Zentralinstitut für Medizintechnik
Technische Universität München

Development of an implant to treat gastro-oesophageal reflux disease

Håvard J. Haugen

Vollständiger Abdruck der von der Fakultät für Maschinenwesen der Technischen Universität München zur Erlangung des akademischen Grades eines

Doktor-Ingenieurs (Dr.-Ing.)

genehmigten Dissertation.

Vorsitzender: Univ.-Prof. Dr.-Ing. Dirk Weuster-Botz
Prüfer der Dissertation:

1. Univ.-Prof. Dr. med., Dr.-Ing. habil. Erich Wintermantel
2. Univ.-Prof. Dr.-Ing. habil. Johann Stichlmair
3. apl.-Prof. Dr. med. habil. Hubertus A. E. J. Feussner

Die Dissertation wurde am 18.06.2004 bei der Technischen Universität München eingereicht und durch die Fakultät für Maschinenwesen am 24.09.2004 angenommen.

Abstract

This study introduces a new method for producing a ring shaped polymer implant, which is to be placed around the oesophagus and passively support the sphincter. This support should reduce the amount of gastric juices in the oesophagus for patients with reflux and hence heal the oesophagitis. Previously, such implants were applied, but failed due to migration along the oesophagus. The idea was to produce an implant with a porous structure, in which tissue could attach to and grow into. This would prevent implant migration.

It has been proven that it was possible to produce the desired porous structure on two different industrial polymer production machine hot pressing and injection moulding, with the novel technique of using water as a foaming agent. The porous structure was adjustable upon the processing parameters. This method was utilized to produce a gastro-oesophageal reflux disease (GORD) implant with a defined pore size distribution. The biocompatible properties of the material were not greatly altered through the new processing method.

Biocompatible tests and enzymatic degradation studies have proven that the injection moulded GORD samples performed better. Enzyme degradation products were found to lay within toxic levels for both machineries. By applying injection moulding process one is also capable of producing far more implants per unit time compared to hot pressing. Material analysis and cell toxicity tests revealed that the most desirable sterilisation method was γ-sterilisation with a minimum dose of 25 kGy. The biocompatibility of the implant was improved by increasing radiation dose, as residual monomers were bound back into the polymer chain. The concentration of methylene dianiline (MDA) was measured to be four times higher for steam sterilisation compared to gamma irradiation of 10 kGy. MDA was undetectable at higher irradiation doses.

Kurzfassung

In dieser Studie wurde eine neue Methode zur Produktion von ringförmiges Implantaten entwickelt. Dieses Implantat soll Patienten, die an der gastroösophagealen Reflux-Krankheit der Speiseröhre leiden, in einem minimal-invasiven Eingriff um die Speiseröhre gelegt werden, um damit passiv den Speiseröhren-Schließmuskel zu unterstützen. Die Menge der Magensäfte in der Speiseröhre soll damit verringert werden und die Reflux-Krankheit könnte geheilt werden. Frühere Implantate, die ebenfalls um die Speiseröhre positioniert wurden, sind jedoch entlang der Speiseröhre verrutscht. Diese Dislokation könnte dadurch verhindert werden, dass Speiseröhrengewebe in das Implantat hineinwächst. Dafür ist eine poröse Innenschicht notwendig.

Es ist gelungen, die gewünschte poröse Struktur und Prototypen des Implantates herzustellen. Dabei wurden eine Heißpresse bzw. eine Spritzgussmaschine verwendet. Die Porengröße und Porosität waren dabei mit den jeweiligen Prozess-Parametern einstellbar. Die biokompatiblen Eigenschaften des Materials wurden nicht entscheidend durch die neue Methode geändert. Das spritzgegossene Implantat zeigte höher Biokompatiblitätswerte und waren in einem enzymatischen Abbaustudium beständiger als die von der Heißpresse hergestellten Proben. Es konnten innerhalb der Toxitätsgrenze keine Abbauprodukte nachgewiesen werden. Verschiedene Sterilisations-verfahrens hatten keine messbaren Auswirkungen auf den Werkstoff, jedoch waren Abweichungen in der Zelltoxizität zu beobachten. Dampfsterilisierte Proben wiesen ein geringes Zellwachstum auf, während auf γ-sterilisierten Proben mit steigender Strahlungsdosis ein erhöhtes Zellwachstum nachgewiesen werden konnte. Generell konnten Fibroblasten an das Material adherieren und proliferieren.

Acknowledgements

The present research work has been carried out during the period of 2002-2004 at the Central Institute for medical engineering, Garching bei München, Germany.

I would like to express my sincere gratitude to my supervisor Prof. Dr. med. Dr.-Ing. habil E. Wintermantel for offering me the opportunity to work in this new institute, for supplying a very interesting PhD topic, state of the art laboratory equipment, electricity to run the machines and for his cordiality and all the support

My referee Prof. Dr. med Feussner deserves my most sincere thanks for all the support, productive inputs during the entire project and particularly for contributing with his expertise to this work.

My second referee Prof. Dr-Ing. Stichlmaier also deserves gratitude for helping me out with the theoretical part of the thesis.

Particular thanks to my tutor Dr. J. Will for her assistance, helpful comments and encouragement through out the entire project. Her kind nature was not just shown through her mentoring, but also by running after bandages for sore skiing blisters and fetching ice cream with fresh strawberries on hot summer days.

I would also like to thank my second tutor, Dr. J. Aigner and Ms U. Hopfner for the entire supervision of the cell studies and useful comments during the write-up. Dr. Aigner has taught me to be critical to my own and other researchers` results. He had as well always time for productive discussions and to give useful tips for publishing scientific papers.

Furthermore, I would like to thank Mrs. S. Schnell for kindly doing successfully SEM images even though hard working construction machines outside the institute and ill-behaving software did all they could to prevent the SEM from working.

Mr. U Ebner deserves severe gratitude for transforming all CAD drawings into real parts, even though the drawings were not always complete. His skills were indispensable.

Also, I would like to thank all students, whom without this dissertation would have been impossible. Their motivation and hard-working mentality gave great inspiration. Their names, in chronicle order: Ms V. Ried; Mr. H. Schlicht; Mr. C. Wende; Mr. L.C. Gerhardt; Mr. M. Brummeisl; Mr. M. Galler; Ms. A. Wagner; Mr. M. Brunner; Mr. F. Pellkofer and Mr. W. Fuchs.

Appreciation also is also given to Dr. S. Guber and Mrs. M. Franke at the Institut für Werkstoffe und Verarbeitung, TU München, for helping out with the EDX analysis.

Special thanks to Sigrid, the Kjuus and the Haugens for their kind understanding and encouragement throughout the whole work, whom without, I would probably never have been able to complete this thesis.

And not at least; Mr. A. Rothberg did a superb proof-reading task.

Two teachers at Volda Upper Secondary School, Norway, Mr. C. Hansson and Mr. E. Berg, were the first ones to bring me true interests into science and engineering. Without their enthusiasm for science and their support for future studies, there would not have been a scientific career path.

All of the above and many others have contributed substantially in one way or another to thesis. I express my deepest gratitude and appreciation to all of them.

Table of content

CHAPTER I
Introduction

1 Gastro-oesophageal reflux disease GORD

1.1 Background

Gastro Oesophageal Reflux Disease (GORD) plays an important role in the development of oesophageal adeno-carcinoma [1]. The number of adenoma carcinomas of the oesophagus and gastric cardia have severely increased over the past decade in western Europe and North America [2-5]. The most alerting rise has been observed for oesophageal carcinomas, which was reported to have escalated in the United States by a factor of six to eight, placing this cancer among the eight most common cancers worldwide [6]. It is one of the most rapid growing of all cancers in western hemisphere [7, 8].

Ten percent of the general population in Western Europe experience reflux of gastric fluids on a weekly basis [9]. Prescriptions for anti-reflux medicine account for six percent of the primary-care drugs budget in the United Kingdom [10, 11]. A similar number has been observed in the remaining western hemisphere [12]. Long-term effects of heartburn will not only, in worst case scenarios, lead to cancer, but also cause profound and prolonged reduction in the quality of life [13]. Hence, heartburn should be taken seriously and addressed with appropriate treatment.

The following pages give a brief overview of GORD and treatment methods. Conclusively, an evaluation of these methods will be made.

1.2 Medical description of GORD

The oesophagus forwards food into the stomach by a wavelike muscle contraction of the oesophageal wall (peristalsis). At the lower end of the oesophagus is a closing muscle (sphincter) located, which exerts pressure within the range of 15 to 30 mm Hg on the opening to the stomach. This pressure

prevents a back flow of stomach fluids. Peristalsis, when swallowing, leads to a slackening of the closing muscle, which makes the passage of food into the stomach possible. After the food has completed its passage, the sphincter contracts itself and prevents the backflow of gastric fluids [14]. Fig. 1 shows a physiological diagram of the stomach.

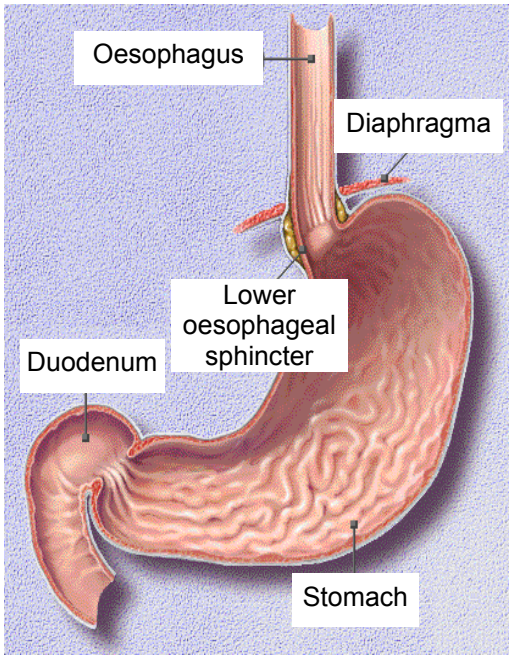

Fig. 1 *Anatomical overview of the stomach: Food is transported through the oesophagus through a wavelike muscle contraction. The opening to the stomach normally closes and opens to let food pass through (By courtesy of Cytosis Fibrosis Trust).*

The most crucial antireflux mechanism is the Lower Oesophageal Sphincter (LOS). To prevent damage to the oesophagus, the following additional mechanisms are necessary: defensive mucous membrane factors and a normal cleaning of the oesophagus through additional peristalsis. The body has several additional barriers that restrict the presence of acid in the oesophagus. Firstly, salvia, which is rich in bicarbonate, can neutralise the remaining acid residue in the oesophagus. Secondly, the oesophageal clearance, described as a second contraction (secondary peristalsis), can push the reflux from the point of irritation back into the stomach. It is triggered by oesophageal dissention or irritation caused by gastric fluids. Thirdly, the oesophagus consists of cell membranes and intercellular junctional complexes, which limit the diffusion rate of hydrogen into the epithelium and thereby protect against injuries resulting from the acid. Finally, the oesophagus also produces a lining of bicarbonate which buffers the gastric fluids and the mucous [15].

The extent and severity level of the oesophagitis depends on the time of contact between regurgitate and oesophagus mucous (quantity), the regurgitate´s composition (quality) and defensive factors of the mucous membrane [16]. However, in some cases, gastro-oesophageal reflux disease affects the contractions of the oesophagus wall, delaying or even preventing self-cleaning. When the lower oesophageal sphincter fails to complete its closure, acids reflux back into the oesophagus, causing heartburn. GORD is defined as the state in which the oesophagus mucosa is exposed to an acidic environment over a prolonged period of time [17].

GORD patients normally have disorders in the above mentioned defence mechanisms. Physicians may classify and diagnose the severeness of GORD by pH-monitoring, radiology and optical viewing of the oesophagus with an endoscopic device [18-20].

1.3 Causes and symptoms of GORD

The reflux is not, according to experts, a result of only one disorder [21]. They assume that the causes of GORD are the prolonged presence of acid reflux in the oesophagus, due to transient lower oesophageal sphincter relaxations, decreased lower oesophageal sphincter resting tone, impaired oesophageal clearance, delayed gastric emptying, decreased salivation and impaired tissue resistance [22]. Nevertheless, the inability of the LOS to perform its function plays the most important role in GORD [23].

There are two pathomechanisms: The LOS can slacken, and/or the intra-abdominal pressure can overcome the sphincter pressure. A hiatus hernia, whereby the top of the stomach „falls out“ through the diaphragma, promotes GORD indirectly, as it weakens the sphincter function and prevents the emptying of gastric acids from the oesophagus. Clinical evidence shows that GORD is rarely observed without the accompaniment of a hiatus hernia [24].

Some factors that may contribute to the development of GORD are smoking, consumption of fatty foods, tight clothing, pregnancy and body positioning [25, 26]. The group most heavily affected are corpulent Caucasians, who are fifty years of age or older [27].

The most common symptom of GORD is heartburn. Heartburn is a burning sensation behind the sternum caused by the return flow of sour stomach mash into the oesophagus [28]. If heartburn

occurs daily, and on a relative empty stomach, it is defined as a GORD [29]. Other oesophageal symptoms are regurgitation, dysfunctional swallowing and chest pains. Dysphagia (difficulty in swallowing) may, however, also occur due to abnormal peristalsis or stricture. Inflammation of the oesophageal leads to odynophagia (pain while swallowing) and dysphagia [30].

Some patients seek help from a physician only after the occurrence of dysphagia. Since the oesophagus wall possesses a certain amount of elasticity, meal can pass through despite the presence of a tumour [31]. Dysphagia appears only in the late stage and as a consequence of reduced elasticity of the oesophagus. In it's advanced stage a tumour is normally already inoperable because it has formed a settlement or broken into neighbouring tissues (Fig. 2) [32].

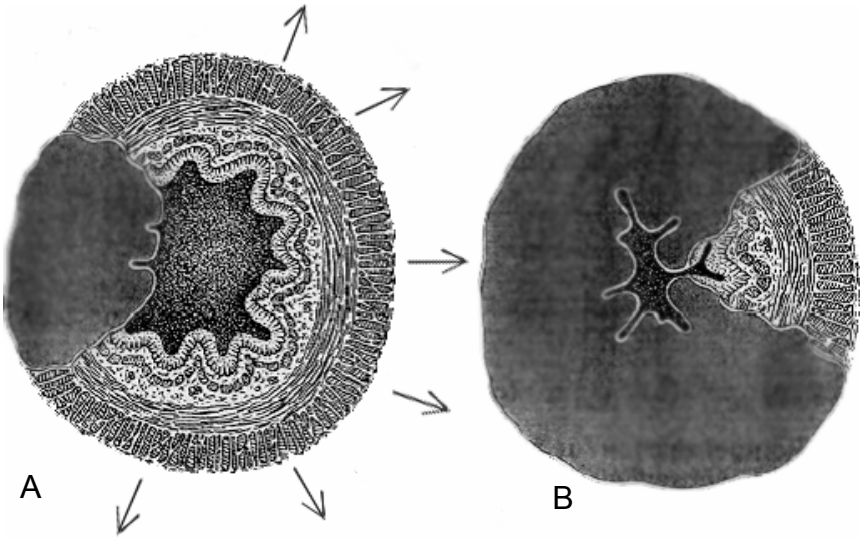

Fig. 2 *Early stage of adenoma carcinoma in oesophagus. Food can still pass through due to elasticity in the oesophageal wall (A). Later-stage tumour: difficulties in swallowing occur as the tumour causes stiffness (B) [33].*

10% of patients with GORD experience pulmonary symptoms which include asthma, chronic coughing, bronchitis, wheezing, aspiration pneumonia and interstitial fibrosis. 45 -65% of adult asthmatics have been found to have GORD [34]. Acid reflux causes decay of teeth and gingivitis. Waterbrash, or the high presence of salvia, is due to a weakly mediated reflex [35]. Injury to the larynx can cause sore throat, hoarseness, laryngitis or a globus sensation. Some patients feel epigastric and /or non-cardiac chest pains. It is also possible for acid to damage the oropharynx and bring about earache [36].

1.4 Treatments for GORD

1.4.1 General Treatment

In most cases, lifestyle changes, that is, diet, clothing, body position and avoiding certain food is enough to achieve some relief from the disease. Lighter cases of GORD can thus be treated without surgical or medical treatments. Such treatments have few side effects and can be a successful remedy for GORD, which involve relatively little effort.

Moreover, higher bed positioning reduces the reflux phenomena during sleep. A reduced intake of alcohol, fruit juices, hot drinks, spicy and fatty food, reduces heartburn distress [37]. Overweight patients may reduce intra-abdominal pressure through weight loss. Avoiding tight clothing might also have the same effect. Patients should avoid food that tend to open the LOS (coffee, tea, sodas, chocolate, fatty foods, peppermint) and should try not to eat later than three or four hours before going to bed [14, 38, 39].

1.4.2 Pharmacological treatment

Known medical treatments for GORD include medications that attempt to decrease acid secretion, or increase gastric emptying. These medications can be divided into three groups: mucosa protective (soothe the oesophagus); prokinetic (increase the strength of tubular contractions and correct weakness in the lower oesophageal sphincter); and acid buffering agents, which decrease amount of acid in stomach. The most common acid suppressant agents are proton pump inhibitors (PPI), e.g. Omeprazole and Esomeprazole [40]. These two medications block the enzyme histamine, which produces hydrochloric acid in the stomach [41]. PPIs are the most common medication for the treatment of reflux diseases [42].

Neutralization of the pH of the refluxate, as achieved by a PPI, effectively eliminates heartburn and the sensation of acid regurgitation. Regurgitation itself, however, cannot be influenced. Patients with acid-related symptoms are often very satisfied with PPI medication [43]. Those with predominantly regurgitative problems may not become entirely symptoms free through PPI treatment. In this latter group of patients, a mechanical solution (restoration of the valve function of the lower oesophageal sphincter (LOS) is preferable [44].

Medical therapies have been quite successful in controlling symptoms in short- and long-term patient follow-up and are highly capable of healing reflux disease. Treatment with acid inhibitors can prevent the recurrence of stricture and maintains symptom remission. Pharmacologic treatment is safe and readily available. Nevertheless, this treatment causes significant costs, and there is often an escalation of dosage required for some patients over time [43]. It is estimated to cost 10 billion US dollars annually [45], and 1300 US$ per person per year is charged for PPIs treatment alone (this may decrease somewhat as generic PPIs become available) [46]. Non-acid alkaline reflux may continue to damage the oesophageal mucosa and, in experimental studies, has been linked to Barrett's oesophagus and oesophageal cancer [47].

1.4.3 Surgical Treatment

Medications are expensive, and such treatment typically has to be continued on a life-long basis [48]. Anti reflux surgery is more cost-effective compared to life-long medications [49]. Many patients are also unwilling to be dependent on medication [50]. Symptoms that arise from complications of the disease, such as persistent or recurrent ulcers, stenosis, volume reflux, and hemorrhagic or confluent oesophagitis, are often an indication for antireflux surgery [45, 51].

Surgical treatments attempt to strengthen the lower oesophageal sphincter by making an incision on either side of the LOS to decrease its volume. This procedure is known as "fundoplication" and is used to prevent the back flow of stomach acids into the oesophagus (Fig. 3) [52].

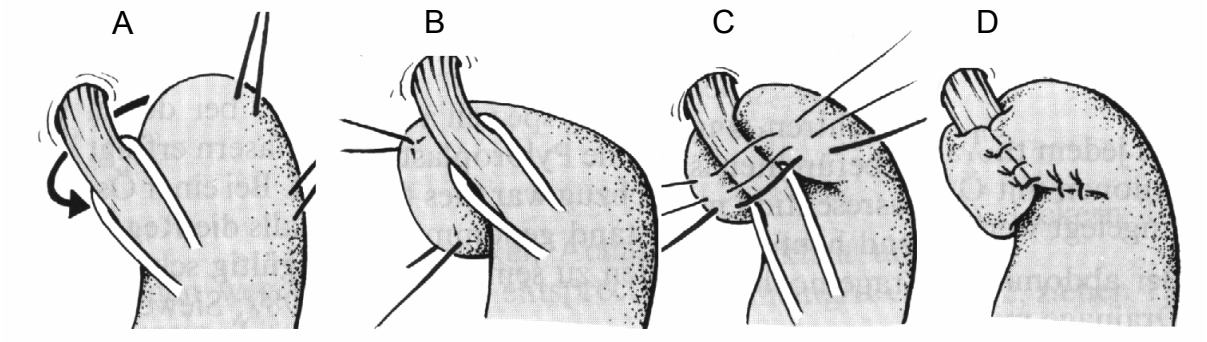

Fig. 3 *The Nissen-Rossetti fundoplication is a method in which the upper part of the stomach is wrapped around the lower section of the oesophagus (A-C) and transforms the LOS into a valve (D) [53].*

The three most common antireflux surgeries are:

- Nissen-Rossetti: Fundoplication [53], as shown in Fig. 3.
- Posterior hemiplication (Toupet) [54].
- Anterior hemiplication [55].

The difference between these methods is the degree of the cuff (Nissen 360°, Toupet 270° and its positioning) [55].

Nowadays, these procedures are performed laparoscopically through 4 to 6 tiny openings in the abdominal cavity. One opening is generally at the navel and the others are in the abdomen. Each incision is between 10-12 mm in diameter. Tubes, called trocars, are inserted into the body through which a telescope-like instrument, called a laparoscope, is passed. The laparoscope is connected to a camera and a video screen for viewing by the surgeon. The surgeon performs the fundoplication, constricting the oesophagus much like the traditional Nissen fundoplication procedure. After surgery has been completed there remain no large incisions, and most patients experience less discomfort than after a traditional Nissen fundoplication procedure. Patients tend to leave the hospital earlier when compared to open-surgery treatments [56, 57].

Even though the success rate of laparoscopic treatment has been well documented in literature [50, 52, 56, 58-60], some post-operative complications are often present. In a study in the US, where 2543 patients were examined, early postoperative dysphagia occurred in 500 of 2453 patients (20.3%), late postoperative dysphagia in 114 of 2068 (5.5%). Additionally, 72 of the 2068 needed dilatation (3.5%), and gastric perforation was occurred in for 1,1 % [61].

Complications of these fundoplication procedures include the inability to belch or vomit, dysphagia, gastric ulcer, impaired gastric emptying and slippage of the repaired area, which may reverse even the best surgical results [57]. Therefore, the fundoplication procedures have been modified to adjust the length and tension of the wrap, including or excluding oesophageal muscle in the sutures and leaving the vagus nerves in or out of the encirclement [62].
Fundoplication treatment heals GORD, prevents stricture reformation and maintains symptom remission. Yet, recent data suggest that between 20% and 50% of surgically treated reflux patients will be back in medical therapy within five to ten years postoperatively [45].

1.4.4 Endoluminal Treatment

Recent interest in developing endoscopic alternatives to medical, or surgical treatments for GORD has generated innovative therapies in three directions: (1) sewing/plicating techniques at the cardia and gastroesophageal junction [63]; (2) radiofrequency thermal application to the lower oesophageal sphincter [64]; and (3) injection/implantation techniques into/across the gastroesophageal junction [65-68].

The first surgical technique using endoscopic sutures was tested on pigs [63], and the first approved method for treating GORD in humans was the Bard® endoscopic sewing machine (Bard Interventional Endoscopic Suturing System®). The procedure requires the placement of an oropharyngeal tube and was developed by the group led by Swain and Mills in London [69]. In the Bard® method, suction is applied, which pulls a fold of gastric tissue into the tube, while a knot is tied outside and pushed into place with a devise designed specifically for this purpose (Fig. 4). The Bard® method is FDA approved and protected under the U.S. patent number 5887594. Clinical results using the Bard device have been relatively successful. In the initial report, 40 out of 67 patients reported improvement, as evidenced by the use of less medications within six months [70]. The inclusion criteria for the participants in this study were very restrictive. Only patients with mild or moderate GORD, minimal oesophagitis, and no hiatus hernia were admitted. Pre- and post-procedure 24-hour pH monitoring was not carried out [71]. Preliminary mid-term data, however, indicate a high recurrence rate

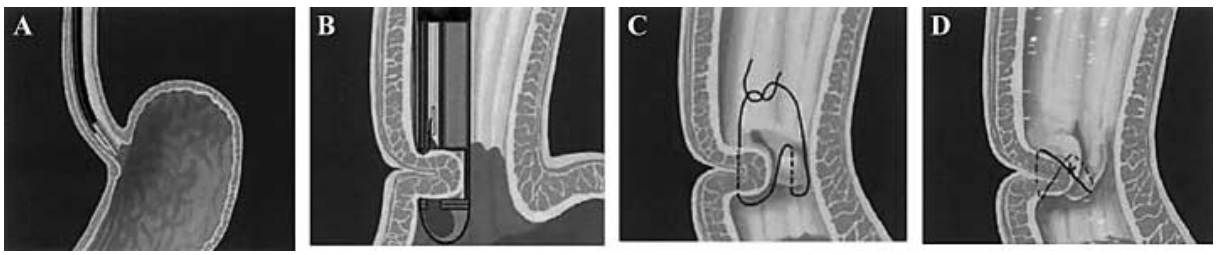

Fig. 4 *The endoscopic BARD® sewing machine is advanced to the gastro-oesophageal junction (A). Suction is applied, which pulls a fold of the tissue into the jaws of the device (B). The sewing machine is applied (C). The knot is tied outside, and pushed into place. (By courtesy of BARD Endochick Ltd).*

The Curon Stretta® device was approved almost at the same time as the Bard method. The device is a special catheter, which is endoscopically delivered to the gastro-oesophageal junction. A

balloon inside the tip inflates and inserts small hooks into the muscles. These hooks serve as antennae for applying radiofrequency heat directly into the muscle (Fig. 5). The amplitude and frequencies used are protected, and have yet to be disclosed by the company. The radiofrequency-induced burns lead to scarring, which seems to create a reflux barrier [64]. This method has also been approved by the FDA and is protected under the U.S. patent number 6321121.

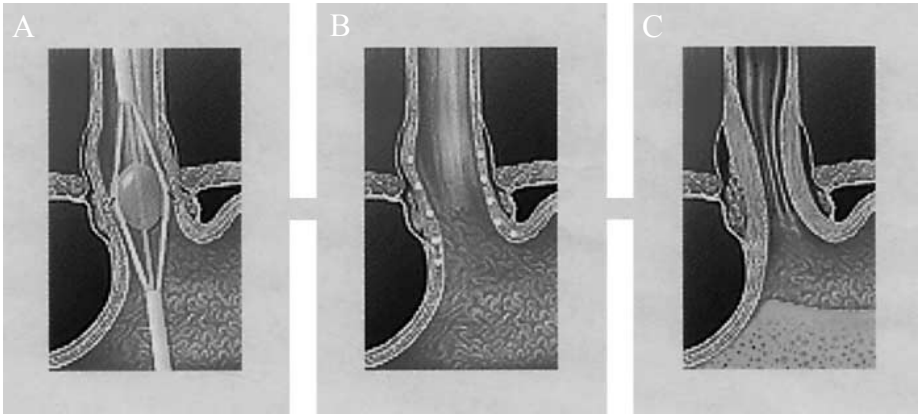

Fig. 5 *The Curon Stretta® device with the antennae is delivered to the LOS junction (A). The antennae induce burns in the LOS walls (B), from which scarring is caused (C) (By courtesy of Curon Medical Ltd).*

Early results from the Curon Stretta® method were similar to those reported by those using the Bard® method [72]. After six months, 67% of the patients had either stopped taking medications or had reduced their dosage considerably. Interestingly, after one year, the percentage of patients who had improved rose to about 80%, although 30% continued to use PPI [73]. This phenomenon is understandable, due to the fact that scars develop slowly after the initial rapid phase and continue to mature for one to two years. This is also worrisome. If the scars continue to contract, at least some patients will develop a narrow stricture. So far, no reports of such a stricture have yet been filed.

Early on, Curon had to recall some of its catheters because of manufacturing defects, but the company has reportedly corrected the problem. In December 2001, Curon Medical announced the completion of two major clinical trials. One of these is a randomized control trial of the Curon Stretta® versus the Sham procedure. The other was an open label study of 590 procedures performed in February 1999. The results have not yet been published, but the company claims they demonstrated efficacy similar to that of the original clinical trial [64].

Self-expanding metal oesophageal stents, which fit across the gastroesophageal junction, have also been tested on animal models [74, 75]. These metal devices function as a one-way valve that hinder the gastric reflux. Wilson Medical has developed a modified stent, where the polyurethane coating has been extended beyond its lower end to form a windsock-type valve [66]. Other valve types are the antirefluxing, mucosal-flap valve [76] and the gastroesophageal flap valve [67].

One of the earlier surgical GORD treatments was an implantation of an antireflux prosthesis, also known as the Angelchik antireflux prosthesis (AAP). A donut-shaped prosthesis of elastomeric polymer filled with silicone was inserted through an incision made in the abdomen. The prosthesis was placed around the intra-abdominal oesophagus. A piece of tape was passed around the oesophagus and tied to the prosthesis to pull the prosthesis into position. The tape ends were then tied and connected by a haemostasis clip used to secure the tightened ends of the tape [68]. One disadvantage of the AAP was that the device tended to migrate from its original position. These migrations often caused obstruction of food into the stomach, and therefore, repeated surgery to correct placement of the AAP was necessary. Another inconvenience was that the prosthesis could not be reinflated if loss of fluid occurred [77]. Due to all these complications the AAP was taken off the market [77-79].

Some scientists have attempted a similar procedure by using a scarf around the oesophagus. The absorbable vicryl scarf was developed to treat traditional reflux-disease management in cases of hiatus hernias. This vicryl scarf induces a subdiaphragmal connective-tissue fixation of the cardia [80]. These semi-absorbable implants have been successful in animal studies [81, 82]. No cases of perforation, stricture formation or other adverse effects were found after years of testing. It has been concluded that this new type of scarf does not have any adverse side-effects [83]. However, it turned out that the antireflux effect was only temporarily.

Initial trials of a bulking agent injection under the mucosa in a refluxing dog model were done by O'Connor and Lehman [84]. Bovine dermal collagen, polymethamethyacrylate and polytetrafluoroethylene paste were shown to increase gastric yield pressures, and there are some evidences to show that the method often causes formation of an antireflux barrier [65, 84-86]. The injection is performed endoscopically [87]. The amount of fluid injected to form the implant

varies with respect to the type of implant material, and optimal volumes have yet to be accurately calculated. The site of implantation is typically near the squamocolumnar junction and is applied in a circumferential fashion.

Boston Scientific Ltd has developed a procedure whereby ethylene vinyl alcohol with tantalum particles is injected endoscopically into the oesophagus's submucosal, and has gained FDA-approval for its product in 2003 [88]. Follow up data from clinical studies showed that, after one year, 57 out of 81 patients (70.4%) treated with Enteryx were able to discontinue their use of daily medication. An additional 8 patients (or 9.9%) were able to reduce their daily dosage by 50% or more [89]. The problems with the Angelchik prosthesis are, however, likely to develop with the newer bulking devices. If erosion into the stomach occurs with a device outside the muscular wall, they are more likely to occur when only the mucosa is a barrier. Most of the inconveniences with the Angelchik prosthesis surfaced after the device had been on the market for a few years. It is suspected that this will also happen with the submucosal bulking devices. Although bulking devices form an effective antireflux barrier, they may also cause dysphagia [64].

1.4.5 Evaluation of current treatment methods

The spectrum of surgical and endoluminal treatments is wide. The preferred surgical treatment at the moment is the fundoplication. Nevertheless, 10-15% of these patients experience post-surgery complication and side effects [46]. Currently, there is no ideal method existing for healing GORD. In the table below some of the advantages and disadvantages with, respect to the heretofore described treatments, are shown.

Treatment	**Pros**	**Cons**
General	cheap, mild cases	only applicable for mild cases [29]
Medical	heals symptoms	Expensive, no prevention of volume reflex [45]
Fundoplication	low mortality rate, definitive treatment	gas bloating, dysphagia [57]
Stretta Curon®	endoscopic technique	scarring disappears after some years [64]
Bard®	endoscopic technique	moderately successful [64]
Angelchik	easy to implant	not in clinical use, migration [77-79]
Enteryx ©	endoscopic technique	little clinical data, migration? [89]

Table 1 *Summarised table of the advantage and disadvantages with the previously presented treatments.*

A completely safe treatment for GORD disease has yet to be developed despite the US Food and Drug Administration's approval of two endoscopic devices for treating gastroesophageal reflux disease. Accordingly, several thousand procedures have been performed to date using these devices. At least 6 other endoscopic devices designed to treat gastroesophageal reflux are in various stages of testing and may soon obtain approval for clinical use. Short-term follow-up studies have consistently reported improvement in heartburn symptoms and quality-of-life scores, as well as decreased use of antisecretory medications. However, oesophageal acid reflux is not fully stabilized after these treatments, nor is GORD improved. Although troubling efficacy and safety issues are currently unresolved, these techniques are becoming routine clinical procedures. Unless careful consideration is given to the scientific validity of these techniques, including comparative trials versus conventional treatments, a cloud of doubt and concern about their role and usefulness in clinical medicine will remain. The rapid flow of these devices into the clinical marketplace, before they have undergone critical scientific scrutiny, increases the urgency to address these issues [90]. It remains to be seen whether the clinical trials will prove them not only effective, but also safe.

The GORD market is increasing, and many researchers are attempting to find a better solution. At present, it is not yet clear which approach will stand the test of time and which of them could actually replace the traditional surgical treatment. At any rate, attempts are required to develop less invasive to cure GORD. This is the topic of this thesis.

2 The new prosthesis, the working hypothesis

The idea was to develop a prosthesis, whereby a polymer ring can be placed on the outside of the LOS. In order to avoid the problem of migration, as has been shown to happen when using the AAP implant, our implant will have a porous inner side, which will enable oesophageal tissue to grow into the implant. Such a ring is displayed below (Fig. 6).

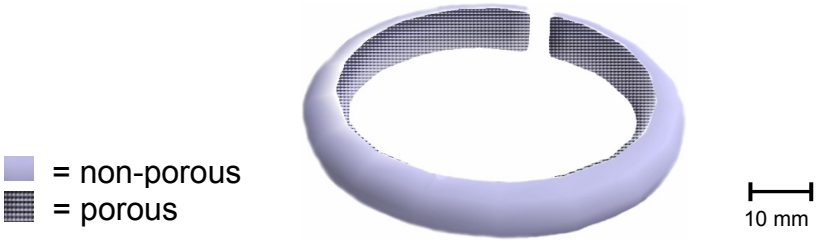

Fig. 6 *Model of the prosthesis with an inner porous and an outer non-porous surface. The goal is that cells will grow into the porous layer, thus preventing the migration of the implant along the oesophagus. The outer side is smooth, which hinders neighbouring tissue attachments.*

The greatest advantage of this implant is supposed to be that it will have a porous inner side, with defined pore diameter and interconnective pores. By having pore diameters of 100-300 µm, interconnective pores of 10-30 µm so that a porosity higher then 65%, fibroblast will automatically grow into the structure and a vasculisation will take place [91-93]. This particular characteristic of the ring will obstruct migration and erosion. The outer surface must be smooth, so that no tissue around the oesophagus could grow into the outer surface of the prosthesis. The implant should also be, in case of explantation, easier to be removed. Fig. 7 shows the intended placement of the ring. The diameter of the ring should be adjustable from 20 mm to 30 mm depending on the patient's oesophagus size.

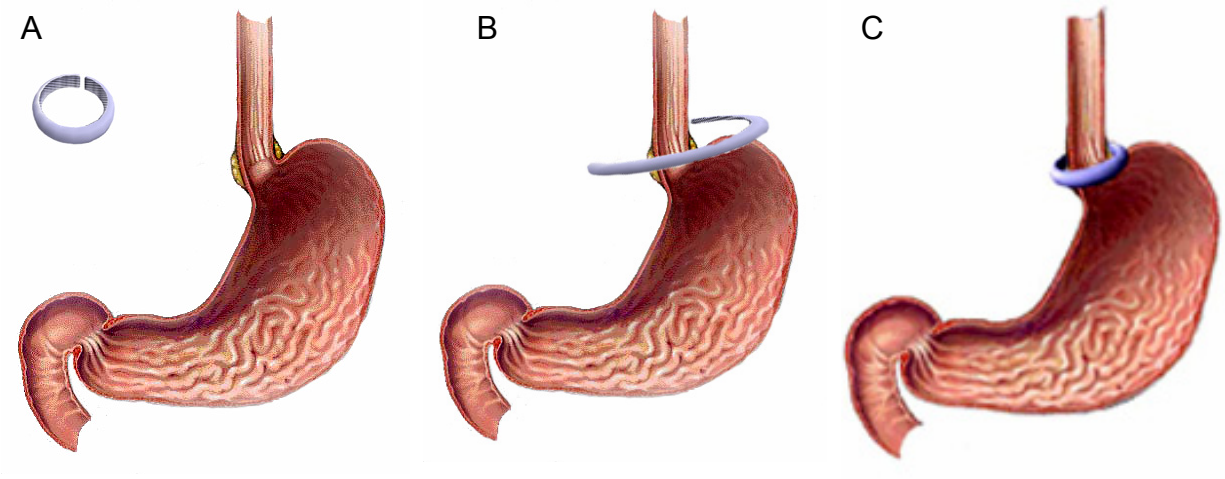

Fig. 7 *Placement of the new prosthesis around the oesophagus at the lower oesophageal sphincter. The implant is flexible and stretched out (A and B). In this manner the implant is placed around the lower oesophagus (C). Its porous structure will prevent the migration of the implant (Courtesy of Cytosis Fibrosis Trust).*

Certain specifications are made in order to ensure the success of the development. The ring shaped prosthesis, which is to be placed around the oesophagus, has to be made of a biocompatible polymer. Secondly, the implantation of the prosthesis has to be minimally invasive (laparoscopic). Thus, to fit into the selected trocar the ring cannot be thicker than ten millimetres. The backflow of acids has to be prevented by the prosthesis and the new treatment should e be cheaper than existing treatments. And finally, the implant should have to display a closing mechanism which enables it to fit all oesophagus sizes. The yearly need of GORD implants in Germany is estimated to be 10 000 [94].

The proposed polymer processing method is combined by using a non toxic blowing agent combined with salt leaching technique. Prior to processing, the polymer is to adsorb water, which will be used as a blowing agent. The processing temperature is high enough for melting the polymer does not affect salt particles. These are, therefore, not to be modified through the processing. The water, however, cannot withstand the processing temperature and evaporates. The water evaporation in the polymer melt creates a myriad of round pores. As the polymer melt vitrifies, networks of round pores are present in the injection moulded implant. These pores are closed, and cannot permit cell growth. The implant is therefore placed in water where the salt particles will dissolve [92, 95-97]. When all particles are leached out, interconnections to the round water pores are created. The proposed foaming method is illustrated below.

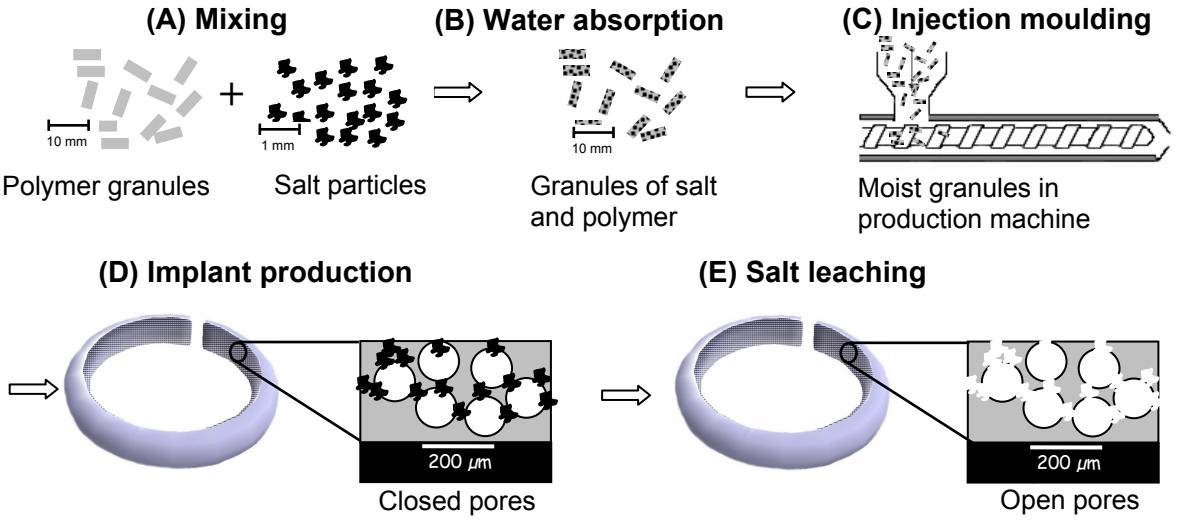

Fig. 8 *Diagram of proposed production of porous polymer. Stage (A): Polymer granules and salt particles are thermally mixed; (B) The granules of salt and polymer absorb water; (C and D) The now moist granules are processed in an injection moulding machine to form the GORD implant. The water evaporates and produces round pore in the polymer. The melt of polymer, vapour pores and salt particles are injected into a cold mould, where the polymer vitrifies. The implant is formed. (E) The implant is, after processing placed in liquid water to dissolve the salt particles. After the salt leaching, interconnections between the vaporised water pore are generated. The rigid imprints from the salt particle can be viewed in the bottom right corner image.*

Polymer granules and salt particles are thermally mixed by a compounder (Fig. 8 A). Prior to injection moulding the granules of salt and polymer absorb water (Fig. 8 B). In the injection moulding machine the granules are heated up (Fig. 8 C). As the polymer melts the water evaporates and produces round pores in the polymer. The salt particles do not melt as the processing temperature is below the melting point of salt. The shape of particles is, therefore, not changed. The melt of polymer, vapour pores and salt particles are injected into a cold mould, were the polymer vitrifies. The GORD implant is formed with a porous structure (Fig. 8 E). However, there is no excess of the vapour formed pores. Thus, the salt particles, which lay between these vapour pores, are leached out in liquid water. Interconnections between the vaporised-water pores are made after this process.

CHAPTER II
Aim of the study

The aim of this project is to produce an implant made of polyurethane, which soothe or even heal the gastro oesophageal reflux disease.

A second objective for this study is to describe the development of a unique manufacturing process to produce a porous structure with a suitable, biocompatible polymer without any toxic compounds. The porosity of the structure has to be from 40% to 90%, and the pore size has to be between 50 µm to 500 µm. The porous structure has to be an open cell structure to ensure that the cells will be able to grow into it, while upholding cell metabolism and nutrient exchange. Additionally, the implant has to be biocompatible so as to guarantee a non-toxic environment for in-growing cells. Hence, a production process that will maintain biocompatible properties of the implant after processing is necessary. The influence of processing parameters on porosity and pore size needs to be obtained.

In order to reach these goals, this dissertation has been divided into three parts: Firstly, a production method that can achieve the desirable porous structure; secondly, the best performing sterilisation has to be found; and thirdly, the integrity in terms of resistance against degradation, needs to be examined. Cell culture experiments will, consequently, be performed to validate the biocompatibility of the material and in growth of tissue into the porous structure as they may be affected during the production and sterilisation processes.

CHAPTER III
Foaming Theory

1 Introduction

This chapter deals with the theoretical modelling for the production process (chapter 1.5) of an implant intended to treat GORD. This method is based on existing theoretical models. Polymer foams are commonly produced by expanding a supersaturated solution of a gas in a polymer melt [98]. Initially, the polymer is saturated with a gas under high pressure. A thermodynamic instability is generated by rapidly decreasing the pressure and/or temperature of this mixture. A porous structure is produced when the gas-polymer mixture tries to reach equilibrium. The state before the pore starts to grow is defined as the critical pore [99]. The pores may grow from a critical radius to any desired size either through amount of gas dissolved in the polymer, geometric confinement of the plastic, rate or magnitude of pressure drop. The pores are distributed uniformly throughout the mixture [100].

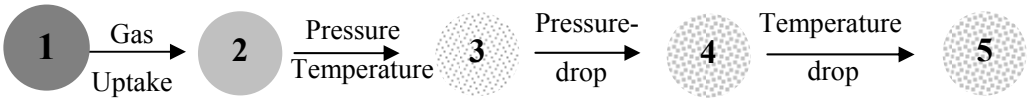

Fig. 9 *Schematic visualisation of the nucleation process: (1) Diffusion of gas into polymer, (2) Plastification of polymer; (3) Homogenous water/polymer phase; (4) Nucleation growth from a critical pore; (5) Vitrified porous structure.*

The most important steps in the nucleation process are [101]; Gas uptake (1); (2) Plastification of the polymer, (3) Homogenous single phase (water / polymer) Nucleate growth and (4) Porous Structure (Fig. 9).

The phenomena-associated pore growth from a critical pore is known as nucleation, and the process can be described by the nucleation theory [102]. The original theory, commonly known as classical nucleation theory, has been extensively reviewed [103-105]. It describes nucleation in terms of thermodynamics arguments, but also takes into account kinetic aspects. Different variation of this theory have also been reported, [106-113], including those based upon intermolecular interactions [114, 115] and molecular dynamics [116]. Besides polymer foaming,

nucleation may be observed in numerous other phase transitions such as boiling, condensation and crystallization.

Once a pore has been nucleated, its subsequent growth is generally described by the continuum conservation equations. Studies of pore growth in infinite [117-120] as well as in finite liquid domains [121, 122] have been reported. Shafi [123], for instance, uses the classical nucleation theory as a basis for the development of a model and additionally takes into account the free volume effects. Their experiments were done using supercritical CO_2 dissolved in polyvinylchloride (PVC).

Shafi's model has been chosen to be used in this study. All models must be modified to fit the system under which the experiments were performed. Shafi's model utilizes dimensionless numbers and is, therefore, more suitable for use in our system. In this model, the pore is considered to be nucleated when it reaches a critical state in which the thermodynamic fluctuations cannot return back to subcritical conditions. This critical state corresponds to the upper limit of the critical pore region described by Zeldovich [124] and Feder et al. [109]. The critical pore was used as the starting point for the pore growth. Shafi's model used the pressure inside the testing vessel as critical pressure. To adapt the model to the injection moulding system, the injection pressure is used as the critical point pressure. Although the number of molecules in the pore at this upper limit is known from the perfect gas law, the radius and surrounding concentration are unknowns.

The critical pore is in thermodynamic equilibrium and will not grow or decay except as a result of thermodynamic fluctuations. The growth of the near-critical size pores is strongly affected by local thermodynamic fluctuations. The details of pore growth dynamics will be discussed in detail in the following pages. To understand the growth of the pore, the nucleation theory has to be firstly understood. Accordingly, the next section will review the nucleation theory and its application in gas-polymer systems.

2 Nucleation theory

Homogeneous nucleation begins when a critical amount of gas is dissolved into a liquid state. This two-component mixture later form a stable second phase, due to elevated pressure and temperature. When the elevated pressure and temperature suddenly vanishes, a thermodynamic

instability is generated, and nucleation is initiated. The rate of homogenous nucleation can be described by the following equations [125] [126]:

$$N_{\text{hom}}^{0} = C_0 f_0 \exp\left(\frac{-\Delta G_{\text{hom}}}{kT}\right) \quad \text{Eq. 1}$$

where N_{hom}^{0} is the number of nuclei generated per cm^3 per second, C_0 is the concentration of the gas (number of molecules per cm^3), f_0 is the frequency factor of the gas molecules, k is the Boltzmann´s constant, and T is the absolute temperature. The term ΔG_{hom} is the energy barrier for homogeneous nucleation, and is given by:

$$\Delta G_{\text{hom}} = \frac{16\pi\gamma^3}{3\Delta P^2} \quad \text{Eq. 2}$$

where ΔP is the magnitude of the pressure drop and γ is the surface energy of the pore interface.
Since the mixture is under high pressure, water is in a fluid state. The surface tension between liquid water and polymer can be described by equation from Reid et al.[125]:

$$\gamma_{\text{mix}}^{1/4} = \bar{\rho}_{\text{mix}} \sum_{i=1}^{2} \frac{X_i \gamma_i^{1/4}}{\bar{\rho}_i} \quad \text{Eq. 3}$$

where χ is the mole fractions, γ is the surface tension and ρ_i is the molar densities (mole/cm^3) of the components.

Knowing the surface energy of the system, as a function of pressure and temperature, the critical size of the nuclei generated can be calculated under any condition using the following formula [127]:

$$r_c = \frac{2\gamma}{\Delta P} \quad \text{Eq. 4}$$

Furthermore, the frequency factor of the gas molecules, f_0, can be expressed as [128]:

$$f_0 = Z\beta^* \quad \text{Eq. 5}$$

where, Z, the Zeldovich factor, which accounts for the fact that a large number of critical size nuclei never grow. Some gas vapour pores shrink back to subcritical diameters, but most gas molecules diffuse into other nucleation sites. The rate at which the gas molecules are added to this site, β^*, can be

calculated by using the surface area of the critical nucleus thickness and the rate of impingement of the gas molecules per unit area (a method suggested by Farkas [128]:

$$\beta^* = \left(4\pi r_c^2\right)\left(R_{impinge}\right) \qquad \text{Eq. 6}$$

Substituting equation 6 into equation 5 results in:

$$f_0 = Z\left(4\pi r_c^2\right)\left(R_{\text{impinge}}\right) \qquad \text{Eq. 7}$$

Equations 1, 2, 3, 4 and 7 form a complete set for the nucleation model of our system. $R_{impinge}$ can be used to adopt Shafi's model to our system. Additional changes were made undertaking the assumption that the self-diffusivity of H_2O is much lower than for a polymer. Therefore, D_{eff}, can be taken as the self-diffusivity of TPU, which is approximately 5-6 x 10^{-10} cm^2/sec. Thus a value of 0.5 x 10^5 sec^{-1} for $R_{impinge}$ has been employed in the calculations.

The quantities C_0, γ_{mix} and ρ_{mix} can be calculated as functions of temperature and gas pressure using the MFLG model [129, 130]. The nucleation model can be solved to describe $\Delta G_{\text{hom}\,o}$, $N^0_{\text{hom}\,o}$ and r_c as functions of temperature and gas pressure. In order to calculate the total number of nuclei generated in the system during injection moulding, the rate of nucleation needs to be integrated over the injection time. Thus the injection pressure was taken as saturation pressure (P_{sat}). Saturation pressure and the pressure at which the polymer vitrifies (P_{vit}) define the rate of integration for nucleation.
Therefore,

$$N_{total} = \int_0^{P_{sat}} N^0_{\text{hom}\,o}\,dt = \int_{P_3}^{P_4} N^0_{\text{hom}\,o}\,\frac{\partial P}{\left(\partial P/\partial t\right)}\,dt \qquad \text{Eq. 8}$$

where P_{vit} can be calculated as a function of temperature using literature data [131].

According to the PVT –diagram for water saturation pressure is the pressure (Fig. 10, Point 3) at which the polymer/water mixture is injected into the mould. The driving force for pore development is the sudden pressure drop which occurs between point three and four (Fig. 10). This stage is assumed to be isothermal. The polymer with the water-foamed pores stabilised as the melt is cooled and vitrified (point four to five).

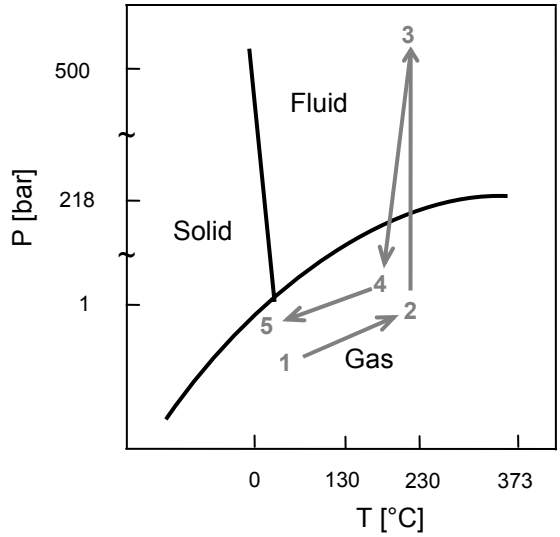

Fig. 10 *PVT-Diagram of H2O, where the foaming process is schematically described. (1-2) Plastification: polymer melts due to temperature rise. (2-3) Injection: Pressure builds up and temperature increases. Water and polymer are homogenously mixed at this critical stage. (3-4) Polymer flows in mould: Sudden depressurization of polymer and water mixture. Pores are formed. (4-5) Cooling: Polymer vitrifies and stable foam is produced. The stages from 3 and 4 have been approximated to be isothermal due to the steep pressure gradient.*

3 Pore growth dynamics

In order to fully understand the growth of the pore, other elements must also be examined.

Consider a polymer melt with a dissolved gas concentration c_o in equilibrium under elevated pressure $P_{G,0}$. With the release of pressure at t = 0, the nucleation and growth of the pores begin. The growth of the pores is inhibited by surface and viscous forces. As pore growth continues the pressure inside the pore and, therefore, the gas concentration at the pore surface decreases. With time t, gas diffuses into the pore, and a concentration gradient propagates in the polymer melt. A schematic of the pore growth is shown in Fig. 11.

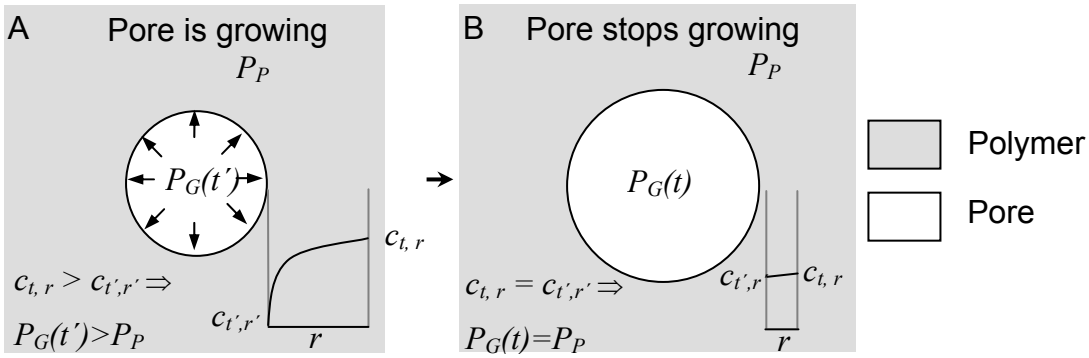

Fig. 11 *Schematic presentation of growth a single pore. The growth occurs as gas diffuses from the surrounding polymer and into the pore (A). This diffusion increases the pressure inside the pore, P_G. The pore grows as $P_G > P_p$. This expansion continues until no more gas molecules diffuse into the pore, $c_{t,r} = c_{t',r'}$(B). At this point the pressure inside the pore is equal to the polymer pressure, $P_G = P_p$. The gas propagates radially. Its gradient is the concentration profile from c_t to $c_{t'}$. The thickness of this boundary layer is r. The pore grows from time t′ with critical radius R(t′) (A) to the final radius R(t) at time t (B).*

The analysis of the growth process will be subject to the following restrictions:

(i) The pore is spherical with radius *R(t)*.

(ii) The gas inside the pore is at pressure $P_G(t)$ and follows the ideal gas law.

(iii) The gas concentration c(r, t) varies only with the radial position and time. The gas pressure in the pore is related to the dissolved gas concentration at the pore surface by Henry's law:

$$P_G(t) = K_H c(R,t) \qquad \text{Eq. 9}$$

(iv) The material properties are independent of the dissolved gas concentration.

(v) The latent heat of the solution and temperature change upon expansion of gas in the pores is insignificant. The growth process can be considered isothermal [118] as the pressure drop is rapid (1-2 msec) compared to cooling time of the polymer (60 sec). The steepness of the pressure gradient is shown in Fig. 10. Inertial effects are small and the liquid is assumed to be incompressible and of Newtonian behaviour. The latter assumption is made due to the fact that the polymer fluid is very viscous (kinematic viscosity < 200 Pa s), the initial pore growth rates are small and hence the inertial effects are negligible.

(vi) Nucleation is homogenous.

Pore growth can be described through coupled mass and momentum conservation equations, with respect to the restrictions mentioned above. A momentum balance across the interface, a mass

balance of the gas in the polymer, and the overall balance on the pore are described by the formulas [119]:

$$\frac{\partial R}{\partial t} = \frac{(P_G - P_L)R}{4\eta} - \frac{\sigma}{2\eta} \qquad \text{Eq. 10}$$

$$\frac{\partial}{\partial t}\left(\frac{4\pi}{3}\frac{P_G R^3}{\Re T}\right) = 4\pi R^2 D \frac{\partial c}{\partial r}\Big|_{r=R} \qquad \text{Eq. 11}$$

$$\frac{\partial}{\partial t} + \frac{\dot{R}R^2}{r2}\frac{\partial c}{\partial r} = \frac{D}{r^2}\frac{\partial}{\partial r}\left(r^2 \frac{\partial c}{\partial r}\right) \qquad \text{Eq. 12}$$

The initial conditions for these pore growth equations are obtained from the state of the pore at the upper edge of the critical pore region [123]:

$$R(0) = R_i \qquad \text{Eq. 13}$$

$$P_G(0) = P_{G,i} \qquad \text{Eq. 14}$$

$$c(r,0) = c_i(r) \qquad \text{Eq. 15}$$

$$c(R,t) = K_H P_G(t) \qquad \text{Eq. 16}$$

$$c(\infty,t) = c_0 \qquad \text{Eq. 17}$$

At a distance very far from the pore surface the solution is not affected by the growing pore, and the dissolved gas concentration remains at c_0, the same as before the onset of nucleation. The subscript i denotes the initial values of the processing variables. New pores nucleate only in the residual volume where the gradients in the dissolved gas concentration are small. The same initial conditions can therefore be used for all the pores. This reduces the many pore problems to a single pore problem and decouples the differential pore growth and nucleation process equations.

Shafi and Flumerfelt [123] used perturbation methods to find the initial conditions for pore growth to a specific size, while also taking into account for the conservation equations.

The solution of equations (10)-(12) provides the pore radius, pressure and the gas concentration profile in the melt surrounding the pore. The pore volume of each pore can then be described as:

$$V_s = \frac{4\pi}{3}\left(S^3 - R^3\right) \qquad \text{Eq. 18}$$

S(t,t') is defined as the radial position at which the dissolved gas concentration equals the nucleation threshold (c_s).

The final pore radii are obtained by performing gas mass balances over each pore. In a state of equilibrium, the sum of gas in the pore and $V_s\left(t_f - \tau\right)$ is equal to the gas dissolved in $V_s\left(t_f - \tau\right)$ at *t = 0*:

$$c_0 V_s\left(t_f, t'\right) = K_H P_G\left(\infty, t'\right) V_s\left(t_f, t'\right) + \frac{4\pi}{3}\frac{P_G\left(\infty, t'\right) R^3\left(\infty, t'\right)}{\Re T} \qquad \text{Eq. 19}$$

where t_f is the time when the final pore structure is formed. $P_G(\infty,t')$ and $R(\infty,t')$ are the equilibrium values of pressure and radius of the pore that nucleated at time t'. Note that at the final equilibrium, the gas concentration in the pore volume is uniform and in equilibrium with the gas in the pore. The final radius and pore pressure are described through the mechanical equilibrium condition using equation 20:

$$R\left(\infty, t'\right) = \frac{2\sigma}{P_G\left(\infty, t'\right) - P_L} \qquad \text{Eq. 20}$$

In order to fit data from our experiments to the Shafi's model, it is needed to utilise dimensionless variables. Only final pore radius and porosity want to be investigated in this study. At this state the residual volume becomes zero. Thus, the following dimensionless numbers can be described (Eq. 21).

$$c^* = \frac{c - K_H P_L}{c_0 - K_H P_L} \qquad c_s^* = \frac{c_s - K_H P_L}{c_0 - K_H P_L}$$

$$J_s^* = J_s / J_{s,0} \qquad P_G^* = \frac{P_G - P_L}{P_{G,0} - P_L}$$

$$P_v^* = \frac{P_v - P_L}{P_{G,0} - P_L} \qquad r^* = \frac{r\left(P_{G,0} - P_L\right)}{2\sigma}$$

$$R^* = \frac{R\left(P_{G,0} - P_L\right)}{2\sigma} \qquad t^* = \frac{t\left(P_{G,0} - P_L\right)}{4\eta}$$

$$V_L^* = V_L / V_{L,0} \qquad V_S^* = \frac{3V_S\left(P_G - P_L\right)^3}{32\pi\sigma^3}$$

$$N_G = \frac{16\pi F\sigma^3}{3kT\left(P_{G,0} - P_L\right)^2} \qquad N_{Pe} = \frac{\sigma^2}{\eta D\left(P_{G,0} - P_L\right)}$$

$$N_{P1} = \frac{P_L}{P_{G,0} - P_L} \qquad N_{S1} = K_H \Re T \qquad \text{Eq. 21}$$

The pore growth governing equations (10-12) with the above dimensionless equations are (22):

$$\frac{dR^*}{dt^*} = P_G^* R^* - 1 \qquad \text{Eq. 22}$$

$$\frac{\partial c^*}{\partial t^*} + \frac{R^{*2}}{r^{*2}} \frac{dR^*}{dt^*} \frac{\partial c^*}{\partial r^*} = \frac{1}{N_{Pe} r^{*2}} \frac{\partial}{\partial r^*}\left(r^{*2} \frac{\partial c^*}{\partial r^*}\right) \qquad \text{Eq. 23}$$

$$\frac{dP_G^*}{dt^*} = \frac{3N_{S1}}{N_{Pe}} \frac{1}{R^*} \frac{\partial c^*}{\partial r^*}\bigg|_{r^*=R^*} - \frac{3\left(P_G^* + N_{P1}\right)}{R^*} \frac{dR^*}{dt^*} \qquad \text{Eq. 24}$$

Equations 23-25 can be solved independently of the equations describing the simultaneous nucleation and growth. These equations are highly stiff, nonlinear and coupled. The moving boundary at the pore surface and the infinite solution domain complicate the problem. Moreover, the boundary condition at the pore surface is a function of time. To avoid such difficulties, the following variables have been defined:

$$y \equiv \frac{R^*}{r^*} \qquad \text{Eq. 25}$$

$$C\left(t^*, y\right) \equiv \frac{1 - c^*}{1 - P_G^*} \qquad \text{Eq. 26}$$

4 Model modification

In order to fit the theoretical data from literature [132], properties of our water/polymer foaming system had to be obtained. The foaming experiments were done with a constant temperature of 503 K, and the injection pressures varied from 300 to 800 bar. The mixture had 5 wt.% water content, hence the presence of the mole fraction is:

$$\chi_{TPU} = \left(\frac{600000\ g/mol}{600000 + 18\ g/mol} \right) \times 0.95 = 0.999$$
$$\chi_{Water} = (1 - \chi_{TPU}) = 0.001 \qquad \text{Eq. 27}$$

From equation 3, one can estimate the surface tension of the mixture. The number for surface tensions was obtained from Table A.6 in DeWitt et al.[133]:

$$\gamma_{mix} = \left(\frac{\chi_{Water}^4 \gamma_{Water}}{\rho_{Water}^4} + \frac{\chi_{TPU}^4 \gamma_{TPU}}{\rho_{TPU}^4} \right) \overline{\rho}_{mix}^4 = 1{,}31\ x\,10^{-2}\ N/m \qquad \text{Eq. 28}$$

The calculation was repeated for the different pressures and temperatures used.

The table below summarises the parameters used in the calculations:

Parameters	**Value**
D	4,28 x 10^{-9} m^2/s
K	4,73 x 10^{-5} mol/Nm
η *(at 503°K)*	1.1 x 10^{2} N s/m^2
σ	1.31 x 10^{-2} N/m
P_{G0}	4 - 8 x 10^{7} N/m^2
P_{L0}	1.01 x 10^{5} N/m^2
T	503 K

Table *2* *Base case value for calculations*

Shafi et al. [134] solved the equation 23-25 computationally by applying the Galerkin method. Based on the parameters in Table *2*, these results can be modified to our system and may be viewed in the graphic presentations below.

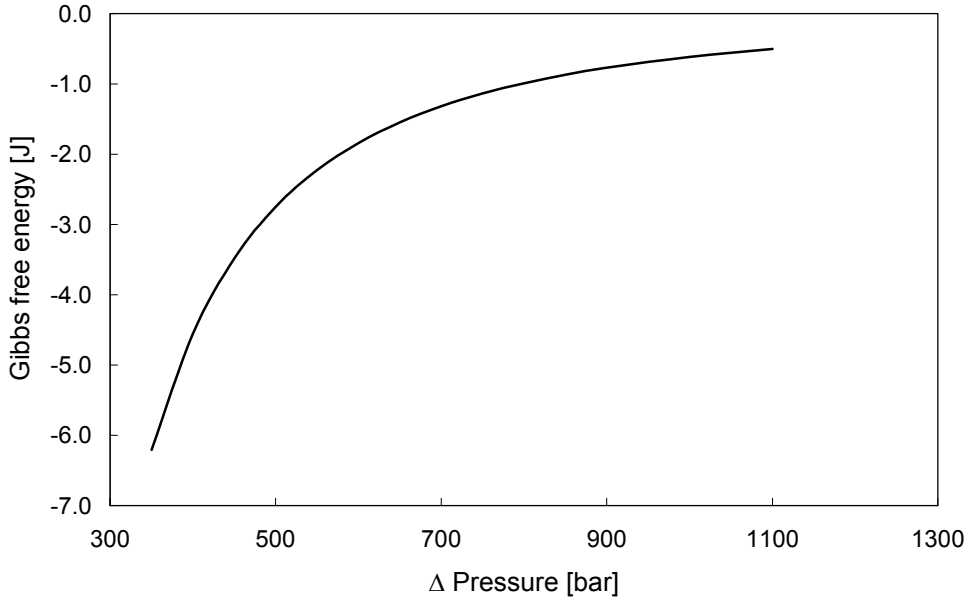

Fig. 12 *Gibbs Free Energy required to initiate nucleation versus pressure difference.*

Fig. 12 represents the Gibbs free energy described in equation 2, which is the minimum energy needed for nucleation growth. The pressure difference is the drop between injection and moulding (Fig. 10). The free energy reaches a plateau at a pressure difference of 1000 bar. Above this value no gain in Gibbs free energy is obtained by further pressure increases. For pressure drops less than 500 bar, a rapid decrease in energy is needed for nucleation.

The porosity for different values of the Gibbs number is represented through N_b, the number of pores per cm^3, with a radius larger than the critical pore size. The Gibbs number (N_G), which is a measure of the energy barrier to nucleation, has a strong effect on the nucleation rate. A slight decrease in the Gibbs number increases the nucleation rate hundreds of times. As the Gibbs number decreases, the number of pores in the foam increases, the final pore radii decrease, and a narrow distribution pore size is obtained. The final pore size distribution will not only depend upon the Gibbs number (N_G), but also on the dimensionless ambient pressure (N_{Pl}) and the Péclet number (N_{pe}).

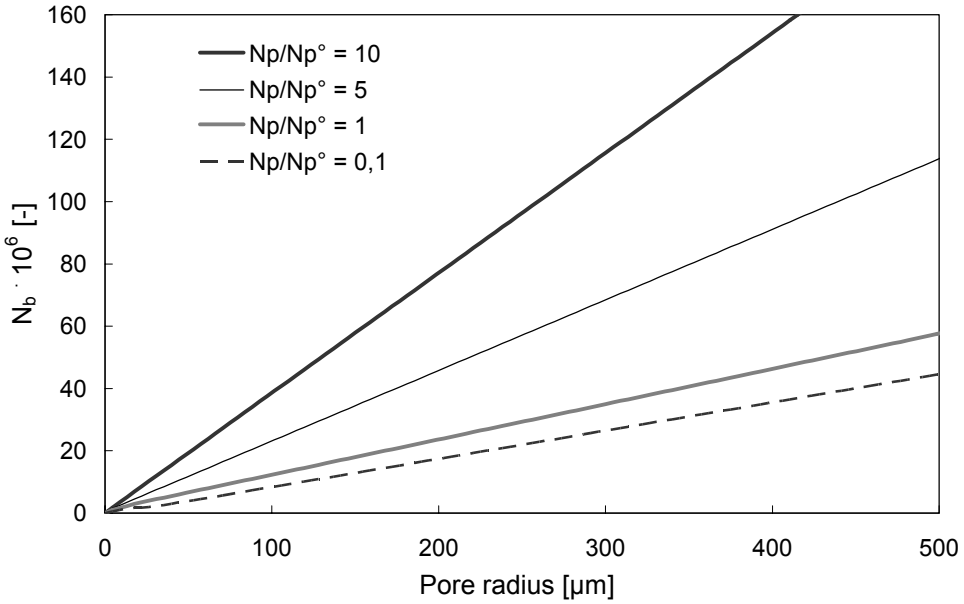

Fig. 13 *Final pore size for different values of the dimensionless ambient pressure against numbers of pores, N_b.. N_{p0}, is the value of the dimensionless ambient pressure at base conditions, and N_p is the number of pores per unit volume whose radii are equal to or smaller than R^*.*

The effect of the dimensionless ambient pressure (N_{P1}) on the pore size distribution is shown in Fig. 13. Pore growth rates and the pore volume expansion rates increase only slightly with a decrease in N_{P1}. Therefore, there is a small decrease in the number of pores.

The effect of diffusion (Péclet number (N_{Pe},)) on pore size distribution is shown in Fig. 14. For a given value of R*, N_b represents the number of pores whose radii are equal to or less than R*. As the Péclet number increases, the nucleation rate is unaffected, the foaming time decreases, the pore growth and pore volume expansion rates increase. The resulting porosity is lower, but the average pore size is larger.

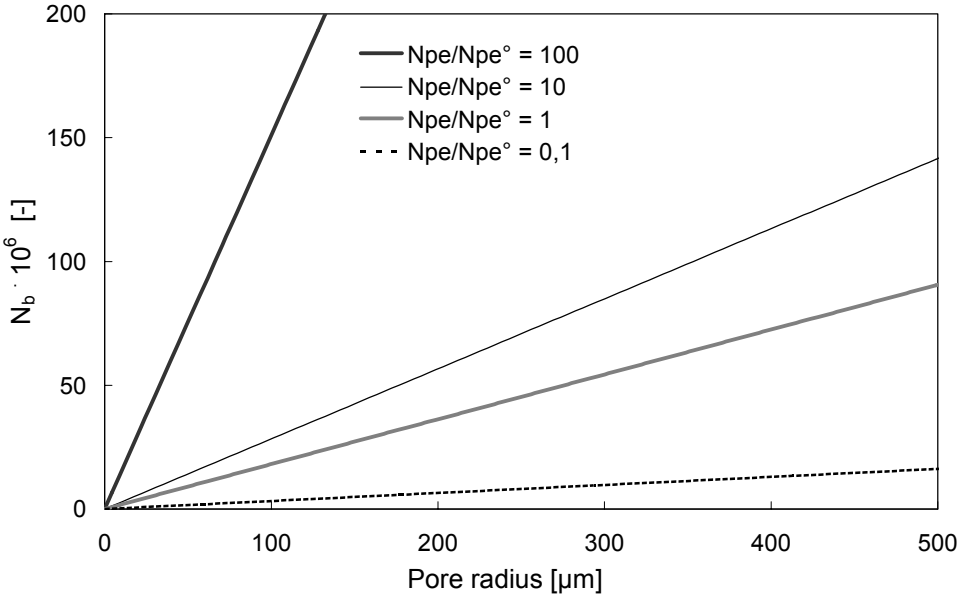

Fig. 14 *Final pore size distribution for different values of the Péclet number. N_{pe} is the value of the Péclet number at the base conditions listed Table 2, and N_{pe0} is the number of pores per unit volume whose radii are equal to or smaller than R^*.*

All the dimensionless groups, N_{Pe}, N_s, and N_p, which appear in the equations of mass transfer, affect the pore growth rate when the fastest growing pores start depleting the gas from the surrounding melt. The Péclet number can be considered as an inverse measure of the gas diffusion rate in the melt. As this number drops, the mass diffusion rate in the melt increases and the pore growth rate are enhanced. The solubility number determines the amount of gas available for pore growth. As the solubility number increases, the pore growth rate increases [123].

The coupled mass and momentum balance equations were solved using the Galerkin method without imposing any restriction upon initial pore volume or dissolved gas concentration. The final pore size distribution depends upon nucleation rate and pore growth dynamics. Any change in processing parameters (here temperature and pressure), which increases nucleation rate or decreases the pore growth rate, will result in higher porosity. Moreover, the pores will have smaller volumes. The final pore size distribution will depend upon the Péclet number (N_{pe}), the solubility number (N_{s1}), the dimensionless ambient pressure (N_{Pl}), and the Gibbs number (N_G). The final pore structure was, after the modified model of Shafi et al, more sensitive to the processing parameters which affected nucleation, especially the Gibbs number, which appears exponentially in the nucleation rate equation up to a saturation pressure of 1000 bar.

CHAPTER IV
Materials and methods

1 Experimental setup

In this chapter the processes for producing a biocompatible porous polymer implant for the use in the GORD therapy will be described. As previously stated, an open porous structure with pore sizes of between 50 μm and 300 μm is necessary. Studies have shown that the ideal pore size for tissue in growth lies within this range [91-93, 135-140]. These pores must be interconnective [91-93], and the implant must be manufacturable on a large scale (> 10 000 implants per year). As a process of this type does not currently exist [97, 141, 142], a new production method is required. The proposed method of production is presented in section 1.5. Due to the high number of implants needed, an injection moulding system has been suggested. Furthermore, this process should not have any major impact on the material biocompatibility, its resistance to degradation stability or on sterilisation. In order to meet the following requirements, the following strategy has been selected (Fig. 15).

Decisions have been made on each level. The outcome of the decision dictates the processing step. That is, if the choice of foaming method is deemed inappropriate by a feasibility study, another method is selected before moving to the next step in the process.

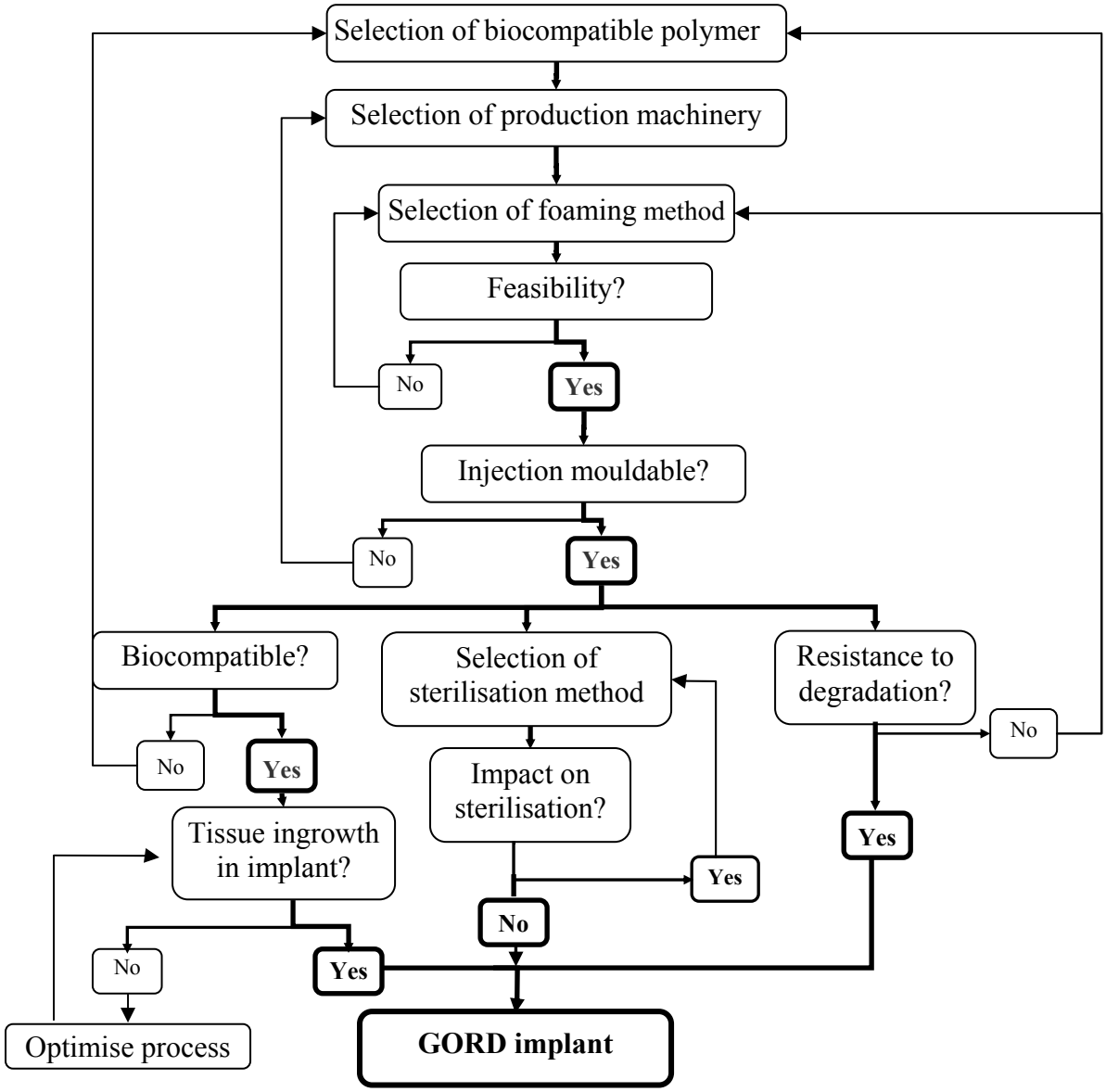

Fig. 15 *Flow diagram of the experimental strategy to obtain a porous GORD implant. The most desirable route to reach the goal is labelled in black. If a level in the flow diagram fails, it is necessary to go back one step and redo the last decision. This route is labelled in bold.*

Choice of polymer:

To guarantee the success of the implant, the following requirements have to be met: (1) The polymer has to be flexible in order to implant it laparoscopically. A porous structure on the inner side of the implant is necessary. Only then will cells be capable of growing into the prosthesis. Hence, the material must be foamable. (2) The material has to be biocompatible and available in medical grade. (3) Finally, the implant material needs to have a high resistance level to degradation

in order to avoid break down of the material in vitro. Degradation of the implant releases products, which may initiate inflammatory reactions and compromise the material's biocompatible integrity [143]. Consequently, thermoplastic polyether-polyurethane (TPU) has been chosen as a favourable candidate. TPU is regarded by scientists as an excellent biomaterial [144-146] and is used for numerous other medical applications (Appendix A).

Choice of processing machinery and method:

As described in section 1.5, the number of implants needed per year, can only be achieved economically through a process using injection moulding. The mixing of a polymer with additives is normally done on extruders. Therefore, the mixing of salt particles and polymer has been chosen to be done on a twin screwed extruder. The double screw enhances mixing properties versus singled ones. The proposed foaming method is a combination of water foaming and the salt leaching technique [96], which is detailed described in figure 1.8. NaCl has been selected for the salt component, as its melting point (790°C) is well above that of TPU (180°C), and it will not change form due to heat. NaCl solubility in water will be used.

Feasibility study:

Injection moulding has up to 30 different changeable processing parameters [147]. Additionally, the mould design and manufacturing is expensive, typically above 10 000 Euro, as well as time consuming (~one to two months) [148]. If the water foaming/salt leaching technique were to fail, much time, effort and money would be wasted. Thus, a feasibility study was performed on a polymer processing machine with lower mould- manufacturing costs (300 Euro) and allow for fewer processing parameters (three), namely hot pressing. If the proposed method is found to function, the next step will be to test the method on an injection moulding machine.

Injection moulding:

The next step, following the feasibility test, was the production of an implant on the injection moulding machine. A study on the processing parameters was performed to obtain the desired porous structure (porosity >60%, pore size 50-300 μm).

Biocompatibility:

After the achieved porous structure had been achieved by injection moulding, the implant was ready for further testing. As the processing method is new, it was uncertain if the polymer material properties would be altered. After the chemical, thermal and mechanical analysis of the material had been done, a biocompatibility test was essential for the realization of the implant.

Release of toxic substances due to implant degradation:

The body fluids attack material, which are implanted. Some of these fluids may initiate a degradation of the implant material [149]. The degradation of the implant may release substances into the body. Some of these compounds may be toxic, and cannot, therefore, allow for cell proliferation and attachment. In order to examine the decay of the GORD implant, a study was performed to observe toxic degradation substances that may be released. Enzyme induced degradation with the hydrolytic enzyme cholesterol esterase (CE) is considered to be the most aggressive degradation mechanism against polyether-urethanes [150-152]. This enzymatic test was chosen to simulate breakdown in the worse case scenario. If toxic substances were being released, the material or processing method would have to be changed.

Effects of sterilisation:

The implant has to be sterilised prior to surgery and implantation. The sterilisation procedure might change the material's properties. Sterilisation may even initiate decomposition of the material, which could lead to the release of toxic compounds [153]. Hence, the material properties and biocompatibility were tested using different sterilisation methods. If no suitable sterilisation procedure for the implant can be found for the material, the proposed implant can never be used.

2 Materials

2.1 Thermoplastic polyether-urethane

Medical grade thermoplastic polyether-urethane TPU (Texin® 986, Bayer Polymers, Pa., USA) was used as material for the implant. TPUs are non-crosslinked polymers and can be generally described as a linear thermoplastic that exhibit an elastic behaviour due to their copolymer structures. They are

composed of short, alternating blocks of soft and hard segments, as shown below (Fig. 16) [154]. These components define the polymer structure. The soft segment determines the elasticity and the flexibility of the TPU and is typically a polyetherdiol in light of its hydrolytical stability in biomedical applications [155]. The hard segments consist of an aromatic di-isocyanate, such as MDI, which gives the polymer its thermoplastic attributes. Additionally, a low-molecular-weight diol is used as a chain-extending agent [154].

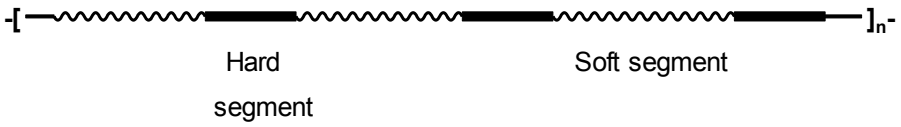

Fig. 16 *Basic structure of linear thermoplastic polyether-urethanes with hard (MDI) and soft segments (polyetherdiol).*

Fig. 17 shows the synthesis of Texin 986 using an aromatic bifunctional reagents diisocyanate (MDI) and a high-molecular weight polyether-diol. A short chain-extending diol increases the hard segment as well as the molecular weight of the TPU [156, 157].

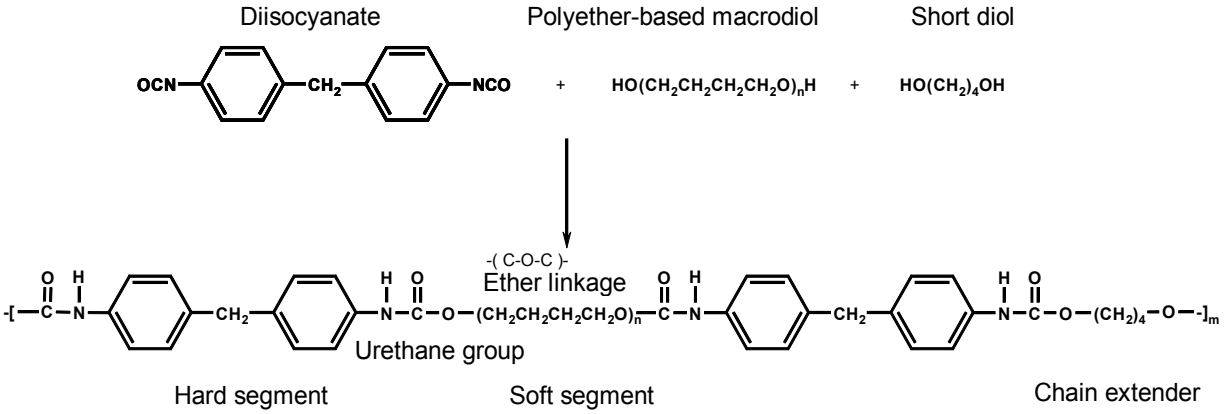

Fig. 17 *Polymerisation of thermoplastic polyether-urethanes using an aromatic bifunctional reagents diisocyanate (MDI) and a high-molecular weight polyether-diol. The short chain-extending diol increases the polymer's the molecular weight.*

2.2 Porogens

Salt particles (NaCl, VWR, Darmstadt, Germany) were used as porogen. In order to achieve the proper size, the NaCl particles were milled in a planetary mill (Pulverisette 6, Fritsch GmbH Laboergerätebau, Idar-Oberstein, Germany) with zirconium oxide milling bowls and balls from the same company. The

mill time was 480 seconds, with a break time of ten seconds at a 350 rpm. Subsequently, they were sieved (AS 200 basic, Retsch GmbH & Co. KG, Haan, Germany) with amplitude of 40 Hz and a sieving time of 10 minutes to obtain the fraction between 100 µm and 200 µm.

2.3 Reagents and chemicals

Enzyme activity measurements were conducted with 4-nitrophenyl acetate (Sigma catalogue no. N8130, Sigma Aldrich Chemie GmbH, Munich, Germany) as a substrate cholesterol esterase from bovine pancreas (EC 3.1.1.13, cat. no. C3766, Sigma Aldrich Chemie GmbH, Munich, Germany) and sodium phosphate buffer (50 mM, pH 7.0, cat. no. 82636, Sigma Aldrich Chemie GmbH, Munich, Germany). Additionally, sodium azide (Sigma cat. no. 19,993-1) was added to avoid microbial contamination. HPLC was calibrated with pure methylene dianiline standards (cat. no. 13,245-4, Sigma Aldrich Chemie GmbH, Munich, Germany), HPLC grade water (LiChrosolv, VWR, Darmstadt, Germany), acetonitrile (Sigma cat. no. 34998) and ammonium hydrogencarbonate buffer (100 mM, pH 10.0), were used as mobile phase compounds. The latter was manufactured by dissolving ammonium hydrogencarbonate (cat. no. 1.01131.5000, VWR, Darmstadt, Germany) in HPLC grade water and adjusting pH with ammonium hydroxide (Alfa cat. no. ALFA035614.K2, Sigma Aldrich Chemie GmbH, Munich, Germany), in accordance with Waters GmbH laboratory guidelines.

3 Polymer processing

3.1 Machinery

A twin-screw extruder (ZK 25, Dr. Collin GmbH, Ebersberg, Germany) was used to mix the salt particles (100 µm - 200 µm, NaCl, VWR, Darmstadt, Germany) with the polyether-polyurethane granule (Texin 986®, Bayer Polymers, Pittsburgh, USA). The extruder was equipped with a counter-rotating twin screw and set to 72 rpm rotating spend to enhance the mixing properties. The composition of salt to polymer was 40 wt.%, and the mixture ratio was controlled using the hopper screw rotating speed (K-CV-KT 20, K-tron AG, Niederlenz, Switzerland), whereby the salt hopper screw speed was set to 125 rpm, and the TPU hopper to 190 rpm.

A heated press (300P, Dr. Collin GmbH, Ebersberg, Germany) was used in the feasibility study. The parameters that were tested were processing temperature, processing time, water and NaCl

content in polymer, heating- and cooling rates. Polymer sheets (Kapton Polymidfolie, 500 FN 131, August Krempel Soehne GmbH + Co., Vaihingen, Germany) are placed between the mould and the covering plates to ensure that the polyurethane will not stick on the plates after the process. The influence of several parameters on the pore building process was investigated. The examined parameters were temperature, filling volume, heating-, cooling- and the water-uptake rate. Samples were produced by changing one parameter systematically, while the others were kept constant. Table 3 shows the examined ranges of the different parameters.

Variable parameter	**Examined range**
Temperature	190 – 235°C
Mould filling volume	50 - 120 wt.%
Heating rate	3 – 15 K/min
Cooling rate	3 – 18 K/min
Moisture content in granules	0.25 - 3.4 wt.%

Table 3 Examined ranges for the initial heated press experiments.

The first experiments were performed without NaCl to identify the important parameters that influence the pore building solely from water. Subsequently, experiments with NaCl were implemented. These initial experiments on the heated press provided the optimum parameters (NaCl content, water uptake, processing temperature and mould filling volume) and were then transferred to the injection moulding. On the injection moulding machine the parameters, which worked out better by the heated press, were held constant.

An injection moulding machine (KM 125 C2, Krauss Maffei GmbH, Munich, Germany) with a 30 cm screw and water mould temperature controlling device (90 S, Regloplas GmbH, Munich, Germany) was utilized for the mass production of the implant. *Table* 4 shows the fixed parameter and Table 5 shows the analysed range of the variable parameters that were used during the experiments.

Fixed parameters	**Value**
NaCl particle size	200 – 500 µm
Filling volume	35 cm³
Cooling time	65 sec.
Dwell pressure	50 bar
Duration of dwell pressure	1 sec.

Table 4 Fixed parameters for injection moulding.

Variable parameters	Examined range
Injection pressure	800 - 1200 bar
Injection speed	30 - 45 mm/s
Cylinder temperature	200 - 230°C
Tool temperature	40- 70°C
Plasticizing rotation	15 - 50 rpm
Plasticizing speed	3 - 5 mm/s
Plasticizing pressure	5 - 10 bar
NaCl concentration	40 – 50 vol.%
Moisture content in granules	4 – 7 wt.%

Table 5 Variable parameters for injection moulding.

3.2 Implant design

The first experiments on the heated press were simplified by producing an oval stick (Fig. 18, A) instead of a ring-shaped GORD implant (Fig. 18, B). The ring structure (Fig. 18, B) was first produced after a controlled porous structure was obtained. All experiments on the injection moulding machine were performed with a ring-shaped GORD implant (Fig. 18, B). The final structure of the GORD implant with a closing mechanism (Fig. 18, C) was not produced. Its design and an initial FEM are discussed in details in chapter VIII.

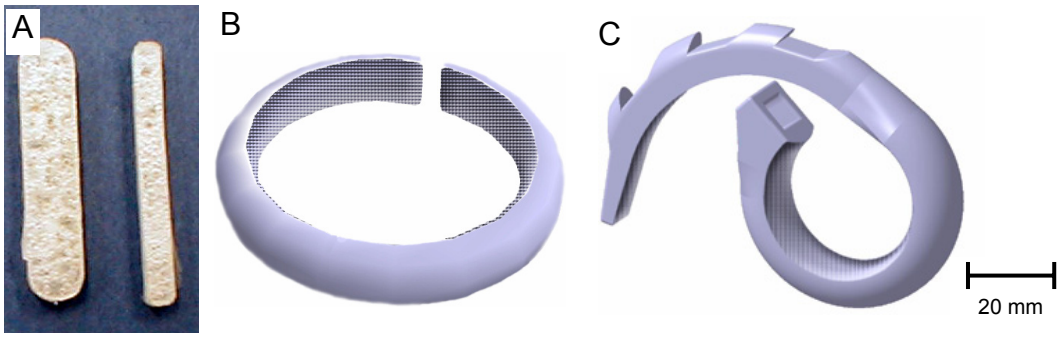

Fig. 18 *The oval stick produced by hot pressing in order to reduce the process parameters (A). The GORD implant produced by heated press and injection moulding (B). Final design of the GORD implant with a closing mechanism (C).*

3.3 Moulds

In order to produce the implant (Fig. 18, B), a particular mould had to be designed. The mould in Fig. 19 was drawn using the CAD program, CATIA © Version 5, and manufactured on non-bored plates using chipping technology (U 630 T, Hermle GmbH, Gosheim, Germany). The mould cavities were eroded (Elox Mondo 2, Agie, Davidson, N.C., USA). Mould standards were bought

(Hasco Normalien GmbH, Lüdenscheid, Germany). The injection mould was equipped to produce six implants at a time.

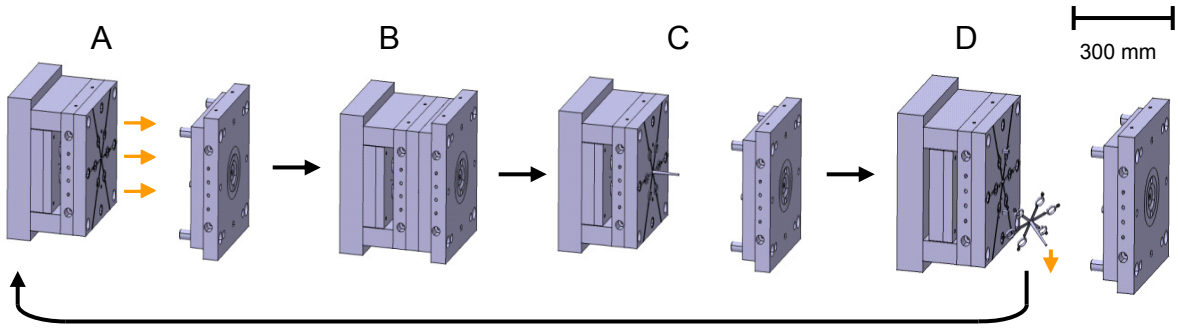

Fig. 19 *Schematic function of an injection mould. (A) The two mould parts close. (B) Polymer melt is injected into the mould and fills the cavities. When the polymer vitrifies, the mould is opened (C). To remove the polymer from the mould, a set of pins are pushed forward and the part falls out. The cycle can now be repeated. Cycle time for the production of six implants was 45 - 60 seconds.*

The plates were constructed of an aluminium alloy (Al Zn Mg Cu 1.5). The mould consists of several different metal parts (Fig. 20), which are mounted together. Four shoulder leader pins and two round interlocks were placed between the mould plates (D and E) to insure a perfect overlay. Appendix B contains mechanical load calculation on the mould.

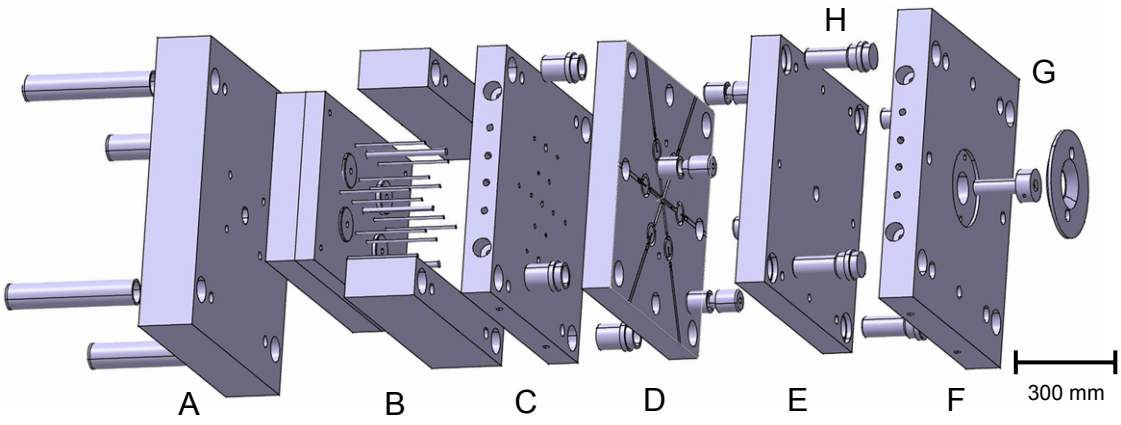

Fig. 20 *CAD model of the mould to produce the GORD implant. From the right: clamping plate at moveable mould part (A); ejector unit with ejector pins, riser strips, retainer and ejector plate (B); cooling plate (C); mould plates (D and E); second cooling plate (E); clamping plate, at fixed mould halve (F) with sprue bushing and positioning ring jacket (G). The cylinders between each plate (H) are centring sleeves to ensure for superimpose of all plates.*

The moulded polymer part, which is produced with this mould, is displayed left side in Fig. 21. Six implants are moulded in one cycle. The thickness of these implants is limited by the size of trocars used during laparoscopic surgery (see section 1.5) and cannot be larger than 10 mm.

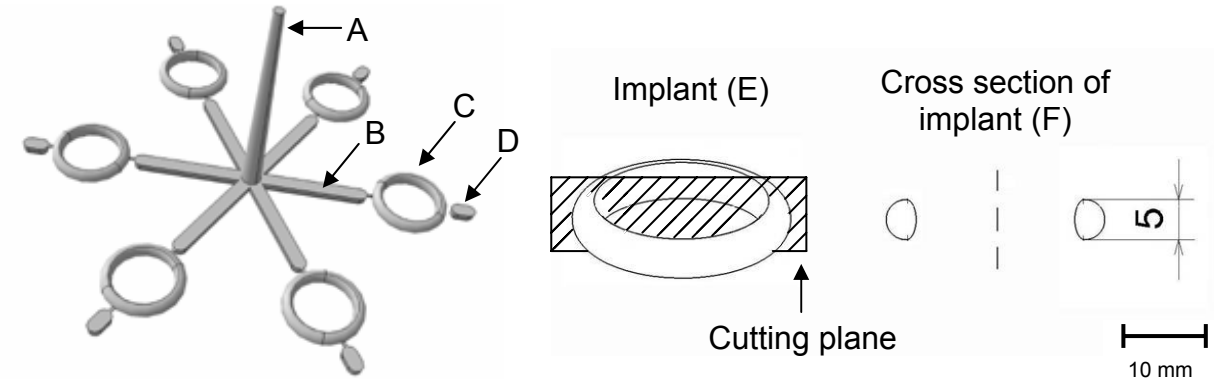

Fig. 21 *Injection moulded part (left), with the sprue (A), runners (B), implant (C) and end runners (D). Far right is a cross-sectional diagram of the implant (E and F). The implant's inner radius is 20 mm and elliptical. The outer surface is rounded. The ring's thickness is 5 mm.*

This implant prototype has a ring radius of 25 mm, which corresponds to a large oesophageal diameter. Far right of Fig. 21 is a technical drawing of the ring implant. This ring was chosen to the prototype of the implant. A closing mechanism is also incorporated and is displayed in chapter VIII.

4 Characterisation of macro- and microstructures

4.1 Microscopy

Closed pores were characterised using a microscope (Stemi 2000-C, Zeiss Carl Jena GmbH, Jena, Germany), which was equipped with a camera (AxioCam MRC, Zeiss Carl Jena GmbH, Jena, Germany). The quantification of the pore sizes was performed visually by selecting a sample area for evaluation. The pore number and pore radius were measured and recorded. The data analysis was performed using Microsoft Office, Excel.

Scanning electron microscopy SEM (S-3500 N, Hitachi Science Systems, Tokyo, Japan) was used for the observation of the internal pore morphology from the samples. The samples were

sliced with a scalpel and then coated with gold (10-20 nm) by using a sputter-coater (SCD 005, BAL-TEC AG, Balzers, Lichtenstein) under high vacuum with a current range between 5-15 kV.

These procedures are qualitative methods, and were only used for initial testing or presentation. Quantitative examinations of macro-and micro structure were performed using various other porosimetry techniques, which are described below.

4.2 Porosimetry

The porosity was examined using a pycnometer (AccuPyc 1330 Pycnometer, Micromeritics GmbH, Mönchengladbach, Germany).

Mercury intrusion porosimetry (AutoPore VI 9500, Micromeritics GmbH, Mönchengladbach, Germany) was used to determine pore size distribution and porosity of the samples. The porous materials were placed in a solid penetrometer with 6 ml bulb volume (model 07-044506-01, Micromeritics, Norcoss, GA, USA). The intrusion chamber was then filled with mercury at a pressure of 3.45 kPa and the samples were penetrated with mercury until a maximum pressure of 30 MPa, at which time the total intrusion volume reached a plateau.

The interconnective pores were examined by capillary flow porometry (CFP – 1100 – AEXL, PMI Europe, Wetteren, Belgium). The samples were glued (Loctite 454, Loctite GmbH, Munich, Germany) on a placeholder and wetted with a wetting agent (Gal wick®, PMI Ltd, Massachusetts, USA), which filled the pores in the sample. A pore distribution, as well as the bubble point (the diameter of the largest pore), were obtained.

Gas adsorption (TriStar 3000, Micromeritics GmbH, Mönchengladbach, Germany) was utilized for surface area characterisation. Fristly, the samples were dried with gas (Vac. Prep. 061, Micromeritics GmbH, Mönchengladbach, Germany). The gas used for this test was Argon 4.8 and helium (Westphalia, Munich, Germany). The total surface area was calculated through the BET isomers from the amount of gas adsorbed on the material.

5 Thermal analysis

A differential scanning calorimeter (DSC, Jupiter Netzsch Gerätebau GmbH, Selb, Germany) was used to determined the melting points, glass transition temperatures and crystallitity of the polymer samples. Each sample weight 25 ± 0.2 mg was heated three times from -100°C up to 190°C at a heating rate of 10 K/min. Cooling runs were done at the same rate. Samples examined for glass transition temperature and crystallinity detection had weights of.

A simultaneously thermal gravity (STA 449C, Netzsch Gerätebau GmbH, Selb, Germany) was used to check the NaCl residue in the implant (analogous to [158]). During the analysis the sample was heated up from 20°C to 1400°C at a heating rate of 20 K/min. Since polyether-polyurethane burns up completely at 400°C and NaCl at 1200°C, the amount of each material can be quantified.

A rheometer (CVOR, Bohlin Instruments, Germany) was used to test the viscosity of the processed polymer. Polymer granules (100 mg) were placed between two 20 mm diameter round plates. Two heating chambers surrounded the measuring chamber to ensure a constant temperature during the testing. The polymers´ viscosity was tested between 180°C and 230°C.

6 Chemical analysis

6.1 Chromatography

After having isolated the extracted polymer solutions, degradation products of the polymer were analysed on a High Performance Liquid Chromatography (HPLC) system (600 E LC, Waters GmbH, Eschborn, Germany) with a 717plus Autosampler, Jetstream column oven and a 2487 Dual UV Absorbance detector. The Waters Empower chromatography software was used to acquire and process data. The polymer extracts were separated with a Waters X-Terra MS C_{18} column (4.6 x 100 mm, 3.5 µm) using a flow rate of 1.5 ml/min and detected by an UV detector at a wavelength of 254 nm. The testing cycle time for one injection was 22 minutes with 3 minutes-delays between each measurement. Prior to use, all mobile phase components (except HPLC grade water) were filtered through a 0.45 µm hydrophilic polypropylene membrane filter (Acrodisc 13 GHP, Waters). The calibration took place by

dissolving 0.1 mg/ml of MDA (cat. no. 13,245-4, Sigma Aldrich Chemie GmbH, Munich, Germany) into HPLC grade water (LiChrosolv, VWR, Darmstadt, Germany) and, subsequently, dilution to ppb range. The fifteen different calibration standards were analysed five times. The Empower software generated a calibration curve with statistical analysis.
The HPLC solvent gradient used is given below (*Table 6*).

Time	Flow [ml/min]	%A	%B	%C	Curve
0	1.5	80	10	10	-
20	1.5	50	40	10	Linear

Table 6 *HPLC gradient used for separation of degradation product. Phase code: (A) HPLC grade water, (B) Acetonitrile, (C) 100 mM Ammonium hydrogencarbonate buffer, pH 10.0.*

The MDA amounts were determined by the UV response with a retention time ranging from 2.0 to 2.2 minutes. The detector response (signal height in µV) was compared to the initial calibration curves and, subsequently, the released MDA concentration was calculated.
The samples runs were repeated three times and compared to the calibration curve.

Following UV detection, the isolated polymer extracts were applied to electrospray ionisation mass spectrometry (ESI-MS), which were carried out on a quadruple mass spectrometer (Micromass ZQ, Waters, Milford). The data were processed by using the Empower operating software. The isolated polymer extracts were delivered with a delay of 0.6 ± 0.05 minutes (n=20) into the ionisation source, using the HPLC pump. The voltage applied to the tip of the ESI needle was 4.0 kV, and the voltage applied to the cone was 27 V. Nitrogen was used as collision gas. The ESI^+ mode was used in order to identify the components in the injected solution. Ion spray mode provides a spectrum of protonated molecular ions (MH^+) in the sample. Additional adducts of the molecular ions could also be produced (MNa^+, MK^+, MNH^4) as other cations are present in the mobile phase and the buffer [159]. Two modes were employed during the MS analysis, single ion monitoring (SIM) and single ion recording scan (SIR). Altogether, three different mass spectra were recorded: A signal for the protonated MDA at a mass-to-charge ratio (m/z) of 199.3 (m+1/z); a spectrum at an m/z ratio equal to the half of MDA (m/z=100); and a scan of the masses between 50 and 250 Da (m/z=50-250). Mass spectrum results were then processed with Empower software and plotted as relative

ion intensity versus mass-to-charge (m/z) ratio. An overview of the process flow of the analytical LC-MS method used in biodegradation experiment is illustrated below (Fig. 22).

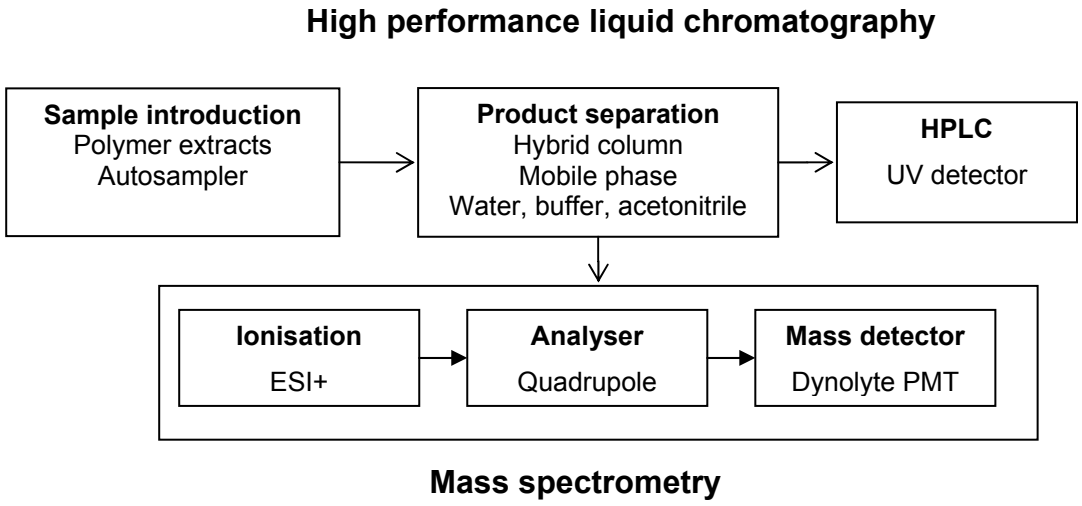

Fig. 22 *Liquid chromatography-mass spectroscopy process flow for the detection of degradation product of TPU.*

Molecular weight analysis of the polymers were measured in a gel permeation chromatography (GPC) system (600 E, Waters GmbH, Eschborn, Germany) with a refractive index detector, Waters 410, a column oven Jetstream, 717plus Autosampler, four Waters Styragel HT 3,4 and 6 were delivered in dimethylformamide, DMF. Again, the Waters Empower chromatography software was used to acquire and process data. The solution for the analysis was HPLC Grade DMF with an additional 0.05 m LiBr to circumvent the hydrophobic interactions between the solvent and the polymer. The columns were calibrated with twelve polystyrene standards (VWR, Darmstadt, Germany) (n=5). All measurements were done at 85 °C to ensure a high viscosity of the test fluid. All samples were filtered through a 0.45 µm hydrophilic polypropylene membrane filter (Acrodisc 13 GHP, Waters) and analysed three times.

6.2 Spectroscopy

Efficiency of an enzyme does not only depend on its weight or volume, but also on its activity grade and purity. Enzymes are quantified according to their activity, namely with activity units (U). In order to assess and determine the cholesterol esterase activity, photometric analysis was

conducted using an Ultraviolet-Visible (UV-Vis) spectral photometer (Specord-210, Jena Analytik AG, Jena, Germany). The generated data was evaluated with the WinASPECT software. A unit of enzyme activity was defined according to Labow and Tang [160, 161],"one unit of cholesterol esterase, CE, was defined as the amount of enzyme required to generate 1nmol/min of p-nitrophenol from the hydrolysis of p-nitrophenyl acetate at pH 7.0 and 25 °C as determined by a spectrophotometric assay at 410 nm." The initial substrate conversion of 1nmol/min is, thereby, directly proportional to CE activity. The chemical path way of the hydrolysis can be viewed below.

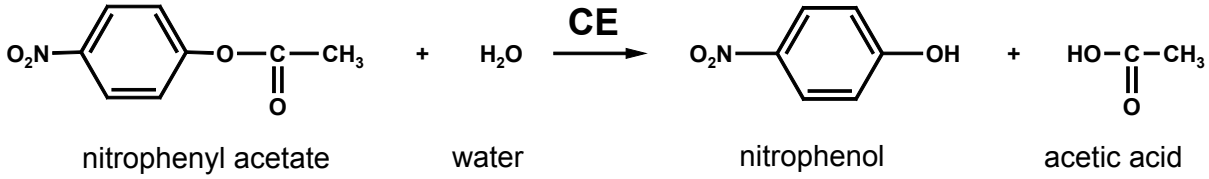

Fig. 23 *Chemical pathway for enzyme cholesterol esterase, CE, activity determination. The CE concentration cannot be measured, and its concentration is thus indirectly determined through the hydrolysis of nitrophenyl acetate and measurements of the end product nitrophenol.*

During the hydrolysis phase of nitrophenyl acetate, changes in absorption/extinction were recorded by UV-Vis spectrometry (Fig. 23). The initial test solution turned from transparent to a deeply neon yellow colour. The activity of one unit can be found by applying the modified Lambert-Beer formula (Eq.29) and back counting the enzyme weight from the dissolved solution. The reaction rate of nitrophenyl acetate to nitrophenol and acetic acid can be calculated as follows:

$$\frac{\Delta c}{\Delta t} = \frac{\Delta A_{410}}{\Delta t \cdot d \cdot \varepsilon_{410}} \cdot \frac{V_{tot}}{v_{cuvette}} \qquad \left[\frac{\Delta c}{\Delta t}\right] = \frac{nmol}{\min} \qquad \text{Eq. 29}$$

where A is the measured absorbance at 410 nm within a certain time interval; ε_{410} is the wavelength-dependent molar extinction coefficient of nitrophenol (ε_{410}=16,300 L*mol^{-1}*cm^{-1}, [162]); d is the cuvette thickness; and c is the analyte concentration. The ratio V_{tot} and $v_{cuvette}$ was used to determine the enzyme concentration. The substrate has to be in excess in order to achieve complete reaction. Some trial and error work was necessary to make sure that absorbance occurred in the linear range of the UV absorbance.

The attenuated total reflection Fourier Transform Infrared Spectroscopy ATR FT-IR (Spectrum one, Perkin Elmer Instruments, Rodgau-Jügesheim, Germany) was used to analyse the chemical structure of the samples after the production process. This analysis provided information regarding the structural differences. All samples were shredded into small pieces (0.5 ± 0.1 mm) and placed into a powder funnel where pressure was applied. This procedure allowed the system to avoid measuring the air gaps in the porous polymer.

7 Mechanical analysis

Ring shaped samples went through a quasi-static tensile-test with a material testing machine (TC-FR 2.5TS.D09, Zwick GmbH & Co., Ulm, Germany) under conditions defined by DIN 53504. Table 7 lists the chosen experimental parameters and shows the test assembly of each porous TPU.

Parameters	**Value**
Ambient medium [gas, °C]	Air, 25
Initial load [kN]	$5 \cdot 10^{-3}$
Initial load speed [mm/min]	50 (DIN 53504)
Test speed [mm/min]	500 (DIN 53504)
Load cell [kN]	2.5

Table 7 *Quasi-static tensile-test defined by DIN 53504 and modified to fit the ring structure.*

8 Biocompatibility analysis

8.1 Cell types

The oesophagus consist of several different cell types, such as muscle cells, epithelia cells and fibroblasts [163]. The most important cells for anchoring the implant to the oesophagus are considered to be fibroblasts [164, 165]. As this implant is designed to fixed onto the oesophagus, and thus preventing migration, fibroblasts were used for the biocompatibility test.

A permanent cell line (Detroit 551, CCL-110, ATCC, Manassas, USA), taken from the skin of a female Caucasian, was used in the study and was cultivated in MEM-Earle-Medium (Biochrom AG, Berlin, Germany) with supplementary ingredients (Appendix D). Fibroblasts

from the oesophagus were not available from the cell bank ATCC Manassas, USA. Therefore, another common fibroblast was used as they do not differ much from the genuine tissue [166]. The cells have a finite lifespan of about 25 serial passages [167].

8.2 Cell culturing

Subcultivation of monolayer culture

The *in vitro* cell studies were performed with a permanent cell line, Detroit 551 fibroblast. The cultivation was performed in Petri dishes (T25 and T75, TPP, Trasadingen, Switzerland). Detroit 551 cell mediums (DMEM, Biochrom AG, Berlin, Germany). Its composition and additives are listed in appendix D. The cell cultivation took place under sterile conditions in cell culture incubators (Heraeus Kendro Laboratory Products GmbH, Langenselbold, Germany) at 37°C and 5% CO_2-atmosphere. For subcultivation, culture medium was removed from the Petri dish and washed twice with phosphate buffered saline (PBS-Dulbecco, Biochrom AG, Berlin, Germany). The cell monolayer was removed by trypsinization (Trypsin EDTA Solution, Biochrom AG, Berlin, Germany), according to Freshney [168].

Vitality and cell number measurements

Cell vitality was assessed using the Trypan Blue method [169, 170]. Non-vital fibroblasts with damaged cell membranes and cell rests will absorb the trypan blue colour (Biochrom AG, Berlin, Germany), whereas vital one will not. The number of vital/non-vital cells was measured with a Neubauer-Haemacytometer (Assistent, Karl Hecht KG, Sondheim, Germany) on a microscope (Axiovert 25, Carl Zeiss GmbH, Jena, Germany).

A second method for determining cell number can be achieved by using the Casy®1-Cell Counter Analyser System, Model TT (Schärfe System GmbH, Reutlingen, Germany). The principle behind the analysis is a combination of electrical resistance and pulse area. A sample was dissoluted one to one hundred using a weak electrolyte (Casy®ton, sterile filtered, Schärfe System GmbH, Reutlingen, Germany) and drawn through a capillary with a constant flow velocity. Voltage is applied to the capillary by two platinum electrodes, and a defined electrical resistance appears. The fibroblasts fill the volume of the capillary and change its resistance. A vital cell will function as an isolator. Resistance is thereby decreased. Its number can be used as a scale for living cells [171]. Vital cells that were monitored were between sizes of 15-30 µm.

Cell seeding

Prior to seeding onto the GORD implant cell, the numbers of vital fibroblast in suspension were counted according to the procedure previously described. The porous TPU samples were fixed in 24 Well plates with sterile paraffin (Histatec®, VWR, Darmstadt, Germany) (Fig. 24, A), preventing buoyancy of the polymer material.

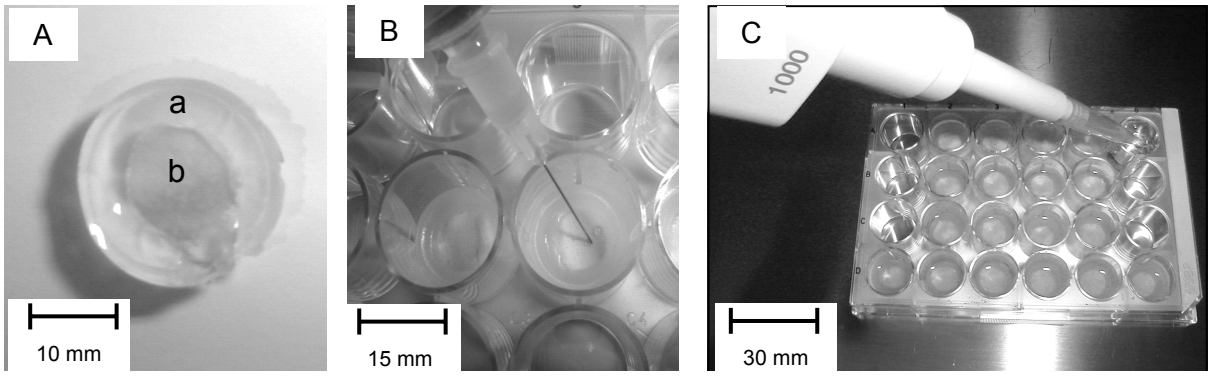

Fig. 24 *(A): Horizontal view of porous TPU sample (a) embedded in paraffin (b) to prevent buoyancy and, hence, inaccurate cell seeding and nutrient supply. (B): The fibroblasts were injected in a suspension into the material. (C): After seeding and imbedding the GORD implant sample and the culture medium was added into the wells.*

Such an event would inhibit an accurate cell seeding. Paraffin was heated to 100°C, and 700 µl of the liquid was injected into the well plate. The polymer sample was set in place with metal tweezers and left to rest until the paraffin solidified. Additional paraffin was added for thicker samples after the paraffin vitrification. A suspension of 12 ml culture medium with $6 \cdot 10^6$ fibroblasts was placed in a beaker. The suspension was drawn into a 5 ml syringe and injected into the sample Fig. 24, B), later the wells were filled with 1.5 mL of culture medium (Fig. 24, C).

8.3 Cytotoxicity test

For the biological evaluation of the implant's material, an *in vitro* cytotoxicity test, based on the European norm ISO 10993-5: 1999, was performed [172]. Sterile samples (30 mg) from the implant were cut into fine pieces each 1 mm ± 0.01. These pieces were washed in sterile water and later incubated in culture medium. The culture medium was added to a well plate containing a monolayer of fibroblasts *(*Fig. 25) in four different dilutions: undiluted; 1:10; 1:5 and 1:2.

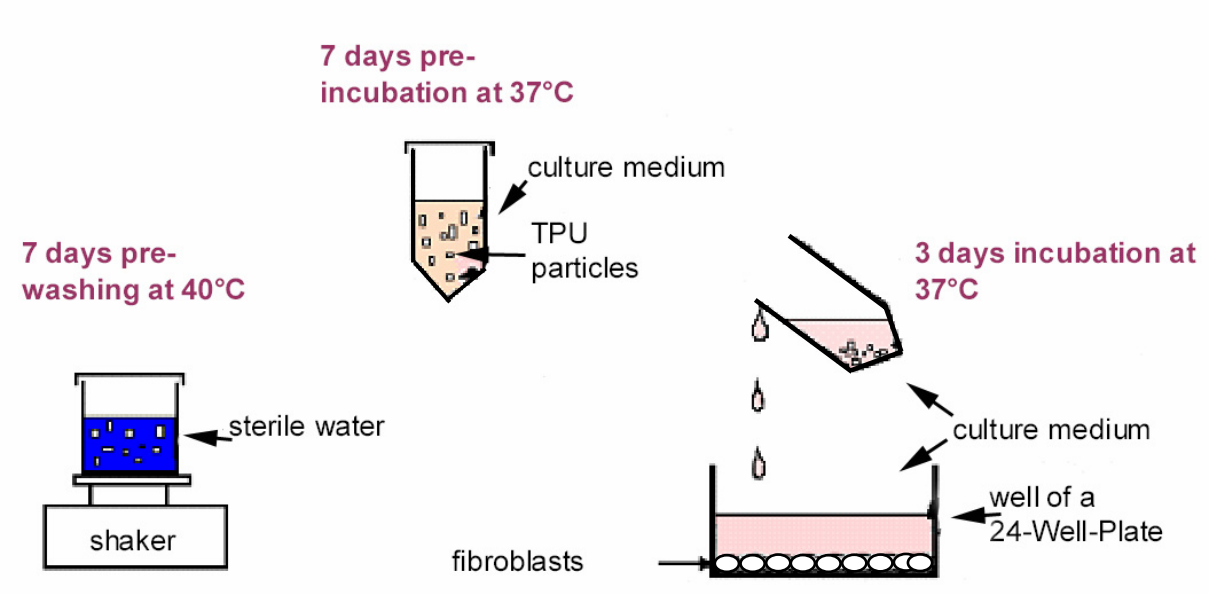

Fig. 25 *Schematic presentation of the eludate test, which was performed to test the cytotoxicity of the implant's material based on ISO 10993-5. Cylindrical samples (radius 9 mm, depth 5 mm) were stamped out of the implant and cut into pieces of 1 mm. These pieces were washed in water and later incubated in culture medium. The culture medium was added to a well plate containing a monolayer of fibroblasts. The behaviour of these monolayers was later analysed.*

Fibroblasts were cultivated for three days at 37°C in a 5% CO_2 atmosphere, as shown in the figure above. 10 %vol. of cell proliferations reagent WST-1 (Roche Diagnostics GmbH, Mannheim, Germany) was added directly into the medium. After 3 hours the behaviour of these monolayers were analysed. Control was the culture medium and 10% WST-1. The photometric measurement of the control took place in a 96-well-Platten with 450 nm (reference wavelength 620 nm) on an ELISA reader (Sunrise, Tecan GmbH, Crailsheim, Germany). The absorption of the control was subtracted from the measured samples. The photometric measurements of the samples were performed three times and with the same parameters as the control. An average optical density (OD) with standard deviation was calculated. The difference in OD percentage from the samples was compared to the control well, which was taken to be 100%.WST-1, is the standard assay used in cytotoxicity test and is recommended by EN ISO 10993-5.

However, this assay did not function well when fibroblasts were seeded directly on the polyether-urethane material, as the photometric signal for WST-1 was similar to the material's colour. The detection of the fibroblasts was, therefore, visually enhanced by applying a second assay, namely the MTT assay. The procedure was performed according to Girotto et al. [173]. The excess culture medium was removed after the desired cultivation period. The samples were washed twice with 300 µl PBS containing MTT (Fluka Chemie GmbH, Buchs, Switzerland). They were then incubated for three hours at 37°C in 5% CO_2-atmosphere. After that, the excess medium was discharged and the sample removed from its paraffin shroud and vortexted in 2 ml Eppendorf beaker with 1 ml 0.01 M HCl in isopropanol for five minutes. The solution was centrifuged (14000 rpm for five minutes), and photometrically measured at a wavelength at 570 nm without reference.

The procedure was performed according to Girotto et al. [173]. The excess culture medium was removed after the desired cultivation period. The samples were washed twice with 300 µl PBS containing MTT (Fluka Chemie GmbH, Buchs, Switzerland). They were then incubated for three hours at 37°C in 5% CO_2-atmosphere. After that, the excess medium was discharged and the sample removed from its paraffin shroud and vortexted in 2 ml Eppendorf beaker with 1 ml 0.01 M HCl in isopropanol for five minutes. The solution was centrifuged (14000 rpm for five minutes), and photometrically measured at a wavelength at 570 nm without reference.

8.4 Histological methods

Scanning electron microscopy SEM

For optical fixation of cell growth on the polyether-urethane material, the following procedure was performed. The samples were washed twice with culture medium and fixed for two days at 4°C with 3% glutaraldhyde (VWR, Darmstadt, Germany). The samples were dehydrated using a graded ethanol (VWR, Darmstadt, Germany) series from 10% to 100%, with three times ten-minute incubation periods for each step. Dehydration was then completed by critical point drying using CO_2 (CPD-030, Bal-Tec AG, Balzers, Liechtenstein).The samples were sputtered and examined in a scanning electron microscope, utilizing the procedure previously described (Section 4.1).

Vitality experiments of the cultivated fibroblasts

A LIVE/DEAD® Viability/Cytotoxicity Assay Kit (L-3224, Molecular Probes, MoBiTec GmbH, Göttingen, Germany) with the reagents Calcein AM (4 mM in DMSO) and Ethidiumhomodimer-1 (EthD-1) (2 mM in DMSO/H2O 1:4, Molecular Probes, MoBiTec GmbH, Göttingen, Germany) was used to investigate the vitality of the fibroblast in the TPU samples [174]. The vital fibroblasts were distinguishable through an esterase activity in the cytoplasma. The visualisations of the different fluorescent colours were performed using a fluorescent microscope (Axiovert 200, Carl Zeiss, Hallbergmoos, Germany). The images were recorded with an AxioCam digital camera and assessed with the software AxioVision 3.0 (Carl Zeiss, Hallbergmoos, Germany).

The microscopic evaluation used two different filters:

-Fluorescent of calcein in vital fibroblasts (Filter number 09, Carl Zeiss, Hallbergmoos, Germany): Excitation 450–490 nm, Emission 515 nm, beam splitter at 510 nm

-Fluorescent of EthD-1 for non-vital fibroblasts (Filter number 15, Carl Zeiss, Hallbergmoos, Germany): Excitation 534–558 nm, Emission 590 nm, beam splitter 580 nm

The TPU samples with the fibroblasts were, after incubation of the desired cell numbers and cultivation time, removed from the 24-well-plate, washed with PBS and cut vertically to thin slices. Half of the samples were further cultivated for fifteen minutes in an incubator at 37°C with 5% CO_2-atmosphere, in a solution of 2 µM EthD-1 and 0.5 µM calcein AM in 1.5 ml Eppendorf beakers. Afterwards thin incisions were made with a scalpel, and stored in PBS to prevent drying. The samples were wetted with PBS during microscopy.

Image-overlaying and cell counting made it possible to quantify the vital/non-vital fibroblasts ratio per area.

9 Effects of sterilisation

Prior to sterilisation, round specimens (n=50) of the implants were punched out from an injection moulded implant with a diameter of 9 mm and a height of 3 mm. Subsequently γ-

sterilisation (Isotron, Allershausen, Germany) was carried out with low, middle and high radiation dosages (10, 25 and 60 kGy) (Table 8). Samples (n=10) were also steam sterilised in a chamber autoclave (Type 23, Melag Apparate GmbH&CoKG, Berlin, Germany) at 121°C, 2 bars for 20 min.

Polymer processing method	**Sterilisation method**	**Dose**	**Sample name**
Injection moulding	none	-	non-sterile (control)
Injection moulding	steam	121°C, 2 bar, 20 min	steam steril.
Injection moulding	γ	10 [kGy]	10 kGy
Injection moulding	γ	25 [kGy]	25 kGy
Injection moulding	γ	60 [kGy]	60 kGy

Table 8 *Test samples for sterilisation experiment (n=10).*

The samples were then analysed to obtain molecular weight (GPC), chemical composition (FT-IR), crosslinkage (DSC) and cell cytotoxicity with WST-1 assay.

10 Degradation behaviour

10.1 Test specimens

During the developmental phase precursor implants were processed either by hot pressing or injection moulding. The release of the toxic breakdown product methylene dianiline (MDA) from the material was considered to be possible. Special attention was given this compound due to its toxic character. Both processing methods were analysed in terms of potential breakdown products after cholesterol esterase incubation. In addition to the physiologically defined enzyme activity (see section 3.10.3), a tenfold increase of cholesterol esterase was used to simulate a very strong chronic inflammation and an abnormally strong enzymatic attack. A total of four different samples were incubated with cholesterol esterase. Likewise, a positive control (embedding medium with CE solution) and a negative control measurement (embedding medium only with buffer) were conducted to investigate the influence of specimen containers. Precursors of the implant, which were 10 wt.% of the entire implant size, were used as test samples (n=1). Four different samples were tested on MDA released due to enzymatic degradation. One was produced by hot pressing and subsequently γ-sterilised at 25 kGy. The three other samples were injection moulded. Two of them were γ-sterilised at 60 kGy and the last was γ-sterilised at 25 kGy. One of the injection moulded samples was sterilised at 60 kGy and was exposed to a ten times greater enzyme concentration than the one described in section 10.3

below. This was to simulate an extremely strong chronic inflammation. The testing chamber had to be tested for inertness. Thus, two controls, one positive and one negative, were monitored along with the implant samples. The positive control contained embedding media (tube, wax etc) and CE solution. The negative control had embedding mediums but no CE enzyme added. The difference in chromatographs from the controls would reveal possible influences of specimen holders. An overview of all tested polymer samples and test parameters is given below (Table 9). Sample preparation for the experiment was carried out at 37°C.

Polymer processing method	**Processing temperature [°C]**	**Sterilisation γ-dose [kGy]**	**Incubation enzyme activity**
Hot pressing	220	25	physiological
Injection moulding	220	25	physiological
Injection moulding	220	60	physiological
Injection moulding	220	60	10-fold increased
No sample, positive control	-	-	physiological
No sample, negative control	-	-	buffer only

Table 9 *Test samples for biodegradation experiment.*

Prior to enzyme incubation, round specimens (n=10), either processed by hot pressing or injection moulding, were punched out from implant rings with a diameter of 9 mm and a height of 3 mm. Subsequently γ-sterilisation (Isotron, Allershausen, Germany) was carried out with radiation doses of 25 kGy and 60 kGy. The samples (n=1) were placed in sterilised silicone tubes to achieve a uniform working surface for cholesterol esterase. Steam sterilisation took place in a chamber autoclave (Type 23, Melag Apparate GmbH, Berlin, Germany) at 121°C, 2 bars for 20 min. Afterwards, the tubes containing the specimens were inserted into 15 ml centrifuge tubes, which were half-filled with a paraffin embedding medium. The specimens were attached with silicone grease (Wacker-Chemie, Munich, Germany) to the paraffin layer before subsequent the enzyme solutions were added. The assembly of the sample in the tube is illustrated below (Fig. 26).

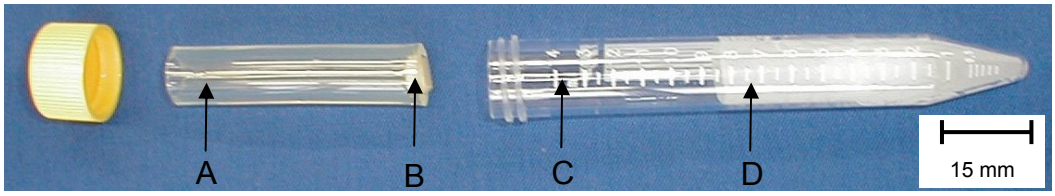

Fig. 26 *Sample preparation for biodegradation experiments (A) Silicone tube, (B) Polymer sample, (C) Centrifuge tube, (D) Paraffin layer.*

MDI is utilised as an aromatic monomer during polymer synthesis and connects the polyether with the urethane linkage (Fig. 27).

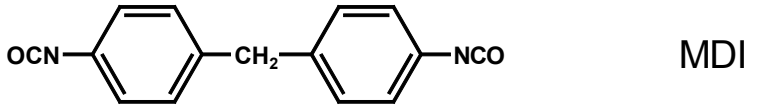

MDI

Methylene bis(p-phenyl isocyanate)

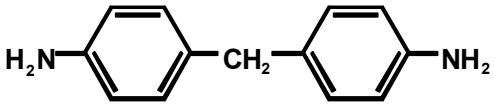

MDA

Methylene dianiline

Fig. 27 *Chemical structure of MDI and MDA. MDI is one of the monomers in the polyether-urethane used in the study. This monomer may break out of the polymer hydrolytically through enzymatic attack with cholesterol esterase or thermal oxidation at elevated temperatures*[143]. *MDI react immediately in aqueous solution to MDA. MDA is regarded as the most toxic degradation product from polyether-urethane* [175].

This linkage can, however, be cracked hydrolytically through an enzymatic attack with cholesterol esterase as well as through thermal oxidation at elevated temperatures at approximately 150°C [143]. This leads to release of MDI, which immediately reacts in an aqueous environment to MDA. The chemical structures of MDI and MDA are shown below (Fig. 27). Other degradation products may be produced [176]. As MDA is the most toxic of the degradation products from polyether-urethane [175], the analysis was only concerned with monitoring the release of this compound.

10.2 Incubation procedure

The incubation procedure was closely adapted to biodegradation experiments conducted by Tang [159]. A physiological relevant enzyme activity was obtained based on data from

Labow [160]. Labow has simulated the amount of CE that can be released through a chronic inflammation (Fig. 28). The duration of the degradation study was 28 days.

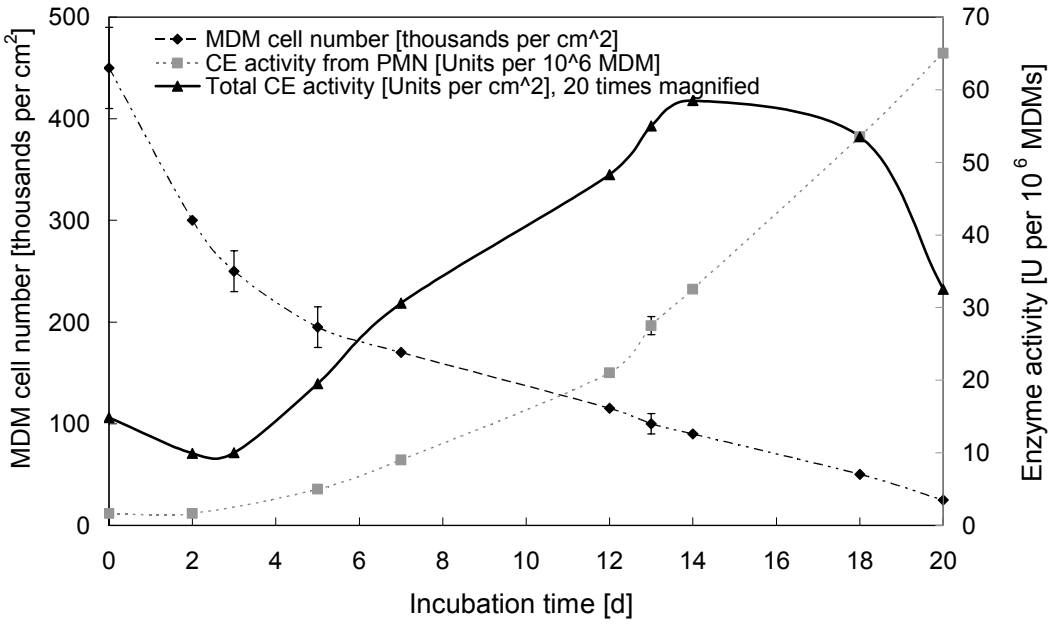

Fig. 28 *To obtain a physiological concentration of CE, a theoretical PMN concentration profile according to Labow* [160] *was plotted (grey). MDM do also release CE. Its concentration is highest just after implantation and decreases with time (black, dotted line). The sum of these two curves gives the total CE released by the chronic and acute inflammation on an implant (black, solid line). This black lined concentration profile of CE was used during the experiments for 16 days. For rest of the incubation time this maximum was kept constant.*

The physiological enzyme activity was obtained from the release of cholesterol esterase, CE, due to a chronic inflammation on a polyether according to Labow [160]. The human body reacts with an inflammatory defence mechanism to biomaterials. This foreign body reaction is principally described through the two phases of acute and chronic inflammation. Polymorphonuclear leukocytes (PMNs) are activated during the acute phase. Here, foreign bodies are normally encapsulated, digested and withdrawn by oxidative compounds and enzymes of giant cells, such as serine proteases like cathepsin G and elastase [177]. In contrast, the leukocytes' response to adhesion and spreading on a biomaterial is termed "frustrated phagocytosis" due to lack of enclosed phagosome [178]. When the inflammation response becomes chronic, monocyte-derived macrophages (MDMs) are the predominant adherent cells in the implant sites. These cells exhibit a considerably greater degradative potential than PMNs

[160]. MDMs synthesise the hydrolytic enzyme cholesterol esterase [179]. Labow [160] has measured the CE concentration released from these mechanisms based on a given implant surface area. This value, only adjusted to the surface area of the GORD implant, was also taken to be "physiologically normal."

Cholesterol esterase incubation and replenishing solutions were prepared by dissolving enzyme powder in a sodium phosphate buffer (50 mM, pH 7.0). The surface area of the GORD implant was measured at 1.27 cm^2 according to section 3.4.2. The polyether urethane samples were then incubated with 2-3 ml of enzyme solution (EC 3.1.1.13, Sigma Aldrich Chemie GmbH, Munich, Germany). The polymer specimens were placed on a tumbling table (Polymax 1040, Heidolph Instruments, Schwabach, Germany) and incubated at 37°C (Binder FD, Binder GmbH; Tüttlingen, Germany). In order to prevent the microbial contamination, 0.1% w/w sodium azide (Sigma Aldrich Chemie GmbH, Munich, Germany) was added to the solutions once a week. As enzyme concentration decreased over time, a fresh quantity of CE was added to the test tubes every second day. The CE amount was monitored every second day. During the incubation period, 1 ml aliquots were removed from the polymer incubation solutions every second day for analysis. The extracts were stored at 4°C prior to preparation for LC-MS analysis.

10.3 Isolation of degradation products

Prior to MDA detection by LC-MS analysis, the extracted polymer solutions from the degradation experiment had to be cleaned. The solution contained enzymes and enzyme breakdown products in addition to polymer-derived and TPU-derived products, which made the MDA detection difficult [159]. A flowchart for the isolation procedure is illustrated below (Fig. 29)

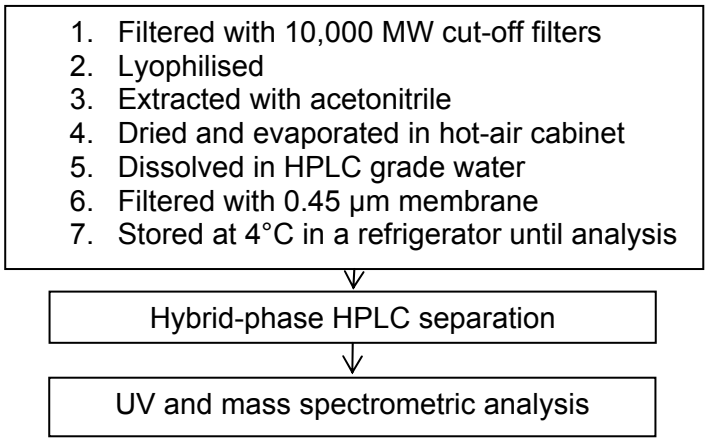

Fig. 29 *Flowchart for the isolation procedure in biodegradation tests.*

Firstly, the extracts (1 ml) were centrifuged about 50 minutes at 4300 rpm to remove high molecular weight protein using centrifugal filter devices (Centricon® YM-10, 10,000 MW cut-off, Millipore, Ma. USA). The filtrate was then freeze-dried overnight in a lyophilsator using a double vacuum chamber with dry flask and ice condenser (Alpha 1-2, Christ, Munich, Germany). The solid residue remaining after this process was extracted with 2 ml acetonitrile and shaken for 90 minutes in an electronic shaking/vibrating unit (Sieve shaker AS 2000 basic, Retsch GmbH & Co. KG, Haan, Germany). Accordingly, the organic polymer degradation products were separated from the salt and residual enzyme protein. Subsequent evaporation of the acetonitrile solution was carried out at 50°C in a drying cabinet overnight. The solid residue after this process was dissolved by using 2 ml of HPLC grade water(VWR, Darmstadt, Germany) and was filtered through a 0.45 µm hydrophilic polypropylene membrane filter (Acrodisc 13 GHP, Waters, Eschboorn). The resulting solutions were stored at 4°C in a refrigerator until LC-MS analysis was carried out. The products from positive and negative control samples were processed identically. The extracts were subsequently analysed in HPLC, where the MDA amount was recorded. An accumulated value was obtained by summing up the single MDA values of respective extraction points over the entire incubation period. The samples were 10 wt.% of the entire implant, and the incubation volume was about 2 ml. Based on these values a total accumulated MDA release could be estimated.

CHAPTER V
Results and discussion
Polymer processing

1 The new processing method

The problem of streaking and the formation of air bubbles when working with moist polymer granules is known. Therefore, polymer granules are generally dried prior to manufacturing. Moisture absorption was here used to create a target porous structure within the polymer. The goal of this study was to inject mould a GORD implant after a specific amount of moisture had been absorbed by the granules. The question arose: would it possible to produce a defined pore structure by means of moisture in the implant? Secondly, would it be feasible to adjust this macro structure by altering the processing parameters?

Several techniques have already been used to fabricate polymers into a porous polymers [96, 98, 180]. Most of these approaches require the use of organic solvents. Residues of organic solvents, which remain in these polymers after processing, may damage cells and also nearby tissue [158]. Therefore, no ideal processing method for a biocompatible porous polymer structure or industrially applicable processing method for medical purposes exists.

2 Water-uptake rate

The rate and amount of water absorbed was dependent on time, humidity in the storage chamber and the amount of NaCl in the polymer. Its relationship is displayed in Fig. 30. The polymer without NaCl particles stagnated its water content by 1.5 wt.% after four days. The granules with NaCl reached a higher concentration and had a faster uptake rate. The same observations were made for granules with 40 vol.% NaCl. Surprisingly, as the graph shows, the water-uptake rate of polyether-urethane with 40 vol.% NaCl was higher than with 52 vol.% NaCl. A plausible reason for this occurrence was the

granule's size. Granules with 40 vol.% NaCl were smaller and, therefore had a greater surface area, which led to a faster water absorption rate.

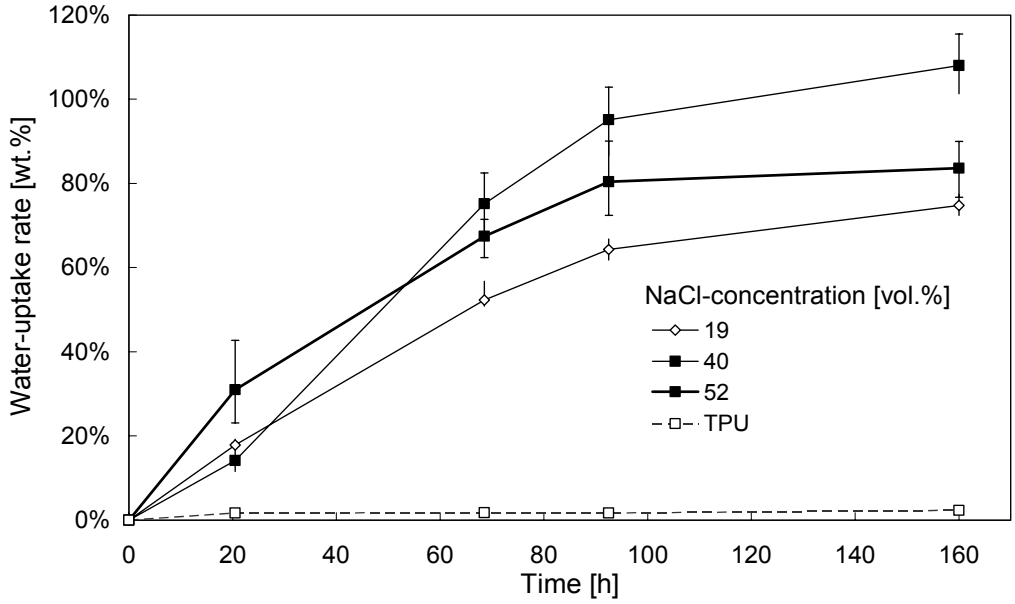

Fig. 30 *Water-uptake rate depended on varying NaCl-concentrations compared to pure polyether-urethane (n=10).*

3 Processing by hot pressing

3.1 Preliminary parameter study

Preliminary experiments were performed in order to verify that water was the main cause of the pore development. Polyether-urethane granules with different moisture uptake (no NaCl) were hot pressed, and showed, indeed, that the initiated porous structure arose from the moisture uptake (Fig. 31). Additionally, pore size diameter was dependent on moisture content and increased with rising water content.

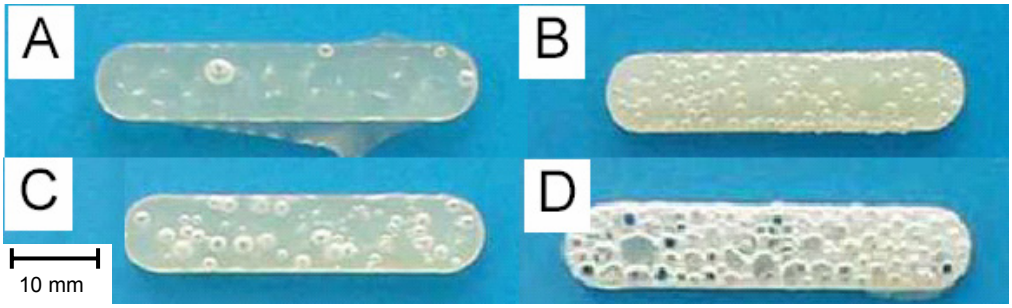

Fig. 31 *Pore growth in pure polyether-urethane with different water content in the granules prior to hot pressing. Sample (A) was hot pressed with 0.2 wt.% H_2O. Samples B, C and D were produced at 0.4, 0.8 and 1.5 wt.% H_2O, respectively.*

An optical analysis was performed to quantify the pore size diameter and the number of pores generated (Fig. 32). Diagram in Fig. 32 shows that both the porosity and pore size increased with elevated water content in the granules prior to processing.

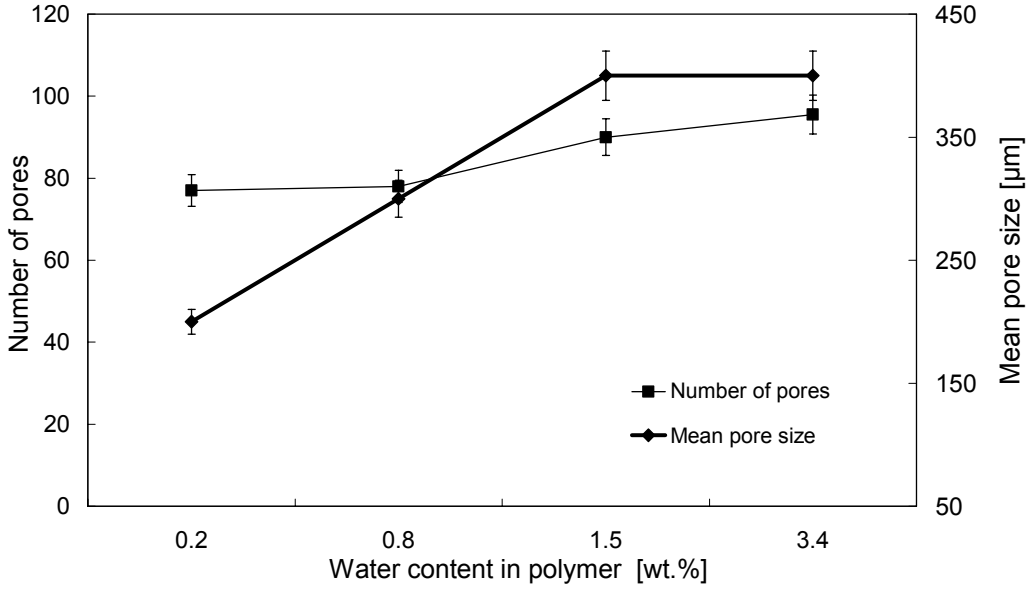

Fig. 32 *Pore distribution depended on the water-uptake rate in the granules prior to hot pressing (n=3).*

Two other parameters, heating- and cooling rates, were examined in the preliminary experiments. Different heating (Fig. 33) and cooling rates (not shown) did not have a significant influence on the pore building effect. Since they had no impact on pore growth in this experiment, their effects were not studied further.

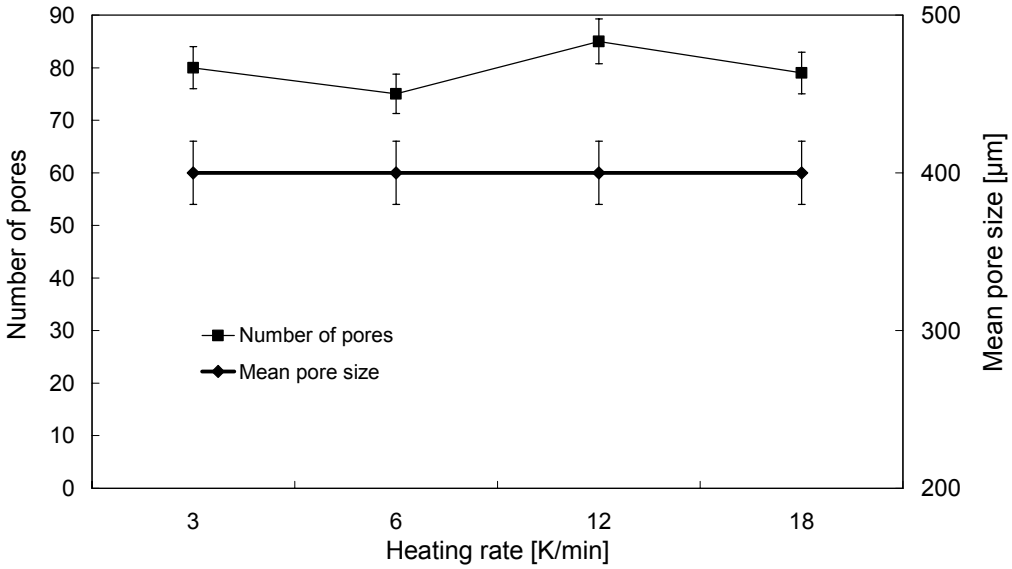

Fig. 33 *Pore distribution depended on the heating rate (left (n=3)).*

3.2 Leaching process

The pores produced in the preliminary tests were primarily closed (Fig. 31). The objective of the study was to obtain an open porous structure however, which could be achieved by adding NaCl particle to the granules prior to manufacturing. NaCl particles have a higher melting temperature (790°C) than polyether-urethane (180°C) and their size was not altered by the processing heat.

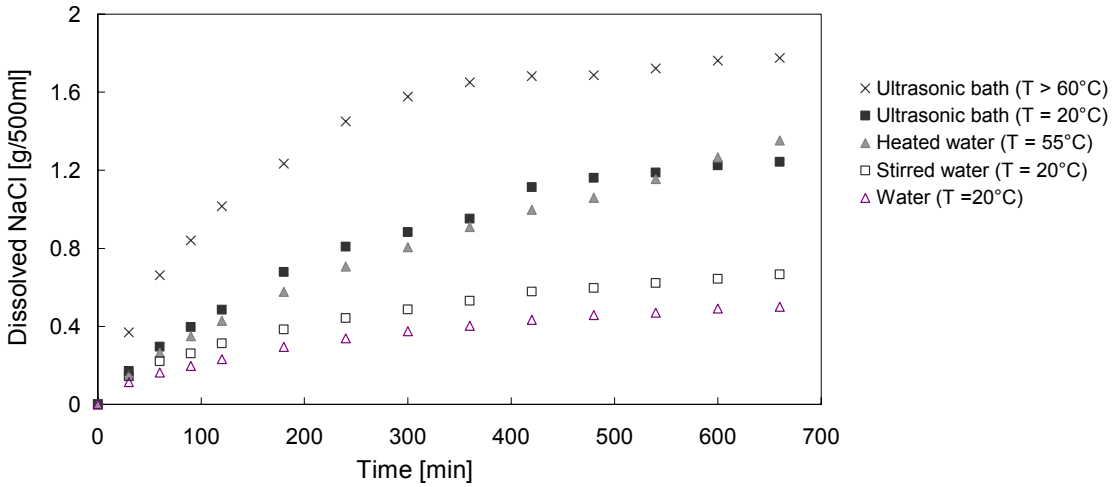

Fig. 34 *Comparison of different leaching method (n=3).*

After processing, these particles were leached out and left behind imprints in the polymer. A comparison of different leaching methods was made. The results are displayed above.

The graph above (Fig. 34) illustrates that some methods accelerate the leaching process effectively. The samples, which were leached in distilled water and at room temperature, displayed the lowest amount leached. Only small improvements could be achieved by stirring the water, whereas heated distilled water showed an improvement in the leaching result. This method was, however, temperature limited. The polymer samples changed colour over a prolonged period of time at elevated temperature. The best leaching results were achieved by the use of an ultrasonic bath. Since the temperature of the solution of the ultrasonic bath went up to 60°C and changed to the colour as well. Therefore, cooling was applied to the ultrasonic bath to maintain a constant temperature.

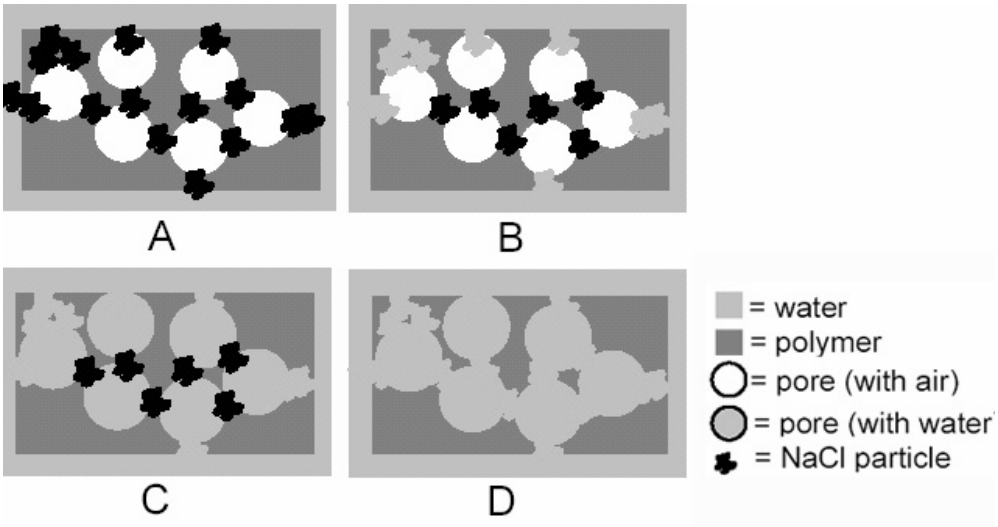

Fig. 35 *Schematic drawing of the air bubbles present in the porous structure, which prevents water from leaching the salt particles out. The polymer sample is placed in water (blue) to leach salt particles out (black) (A). The first NaCl particles are dissolved. Pores with air prevent the water to excess the next salts particle further inside porous structure (B). When the entrapped air was forced out, water came in contact again with the salt particles and could leach them out. This generates a fully open pores structure (C and D).*

The leaching process was decelerated by air bubbles. Bubbles appeared because air was present in the sample itself and prevented the water from coming into contact with the salt particles (Fig.

35). Similar to the ultrasonic bath, stirring the water led to the detachment of the bubbles. The leaching process could also be improved by heating the water since the gas solubility in water decreases with increasing temperature, according to Henry's law.
Therefore, the leaching process was chosen to take place at the highest temperature, 40°C, where the polymer could not be affected.

STA analysis monitored the NaCl content. The remains from the burn-out of pure TPU were carbon ashes. This ash content was found to be 1.2 wt.%. Porous samples that have not been fully leached show a significant drop in the mass percentage in the region from 800-1200°C as is seen in (Fig. 36). NaCl has a melting peak at 790°C, and hence the salt evaporated in this region. By subtracting the ash content of carbonated TPU, the exact amount of NaCl remaining in the samples was obtained.

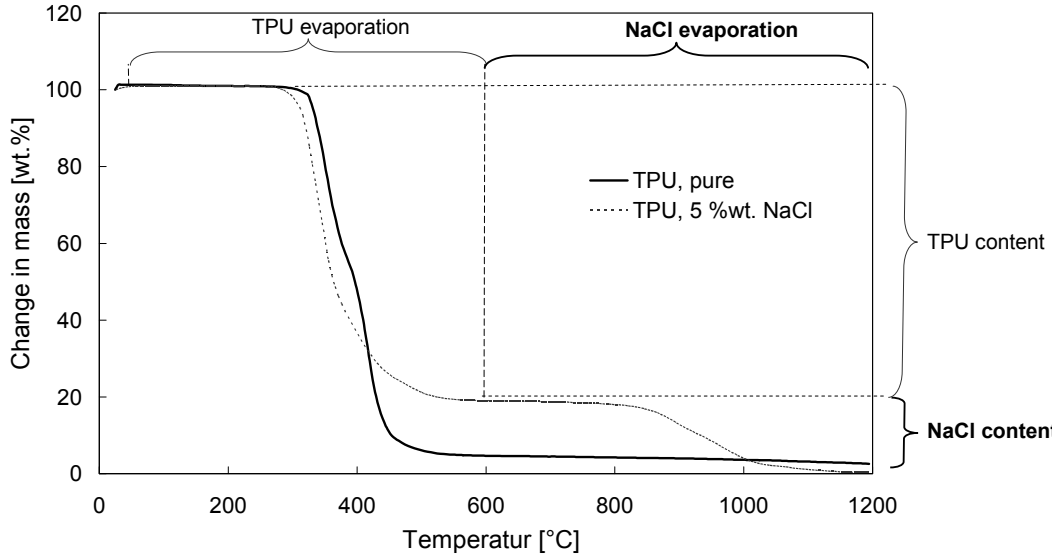

Fig. 36 *STA measurements to obtain the remaining NaCl content after leaching. The mass difference between 800 and 1200°C, the region where NaCl evaporates, was the remaining NaCl mass.*

The following method proved to be an accurate tool for measuring NaCl remaining in the polymer after leaching, and to ensure that the implants contained less than 1 wt.% NaCl.

3.3 Main parameter study

3.3.1 Pore size and mould filling volume

Fig. 37 shows a summary of mercury intrusion porosimetry measurements. The porosity was calculated from the total intruded Hg volume, and the mean pore diameter was taken at the peak intrusion. Samples filled with 100 wt.% of the volume had hardly any porosity. When the water molecules have no space to expand, a foaming process cannot take place. The 10 % porosity was the volume of the imbedded salt particles. Fig. 37 demonstrates that the porosity increased excursively with decreased filling volume. Additionally, the median pore diameter displayed that the pore size also decreases when the mould was more filled. Samples with a filling volume of less than 70 wt.% could not been produced since the amount of granules was not enough to plasticize the polyether-urethane.

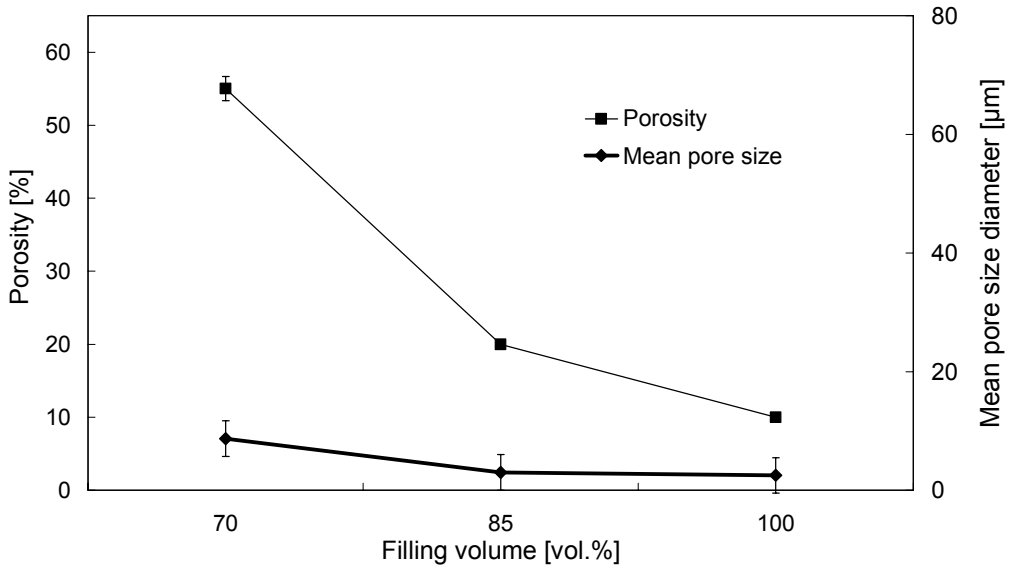

Fig. 37 *Pore distribution depended on the filling volume (n=3).*

3.3.2 Pore size and NaCl-concentrations

Fig. 38 illustrates that with increasing NaCl-concentration the pore size was practically unchanged since the median pore diameter only increased from 7.5 to 21.9 µm, which was one and a half the magnitude below the required mean pore sizes (200-400 µm). The porosity, however, increased from about 20% to 60%. It was not likely that the increased salt volume itself was the sole reason for the tripled porosity. Hg intrusion porosimetry can only measure open pores. The elevated NaCl amount

present in the samples led to better connections between the pores formed from the evaporated water, which increased the excess to the round vapour formed pores.

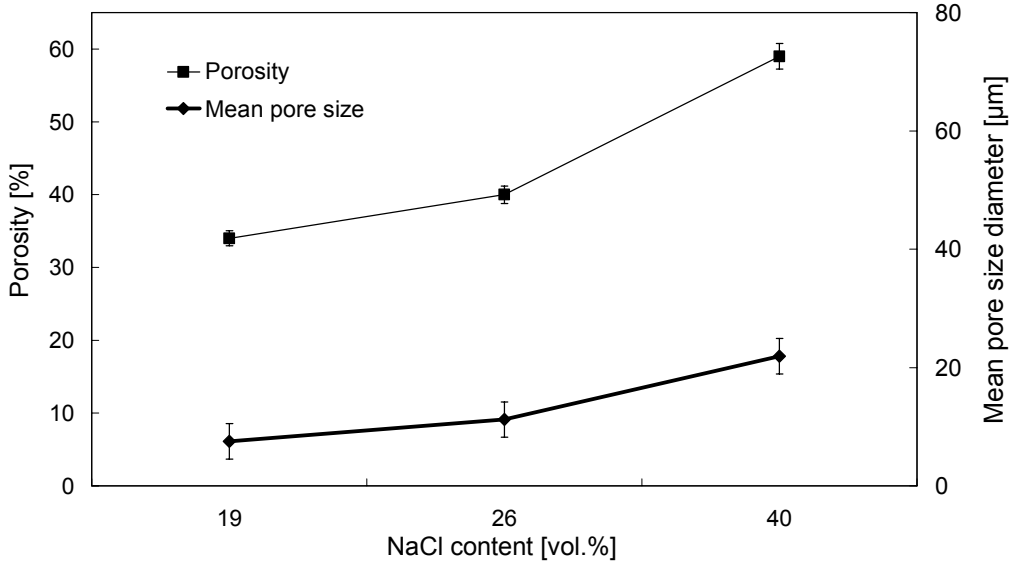

Fig. 38 *Pore size depended on NaCl concentration.*

The assumption that interconnection increased in numbers was verified by SEM pictures (Fig. 39 and 40). The images show circular pores, which are the ones generated as the water evaporates. The same water content was used in both experiments. The amount and dimension of spherical pores were, accordingly, similar for both images.

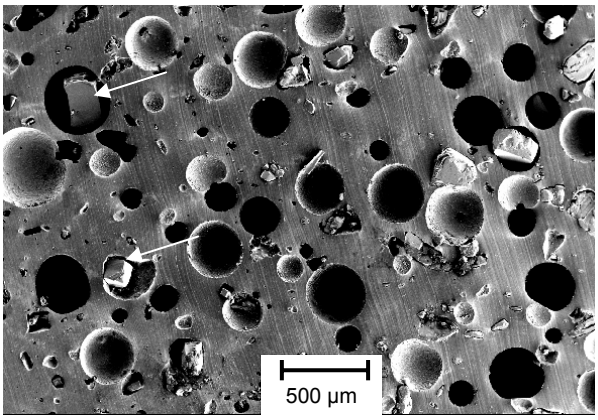

Fig. 39 *Cross section of a sample produced with 19 vol.% NaCl shows cubic and rigid-shaped NaCl-residuals entrapped in the middle of vapour pores.*

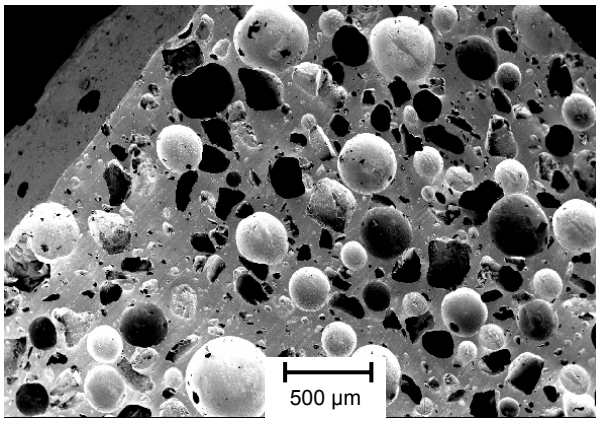

Fig. 40 *Cross section of a sample produced with 40 vol.% NaCl with imprints of NaCl-particles and no NaCl residuals.*

The sharp edged pores are imprints from NaCl particles. It can be seen from image Fig. 39 that NaCl particles were not completely leached out. Additionally, some cube-shaped objects can be seen (white arrows). They are NaCl particles, which were dissolved but not transported out of the porous structure due to lacking diffusion properties between the vapour pores. Prior to SEM preparation the samples were dried and a recrystallisation of the dissolved NaCl took place. Hence, the cubic shaped objects were present. However, the image in Fig. 40 displays another situation. Here, no NaCl can be observed, and far more entrances to the round vapour pores can be found. These observations confirmed that the salt particles played an important role in the formation of interconnections. Samples, which contained more than 46 vol.% NaCl, did not plasticize in the heated press.

3.3.3 Pore size and processing temperature

Porosity grew from 25 to 58% with a process temperature rise from 190°C to 220°C (Fig. *41*), while heat seemed to have marginal impact on pore size diameter. Fig. 42 and 43 illustrate the correlating SEM pictures of the samples.

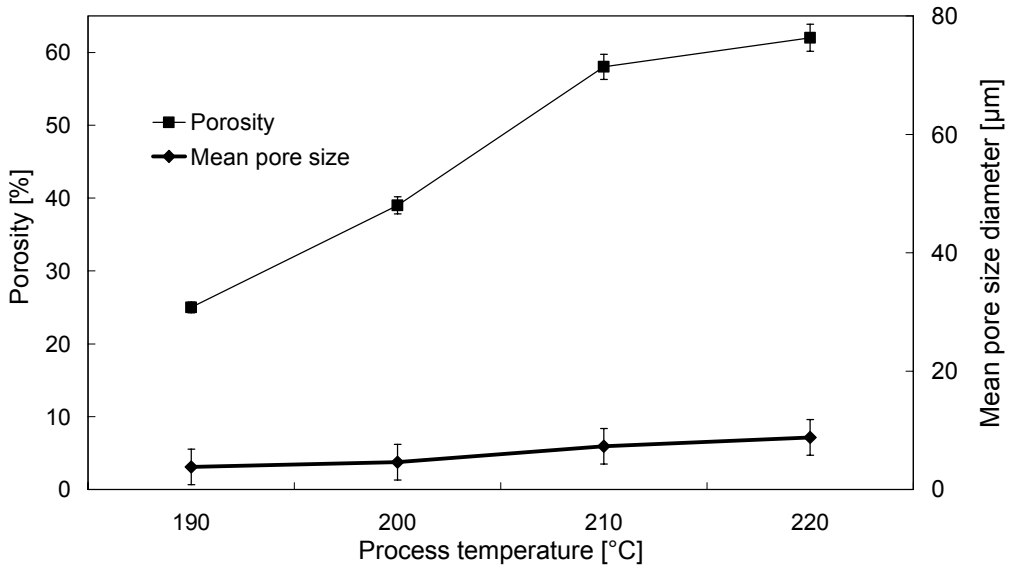

Fig. 41 *Pore distribution depended on processing temperature (n=3).*

The sample, which was produced at 190°C, shows only small vapour pores with a deformed shape instead of the large spherical shaped vapour pores. These round pores were present at a production temperature of 220°C. Hence, the viscosity played a major role in the pore growth. The viscosity dropped as the polymer was further heated and the vapour pores could be fully develop. Therefore, porosity could also be influenced by varying the processing temperature.

The best results were obtained with temperatures of 220°C. Higher temperatures led to a degradation of the polyether-urethane with low mechanical stability. Samples that were produced at temperatures higher than 230°C disintegrated.

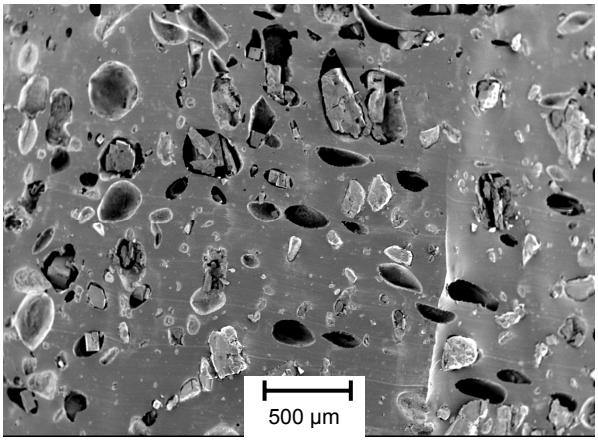

Fig. 42 *Cross section of a sample produced with a temperature of 190°C shows small, not fully-developed vapour pores and entrapped NaCl particles.*

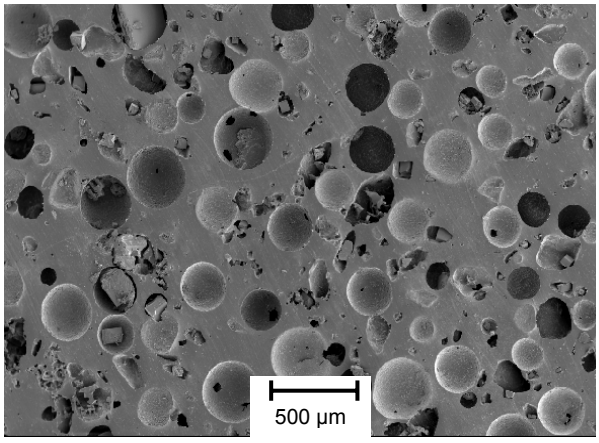

Fig. 43 *The cross section of a sample produced with a temperature of 220°C shows large vapour pores with a spherical shape.*

3.3.4 Pore size, porosity and processing time

The pore growth was dependent not only on the viscosity, but also on the diffusion. Diffusion was again dependent on temperature and time.

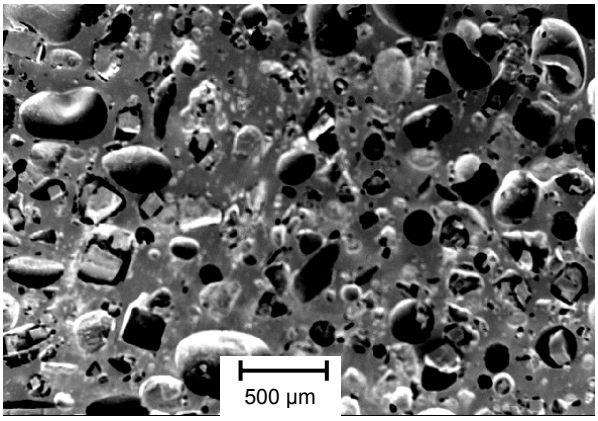

Fig. 44 *Cross section of a sample processed for 180 seconds with small, deformed vapour pores.*

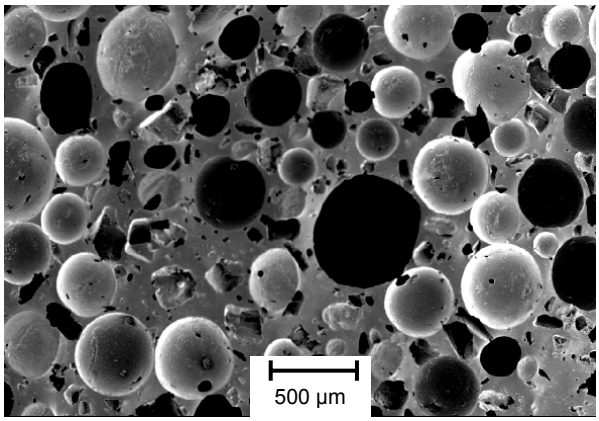

Fig. 45 *Cross section of a sample processed for 540 seconds with large, spherical vapour pores.*

Fig. 44 shows that pores are underdeveloped after a short processing time. Similar shaped pores are seen in Fig. 42. At longer processing times (>360 sec), fully circular pores appeared (Fig. 45). The pores need to have time and the right viscosity to develop fully; if not, the pore growth becomes suppressed. Analogous to the process temperature results, the porosity was greatly increased (35%-55%) and the median pore sizes remained almost constant (Fig. 46). The four SEM images above show an increase in pore size diameter at elevated processing time and temperature. The porosimetry results did not show any major changes pore sizes. The cause was the measuring technique of the mercury intrusion porosimetry.

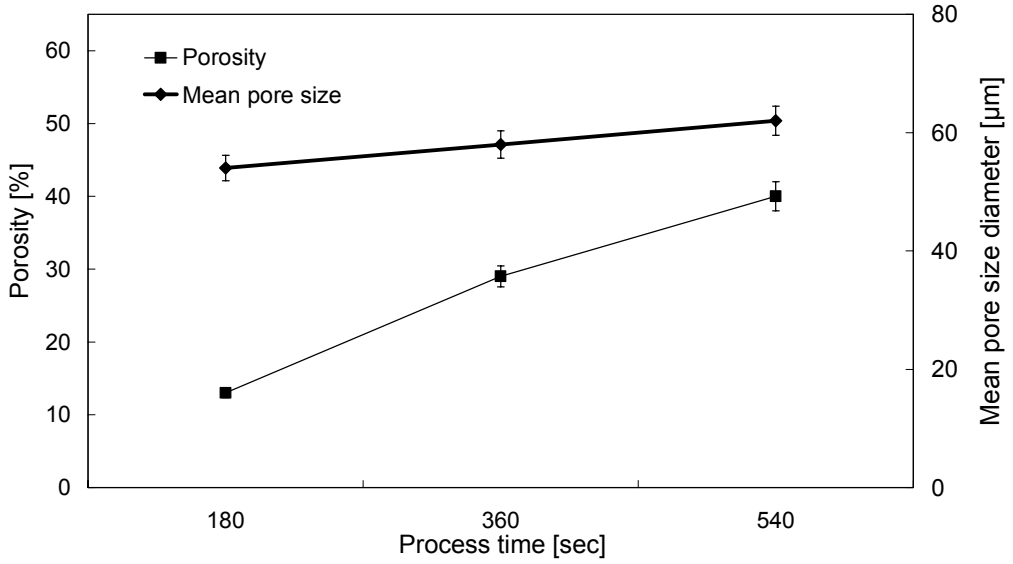

Fig. 46 *Pore distribution depended on processing time (n=3).*

Fig. 47 shows that with increasing water-uptake the mean pore size diameter increased as well. The graph shows a lift in the mean pore size for higher water content. Unexpectedly, the porosity of all samples did not differ and stayed between 60% and 64%. This means that the numbers of pores were almost constant, and the water content in the polyether-urethane changed only the pore size diameter.

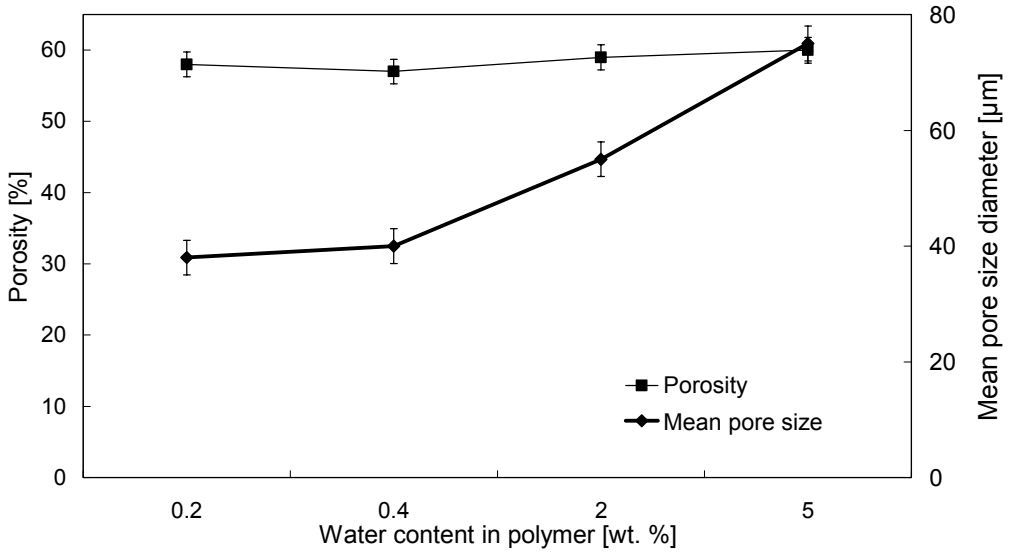

Fig. 47 *Pore distribution depended on the water-uptake rate (n=3).*

3.3.5 Summary of the hot pressing results

It has been proven that a controlled moisture uptake in granules prior to injection moulding can be used to generate porous polymers. Secondly, it has also been shown that this pore structure can be adjusted through processing parameters. The porosity can be increased by altering the filling volume, processing time and temperature. The diffusion of water molecules were enhanced by amplified processing temperature. Diffusion is constrained by time. Thus, higher processing temperatures and prolonged processing time led more water molecule into the nucleation sites and induced more pores. The interconnections were multiplied by additional NaCl mixed with the polymer. The pore size was adjustable with changing the water uptake level prior to processing. Using the optimal parameters, a GORD implant with $64 \pm 3\%$ porosity, mean pore size of 80 ± 10 µm and pores within the range of 50-500 µm was produced. A second undertaking was to use the same knowledge from the water foaming process on an injection moulding machine. The next section will, therefore, answer the question if it is possible to use the same method on an injection moulding machine and also meet the requirements for the porous structure in the GORD implant.

4 Processing on an injection moulding machine

4.1 Processing parameters study on pore size and porosity

The mould described in chapter III was used to produce the GORD implant ring on the injection moulding machine. Parameters gathered from the hot pressing experiments were used as a starting point, and the additional six processing parameters were adjusted to generate the desired porous structure. This section presents the effect of the processing parameters on this porous structure. Again, the samples were produced by varying one parameter while the others were held at a constant.

4.1.1 Pore size distribution, porosity and plasticizing speed

Fig. 48 shows the pore size distribution, measured with a mercury intrusion porosimetry. The peak of the curve is the mean pore size diameter and the integrated area below is the porosity. The speed varied between 3 and 5 mm/s. The mean pore diameter at a speed of 3 mm/s was 270 µm, and at 5 mm/s 10µm only.

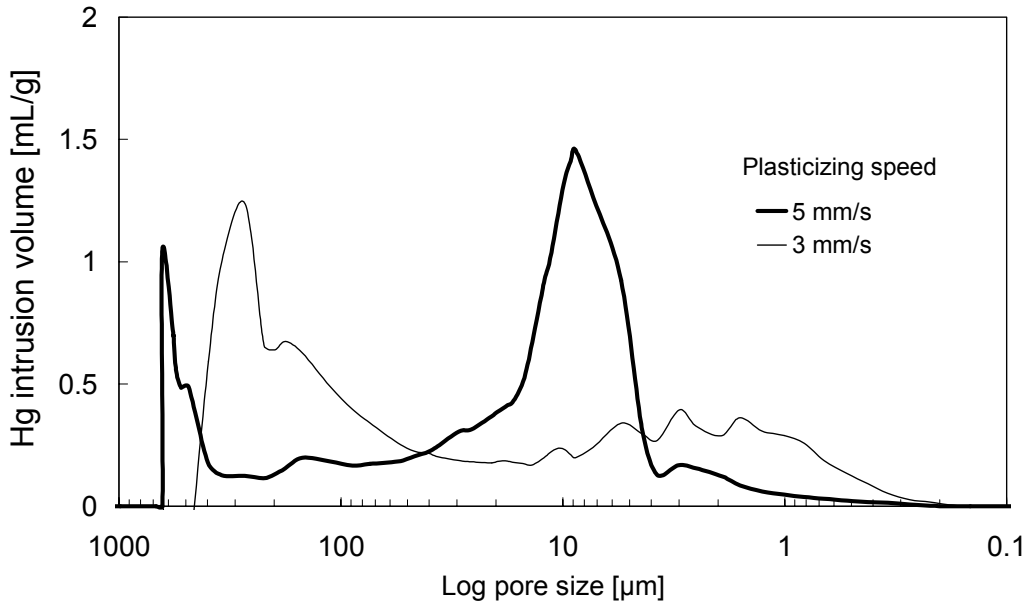

Fig. 48 *Pore size distribution depended on the plasticizing speed (n=1).*

Hence, a lower plasticizing speed increased the pore sizes. At lower speed granules had more time to homogenise. The water molecules were better distributed across the polymer, and fully developed pores could grow. The porosity was unaffected by the plastification speed.

4.1.2 Pore size distribution, porosity and plasticizing rotation

The intrusion porosimetry data showed that the rotation per minute did not have a significant influence on the pore size distribution (Fig. 49). The mean pore diameter was with a rotation speed at 20 rpm about 400 µm, which was in the range of the desired pore size.

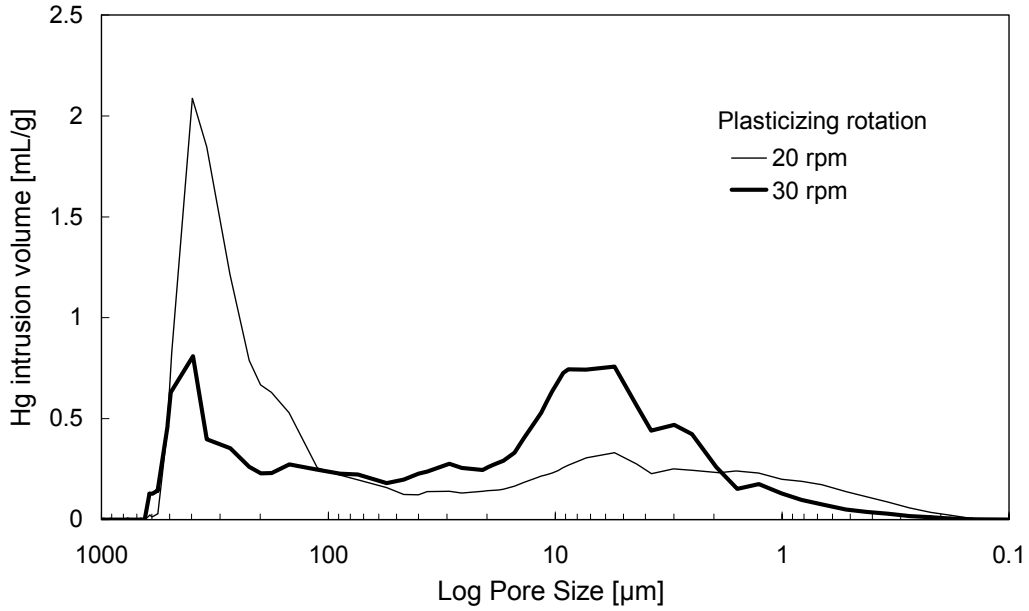

Fig. 49 *Pore size distribution depended on plasticizing rotation (n=1).*

4.1.3 Pore size distribution, porosity and processing pressure

Unsurprisingly, pressure had a major effect on pore growth. The nucleation theory also supports this fact. Pressure can be generated in the injection moulding machine through several parameters, plasticizing pressure, injection speed and pressure. Plasticizing pressure of 5 bars produced porous implant with a mean pore diameter of 25 µm (Fig. 50).

By doubling the plasticizing pressure the pore grew to more then ten times the diameter (340 µm). The pore size distribution was narrower at this pressure compared to 10 bars. The second porous region, with a peak at 5 µm, was also measured (Fig. 50). This region, which ranged was from 0.5-50 µm, must be developed from the NaCl particles. Interestingly, the size of these pores was from ten to one hundred times smaller than when the NaCl particles were mixed with the polyether-urethane. The particles have, most likely, been minced by the shear of the

screw in the injection moulding machine. Porosity was practically unchanged by the plasticizing pressure.

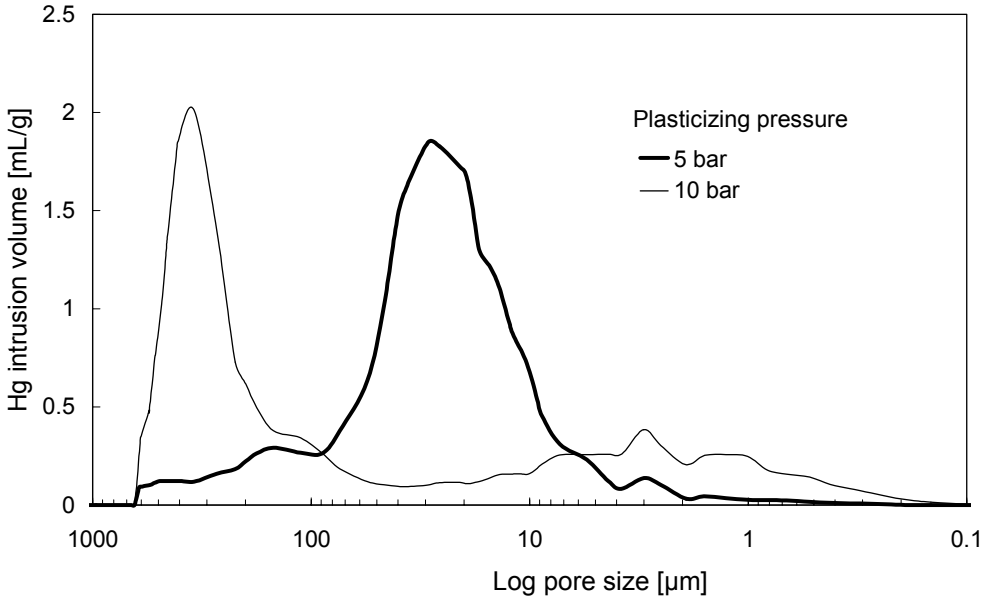

Fig. 50 *Pore size distribution depended on plasticizing pressure (n=1).*

Injection pressure and speed also had a major influence on pore size distributions. The result was similar to Fig. 50. Again, an increase in pore diameter with a more confined pore size distribution was observed (Fig. 51). The mean pore diameter was increased from 10 to 340 µm by raising the injection pressure and speed from 1000 bar and 40 mm/s to 1100 bar and 45 mm/s. Pressure drop was the driving force for the pore development. According to the nucleation theory, as the pressure rises, the pore has more momentum to grow larger. The nucleation theory does not, however, explain why the pore distributions were more distinguished for higher pressure. Similarly, the second porous region showed pores in the range from 0.5-10 µm, and was expected to be the interconnections between the pores. The pore diameter and its distribution of the interconnections are discussed separately at the end of this section.

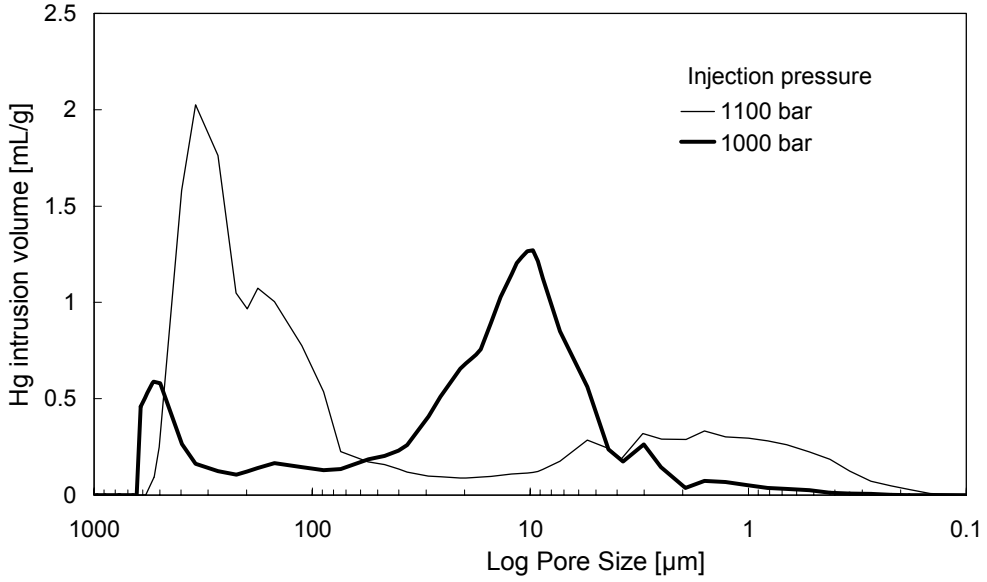

Fig. 51 *Pore size distribution depended on injection pressure (n=1).*

4.1.4 Pore size distribution, porosity and NaCl concentration

Fig. 52 shows that the second region was moved to the left by adding larger NaCl particles. Since the area below the curve is greater, the number of these pores also increased.

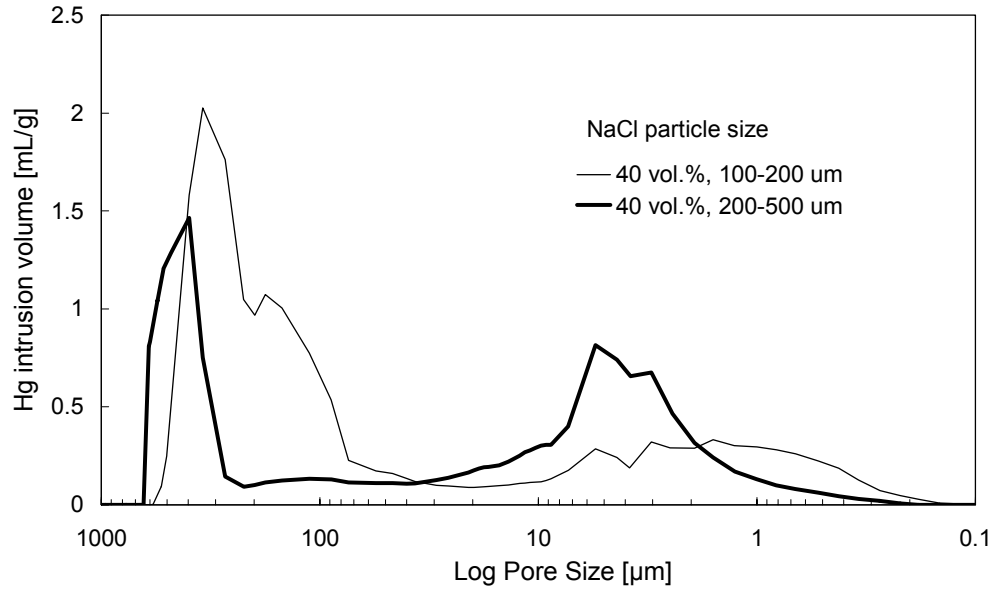

Fig. 52 *Pore size distribution depended on NaCl particle size in the polyether-urethane prior injection moulding (n=1).*

4.1.5 Pore size distribution, porosity and processing temperature

A higher cylinder temperature produced larger pores in similar to the hot pressing experiments. The mean pore diameter was 10 µm at 210 °C and 270 µm at 230 °C (Fig. 53). The reasons for pore growth due to the enhanced diffusion and lower polymer viscosity were discussed in the previous section.

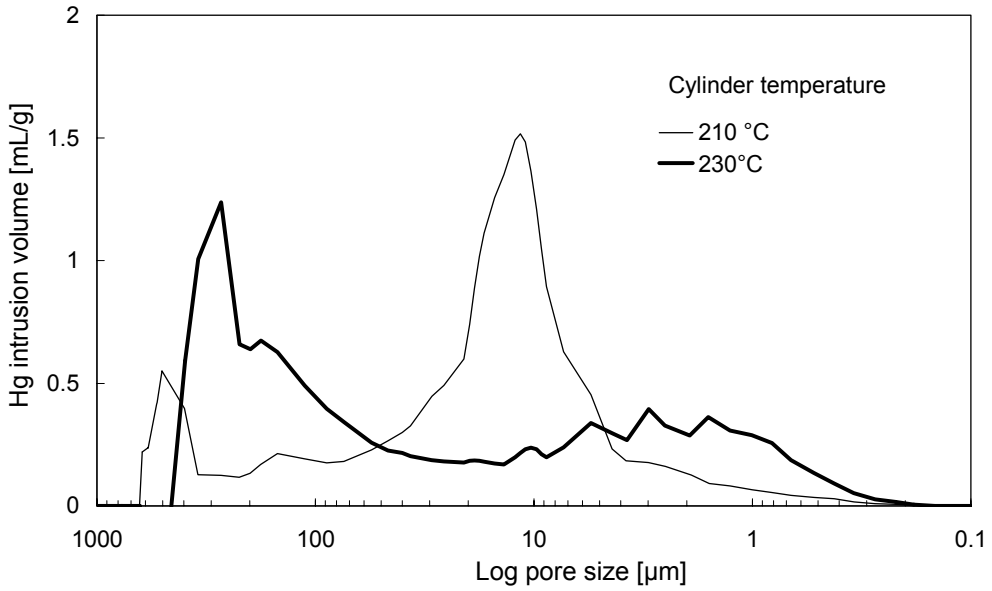

Fig. 53 *Pore size distribution depended on cylinder temperature (n=1).*

The mould temperature had three effects: A lower temperature reduced the cycle time from 60 to 45 seconds. But at lower temperatures (<50°C), the implant was difficult to remove from the mould. Additionally, the lower temperature decreased the pore diameter, which made it impossible to operate at low mould temperature. Porosimetry measurements showed a mean pore diameter of 270 µm at 70 °C, and 30 µm at 40°C (Fig. 54).

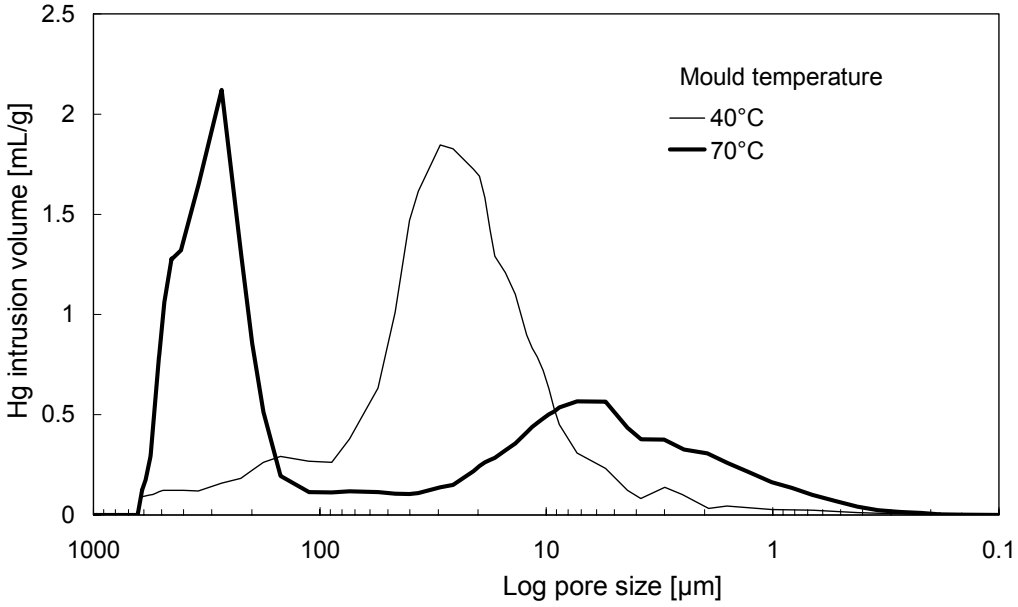

Fig. 54 *Pore size distribution depended on mould temperature (n=1).*

These results can be explained by the experiments performed by hot pressing: Fig. 44 showed that pores were underdeveloped after a short processing time. After a longer processing time (>360 sec), fully circular pores were developed (Fig. 45). Therefore, the time factor was important to allow for larger pore (>100 µm) to grow. If the mould was kept cooler, the implant vitrified faster, due to more rapid heat transfer. Thus, the cycle time was reduced. For shorter cycle times, the pores did not have enough time to fully develope before the polyether-urethane hardens. Thus, the pore diameter was suppressed.

4.1.6 Short summary of the results

Similar to the samples obtained through the hot pressing method, the GORD implant was also producible by injection moulding machine implant with a defined porous structure. Previous section described significant influences upon the porous structure by temperature changes. The heat press had only one temperature parameter, whereas with injection moulding the mould and the cylinder temperature can be controlled. These two parameters were most important for pore size diameter adjustment. The major influence on porosity was the injection pressure. The injection moulded did not produce samples with higher porosity. However, the narrower pore size distributions were made, and are thus easier controllable.

4.2 Pore size distribution of the interconnections

Fig. 55 shows the mean pore size of the interconnective pores in the ranged from 20 – 45 µm. Bubble point (interconnective pore with the largest diameter) was found to be 48 ± 7µm. Pore size distribution of the interconnective pores showed that the most common pore size was 45 ± 3µm (Fig. 55). The results corresponded with the aim of the study.

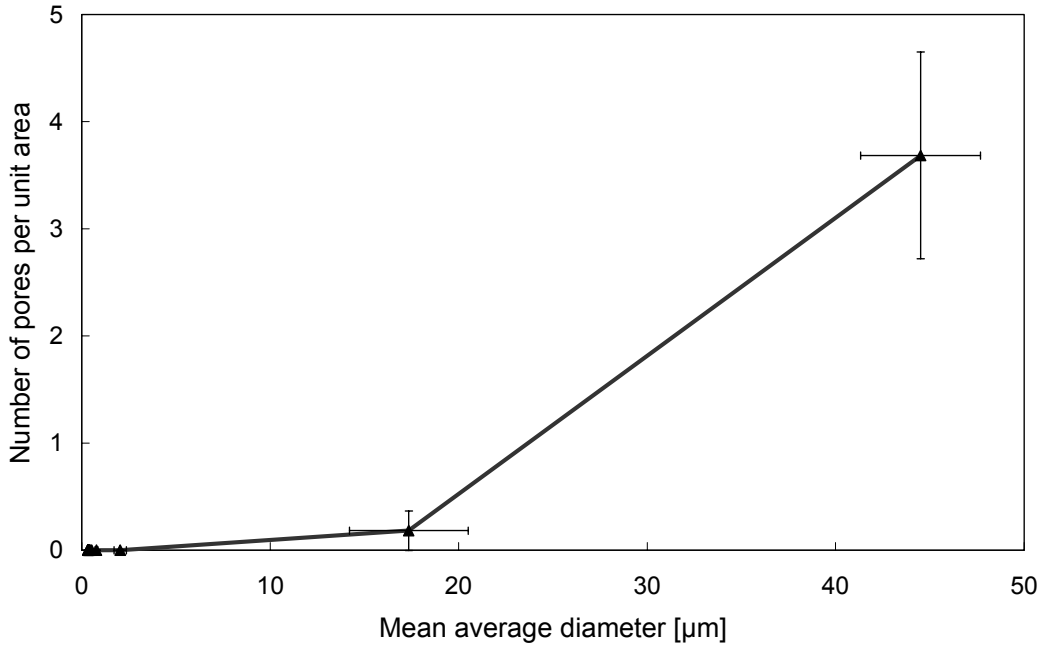

Fig. 55 Pore size distribution of the average interconnective pores diameter (n=6).

The interconnections between the pores were found by the extrusion porosimetry, however, the predominately pore size diameter of the interconnections were smaller than the added NaCl particles. Thus, the salt particles were minced by the process to one ten of its original size.

The fairly large standard deviation was found due to the measuring technique. Fig. 56 shows the gas flow through the samples and its respective pore size. The pore size increased by the numbers of runs, which indicated that the gas pressure used to analyse the samples, actually expanded some of the interconnections. Since the gas flow also went higher after each test, extra interconnections were made. Thus, the gas pressure used (<2 bars) was capable to break the polymer walls between closed pores.

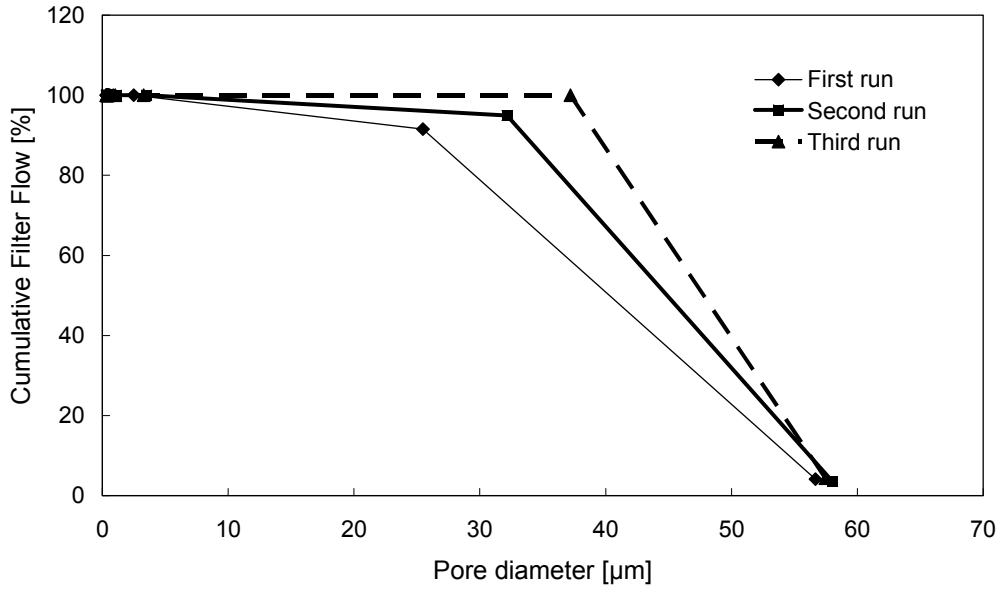

Fig. 56 *Pore size of interconnective pores and cumulative flow depended on number of runs (n=3).*

4.3 Standard deviation on porous structure

Seven measurements mercury intrusion porosimetry revealed slight fluctuations (Appendix C, Fig. C.1). The standard deviation of the porosity was 2.1% (n=7). The mean pore diameter was 364 ± 62 µm (n=7). The standard deviation on porosity was calculated to be 4.8% (n=36), and the mean pore diameter was 387 ± 92 µm (n=36). The pore size distributions were practically identical and can be viewed in the Appendix C.

The reason for the low deviations in the porosity can be explained in the following manner: The driving force for pore growth has been found to be predominately pressure drop and its rate (Fig. 51). In order to generate a uniform pore structure within the entire implant, the pressure drop inside the implant had to be constant.

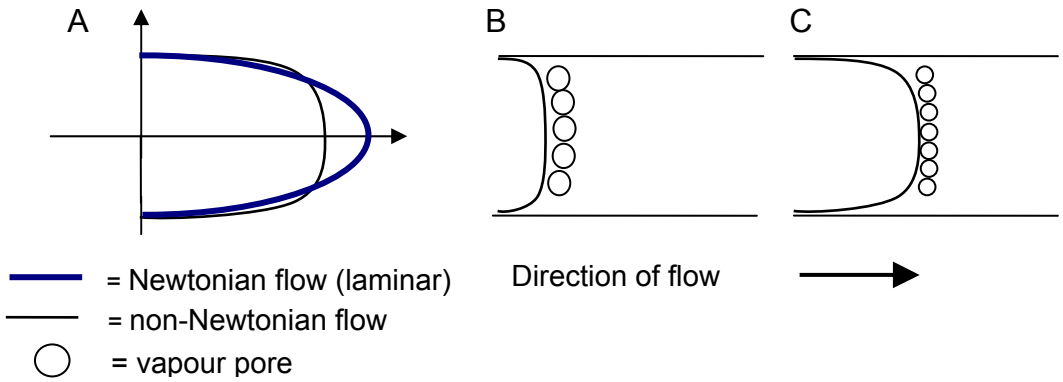

Fig. 57 *Velocity profile from Newtonian and non-Newtonian flow (A). As the injection speed or pressure increases in the mould, the velocity profile is shifted in the direction of flow (B and C). The velocity gradient was steeper for higher velocity profiles (C) compared to those at a lower speed (B).*

The Reynolds number of the polymer flow was below 4000, and was thus not turbulent [181]. Firstly, a laminar velocity profile of the flow is to be assumed. However, the polymer melt with the NaCl particles was proven to be non-Newtonian, as the viscosity was dependent on the shear stress (Appendix C, Fig. C.2). The melt was structure viscous as the viscosity dropped by applying shear stress. Thus, the polymer melt follows a non-Newtonian velocity profile drawn schematically in Fig. 57, A. For non-Newtonian flow, the velocity profile is characterised by a plateau of constant velocity between steep boundary gradients [182, 183].

The main driving force for the pore building was, as already mentioned, the pressure drop. When this pressure drop was equal throughout the implant, the same number and same-sized pores were formed. This pressure is closely related to the velocity profile in the polymer melt [183]. Since the non-Newtonian flow produces a nearly constant velocity profile, the pressure gradient must also be practically constant. This explains why the pore structure within the implant was uniform.

As the injection pressure was increased, the velocity profile was pushed forward in the flow direction [184]. The plateau did not change. Hence, changes in the processing pressures would not change the consistency in the porous structure. The only change in the velocity profile due to varying processing pressure was the altered boundary velocity gradient. In this boundary layer

the pressure was below the critical nucleation pressure. Therefore, no vapour pores could grow and a solid layer was formed. When the injection pressure increased, the gradients became steeper and the boundary layer was made thinner and thus thinner walls were formed.

Attempts to find the nucleation sites by EDX, which must have been where evenly distributed across the TPU in order generate a uniform pore structure, were unsuccessful, as no particle was found evenly distributed.

4.4 Surface properties of the GORD implant

The aim of the project did not only include a specific internal porous structure of the GORD implant, rather a porous inner side and a solid outer surface as well. The entire implant had a solid surface after being removed from the mould (Fig. 58). The reasons behind the solid layer are presented in previous section. The inner skin was mechanically removed from the inner-side of the porous structure with a specially designed cylindrical stamping device.

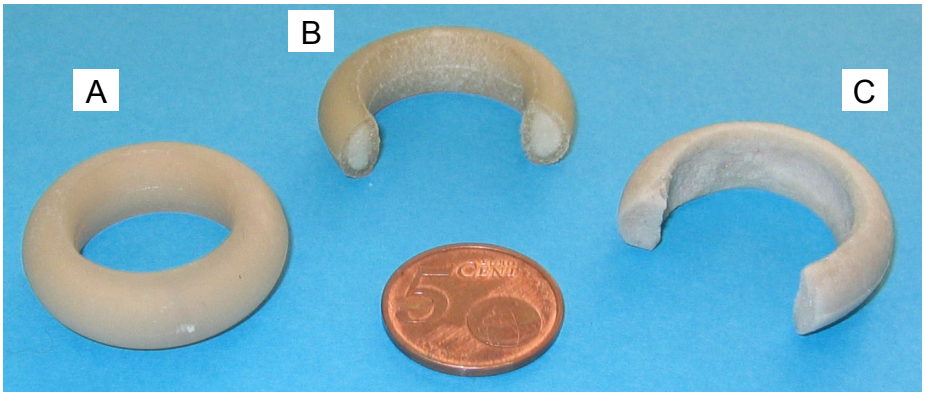

Fig. 58 *The GORD implant after being removed from the mould (A). The entire implant had a porous core surrounded by solid outer surface (B). The inner side of the GORD implant was mechanically removed (C), which produced a ring structure with a porous internal structure (3).*

The thickness exterior layer was found to be adjustable by varying the mould temperature the injection speed (Appendix C, Fig. C.3). At higher mould temperatures (>70°C) this layer was found to be 0.52 ±0.12 mm (n=14) compared to lower 0.66 ±0.14 mm (n=14) at 40°C. When the polymer vitrifies rapidly, the boundary layer (Fig. 57) was forced away from the outer walls, and the solid surface became thicker.

It was best to make this layer as thin as possible, as less material had to be removed. The optimum parameters to produce a thinner layer were the same as for making the required porous structure.

4.5 Chemical analysis

Annotated Transmission Reflex Fourier Transmission Infrared ATR FT-IR analysis

No significant changes (< 5% transmission) were found within samples produced by hot pressing or injection moulding. Three spectra are, as an example, compare unprocessed TPU granules with GORD implant injection moulded at different temperatures presented below (Fig. 59). The identification of the respective peaks were compared to other experiments [185] and found to lay within ± 3 cm^{-1}.

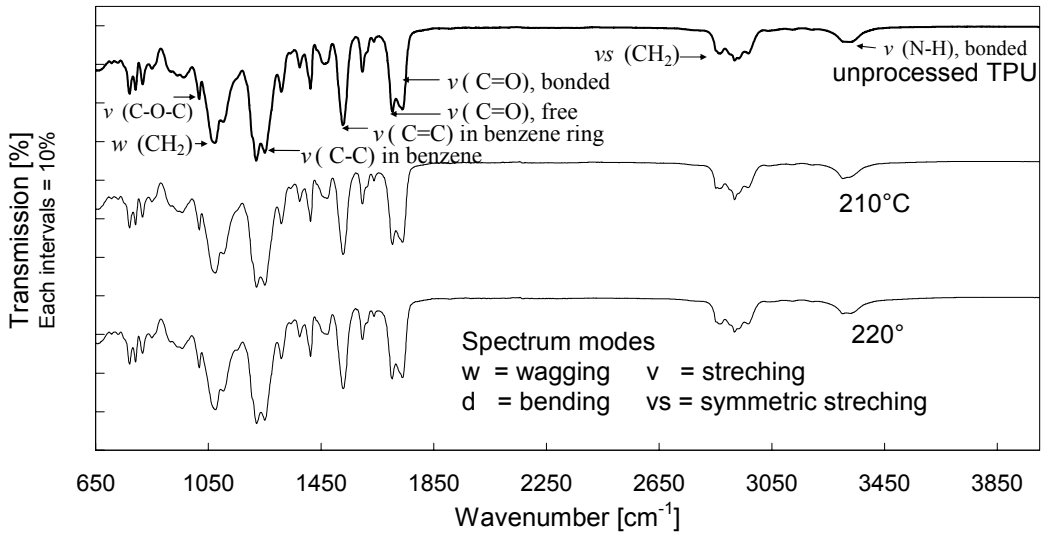

Fig. 59 *ATR FT-IR-spectra of two samples of the GORD implant injection moulded at 210 and 220°C compared to unprocessed TPU granules.*

4.6 Mechanical properties

Fig. 60 shows the mechanical properties of the GORD implant (n=20) when processed by hot pressing and injection moulding. The tensile strength for the injection moulded implants were double

(4.3 ± 0.52 MPa) compared to the hot pressed implants (2.0 ± 0.98 MPa). The elongation at break was also substantially improved by the injection moulded implants. The value was three times higher (176 ± 16.4 %) compared to the hot pressed polymer implants (56.6 ± 26.1 %).

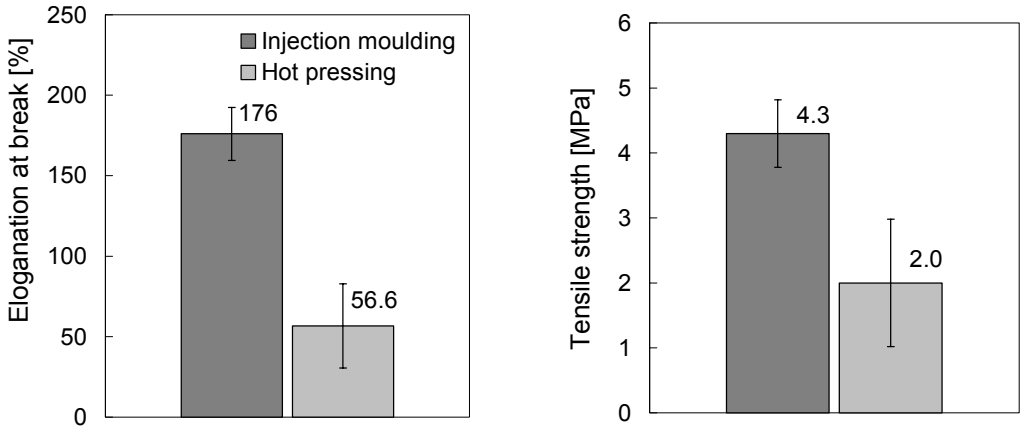

Fig. 60 *Mechanical properties of the GORD implant (n=20) processed by hot pressing and injection moulding. The mean values of the respective properties are displayed in the diagrams.*

4.7 Biocompatibility test

Fig. 61 illustrates a comparison of a cytotoxicity tests defined by EN ISO 10993-5 from GORD implants produced by hot pressing and injection moulding. Pure medium was used as control. Fig. 61 shows the effect of the culture media, which were pre-incubated with the GORD implant for seven days prior the WST-1 assay. Toxic compounds would diffuse into this culture medium if they were generated during processing, and the optical density (OD) would decrease. A graphic representation of the result showed that the eludate media (pre-incubated media) did not have any effect up to 1:2 dilutions. A slight cytotoxicity was observed for the injection moulded implants with mean OD level of 81.6 ± 14.8% (n=3) for the undiluted medium. The mean value for the heated press were 64.6 ± 10.2% (n=3). Due to the magnitude of the standard deviation it was difficult to tell with high confidence that the hot pressed implants performed less well.

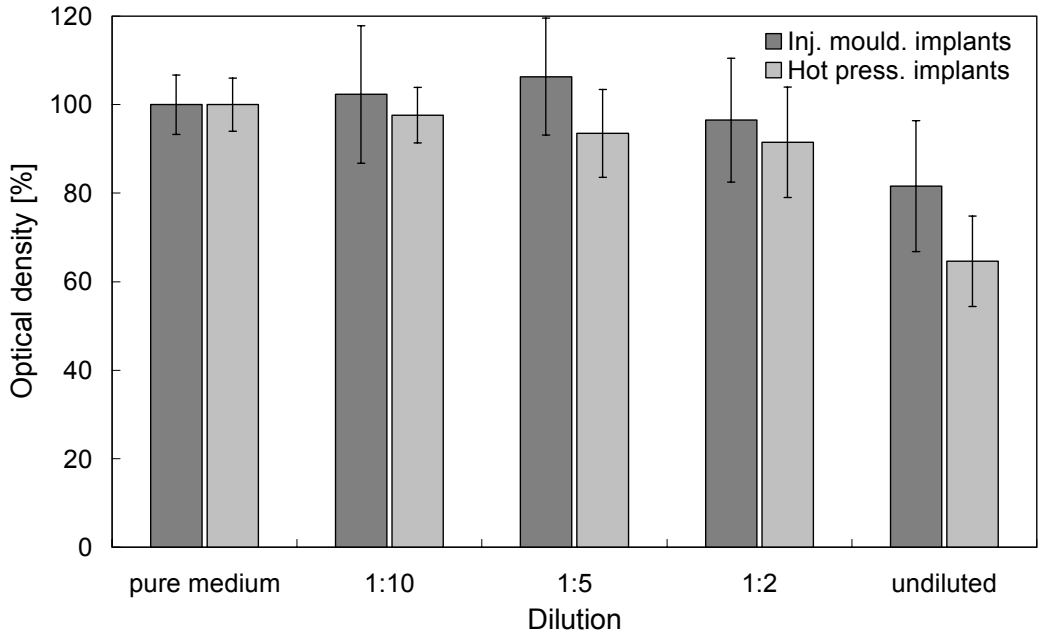

Fig. 61 *WST-1 assays with fibroblastic cells to compare the GORD implants' cytotoxicity levels produced by two different manufacturing methods. The right column serves as control; the others are different dilution levels of the eludate medium (n=3).*

A LIVE/DEAD colouring of the fibroblasts from the experiments described above was also performed (Fig. 62). The Fig. 62 A, B and C) pictures were made with an undiluted eludate medium. The tendency was observed that the cell toxicity was higher for the hot pressed GORD implants (Fig. 61). The highest cell vitality levels were observed in the control. A slight decrease, compared to the control, is seen in the injection moulded implant. By counting the number of vital fibroblasts cells in a 1 mm^2 area and comparing the result with the control (Fig. 62 B), the percentage of vital cells was 85%. This result corresponded with the WST-1 assay. Fig. 62 C presented a clear decrease in vitality. Here 136 vital fibroblasts (green) were found in comparison with the 348 in the control. The non-vital cells were 48 pro mm^2 weighed against the 8 from the control.

One has to take into account that dead cells tend to detach from the scaffold and the samples are washed in performing the LIVE/DEAD test, which tends to remove dead cells. Both factors tend to decrease the number of dead cells that are counted.

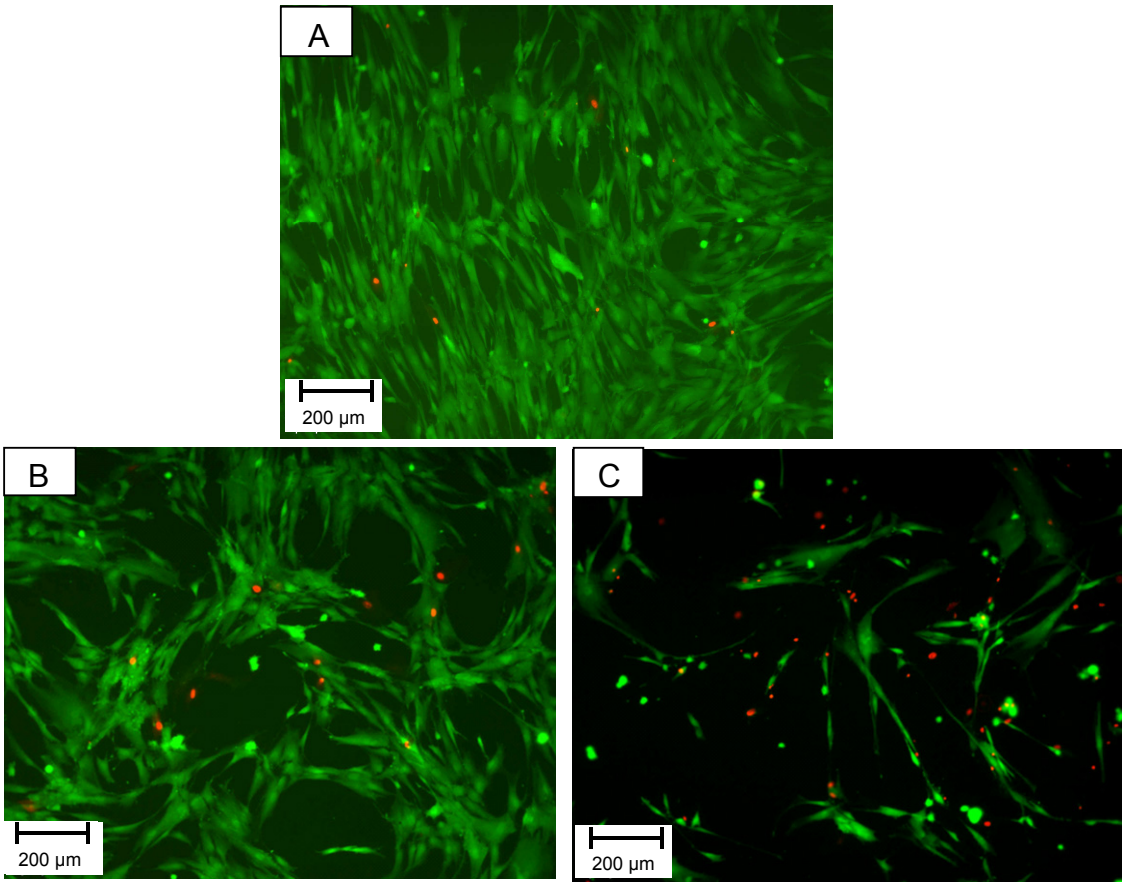

Fig. 62 *Vitality colouring after cultivation of fibroblastic cell line Detroit 551 with eludate medium (non-diluted). Green is vital cells and red is cell nuclei of non-vital cells. Labelling; A: control; B: Injection moulded sample; C: Hot pressed sample. The vitality was lowest for the GORD implant produced by hot pressing, whereas more cells are vital for the test material which was injection moulded. All processed samples had lower vitality compared to the control.*

The reason why the hot pressed implant performed worse than the injection moulded ones was most likely due to a longer processing time (30 min. compared to 60 sec), which released derivative products into the culture medium. This matter is further discussed in chapter VII.

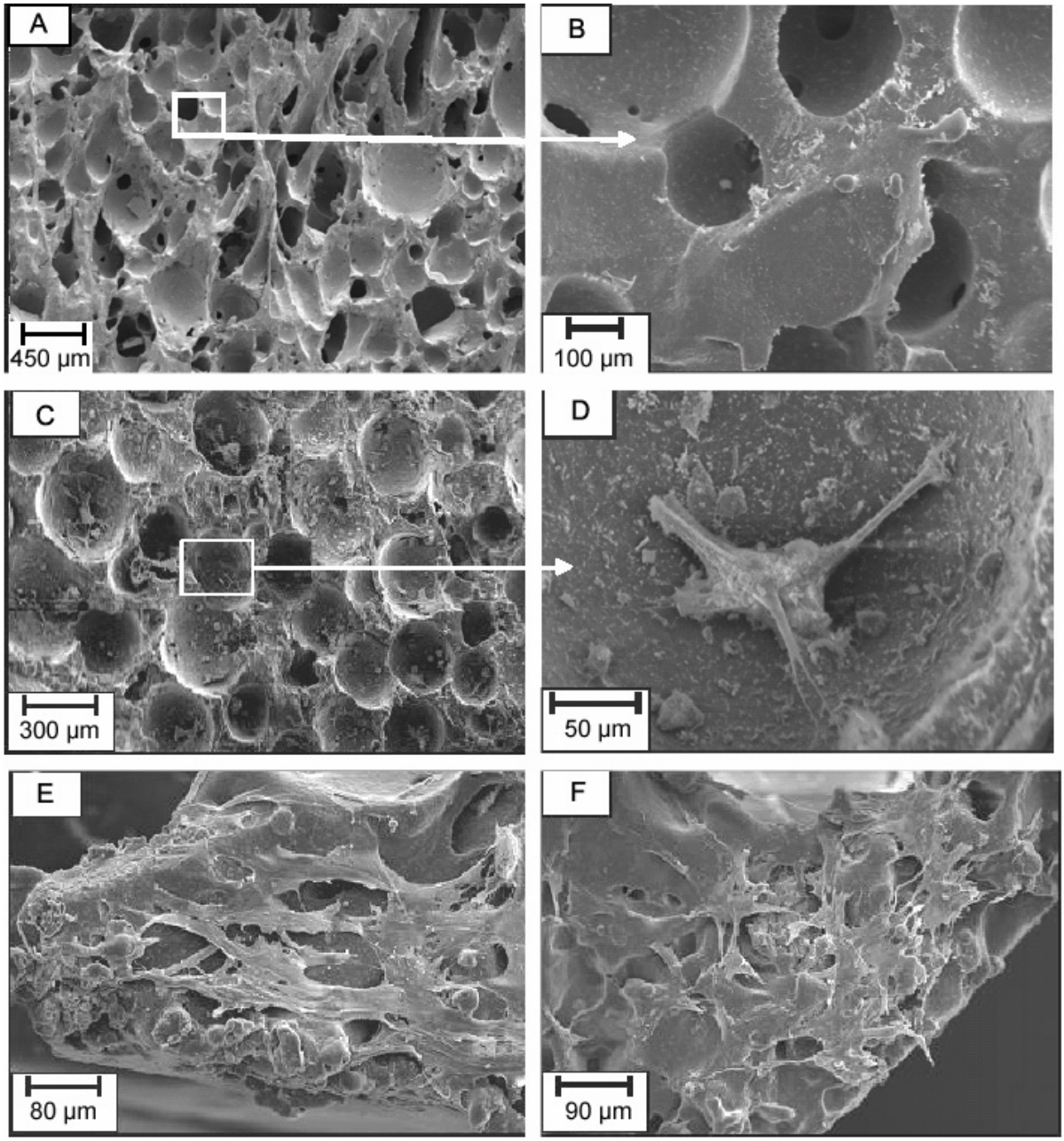

Fig. 63 *SEM micrographs of the surface of the implant after different incubation periods. Pictures (A) and (B) are images of the GORD implant without cells. (C) and (D) were taken after an incubation for 3 days with initial cell number of 10.104 (E) shows the material after incubating for 7 days with an initial cell number of* $10 \cdot 10^4$*, and (F) After incubation for 14 days with an initial cell number of* $10 \cdot 10^4$

Fig. 61 and 62 showed that there was only a slight cytotoxic behaviour with the injection moulded GORD implants. In order to prevent the implant from wandering on the LOS, cells and

tissue from the oesophagus have to grow into the porous structure. Before this can happen, the cells must be capable of attaching themselves to the surface of the polyether-urethane. Fig. 63 shows SEM micrographs of the porous structure at different incubation stages. Only a small number of fibroblasts could be seen after three days incubation (Fig. 63 C). A single cell had attached itself onto one of the pores in the material (Fig. 63 D). The surface area, covered with fibroblasts, was enhanced by increase in the incubation time (Fig. 63 D and E). After seven days cluster of cells were formed. The typical morphology of the fibroblasts, where the cells stretch out on the surface, was visible. The fibroblasts proliferated in linked networks.

The network-like fibroblastic growth can also be viewed in Fig. 64. Cell density increases with incubation time. After 14 days there was hardly any polymer surface left for further cell adhesion. The number of non-vital cells (in red) rose with an increase in incubation time. The high cell density, chosen to simulate *in vivo* conditions, prevented fibroblasts from growing in monolayer. After a certain incubation time, the fibroblasts have to proliferate on top of each other. Further proliferation cause cell death and this might be the reason for the increasing numbers of non-vital fibroblastic nucleus.

The 3D seeded of fibroblast into the porous region of the GORD implant was not performed.

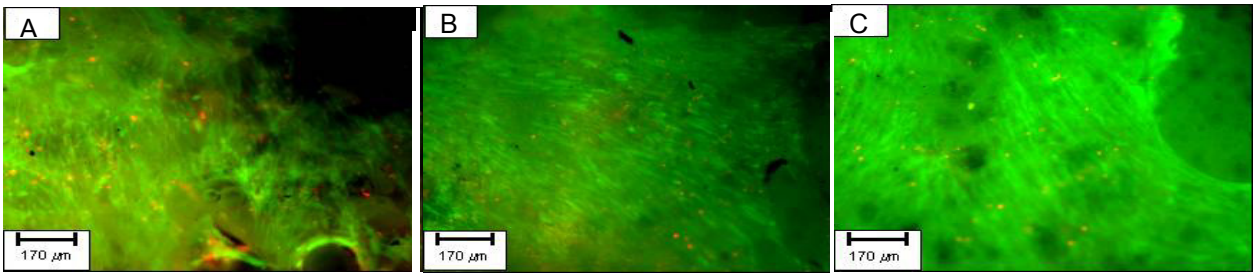

Fig. 64 *Vitality colouring seeded fibroblast onto the surface (top view) of the GORD implant after different incubation periods. The implant surface was incubated with 50x104 Detroit 551 fibroblasts. The images were shot after 3 (A), 7 (B) and 14 (C) days. Green = vital fibroblast. Red = nuclei of non-vital fibroblasts*

An MTT assay (3-(4,5-dimethylthiazolyl-2)-2,5-diphenyltetrazolium bromide) was added to the medium solution of seeded fibroblasts (Fig. 65).Colour intensification occurred after increasing incubation time, which verifies observation done on the SEM images, where a growth increase

against time was observed. However, the SEM images only examine a small surface area. The images below show that the colouring is uniform, meaning that the adhesion and growth of the fibroblast was homogeneous across the entire inner surface of the implant.

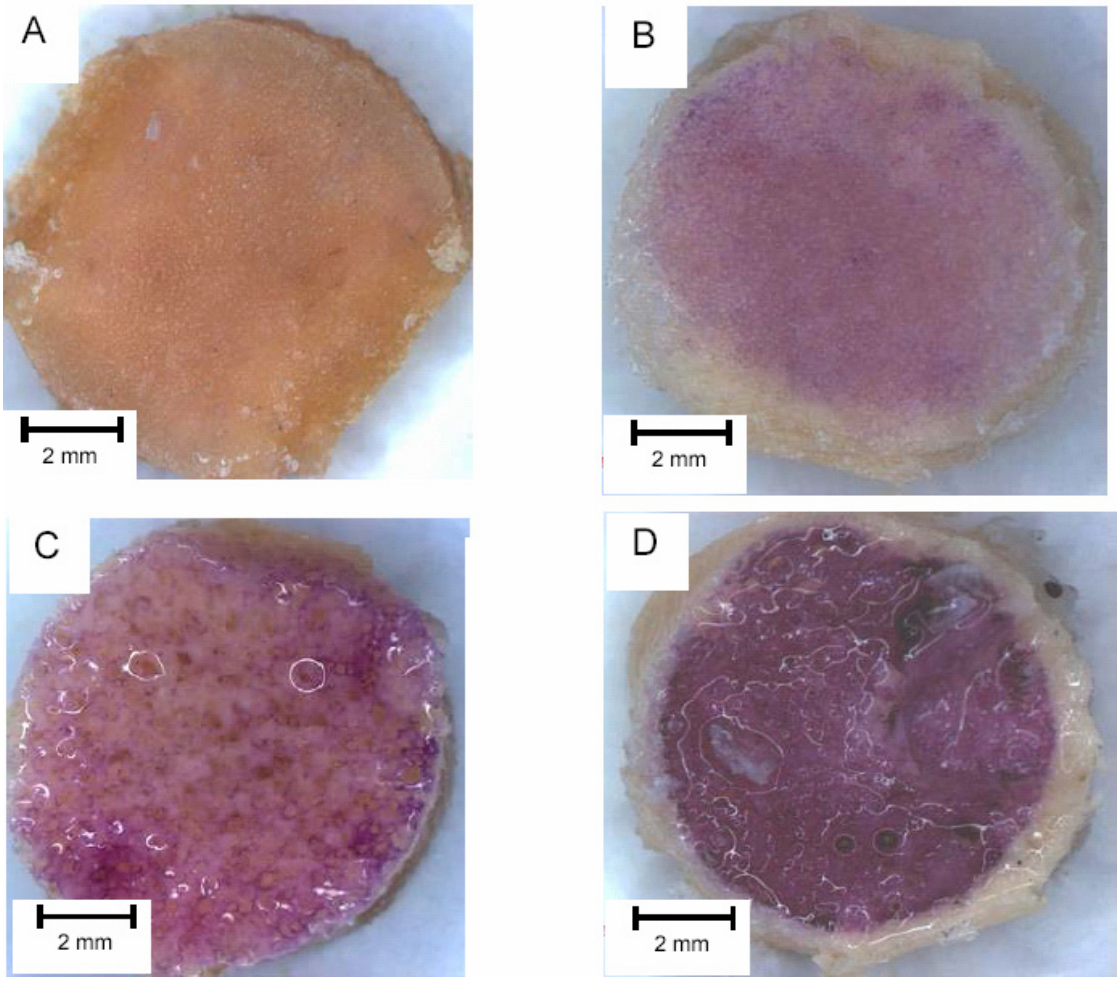

Fig. 65 *MTT assay colouring of the Detroit 551fibroblast seeded onto the GORD implant surface after 3 (B), 7 (C) and 14 (D) days with an initial cell number of 1.104. The control (A) was the same implant with MTT colouring, but without fibroblast.*

CHAPTER VI
Results and discussion
Influence upon sterilisation

1 Spectroscopy analysis

No major difference in the spectra (<5%) between unprocessed polyether-urethane granules compared to the steam sterilised and γ-irradiated GORD implants (n=20) was found by ATR FT-IR analysis. Representative transmission spectra are presented below (Fig. 66).

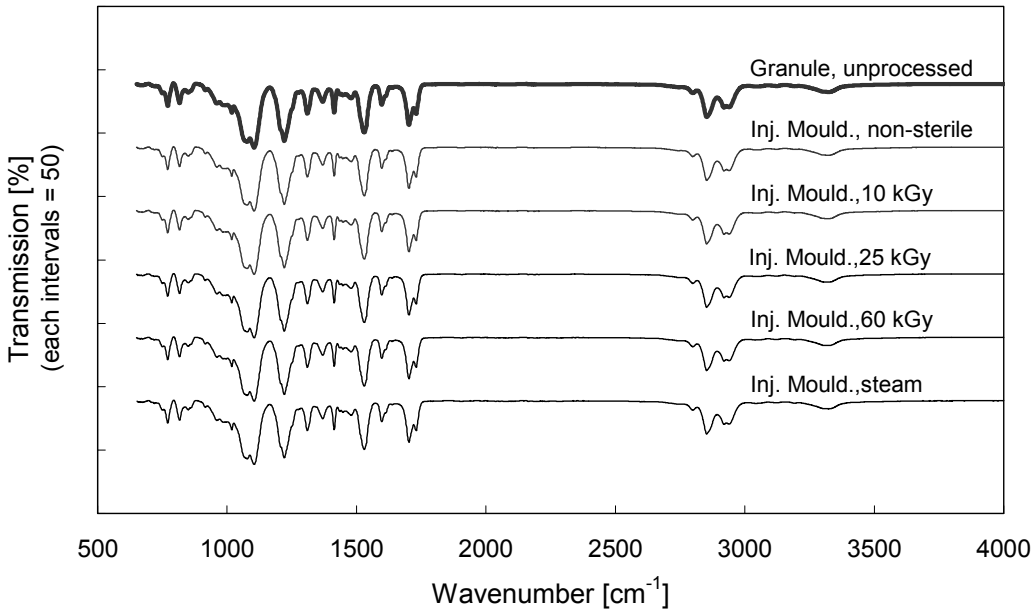

Fig. 66 *ATR FT-IR analysis of the sterilised GORD implants versus unprocessed granules and non-sterile samples. Labelling: Inj. Mould = injection moulded GORD implants.*

2 Gel permeation chromatography

A loss in the weight average molecular weight number, M_w, of 11.9 ± 1.58% was detected for the steam sterilised samples against the non-sterile GORD implant, which was used as a control. The irradiated GORD implants behaved reversely and gained molecular weight. The improvement of the M_w, was 8.6 ± 1.60%, 13.3 ± 1.57% and 20.0 ± 1.59% for the 10 kGy, 25 kGy and 60 kGy γ-

sterilised implants (Fig. 67). The figure below displays the M_w also for the granules after extrusion, where salt and polyether-urethane was mixed. Therefore, this M_w was the weight average molecular weight number prior to injection moulding. The loss of M_w during injection moulding was not compensated by the γ-radiation.

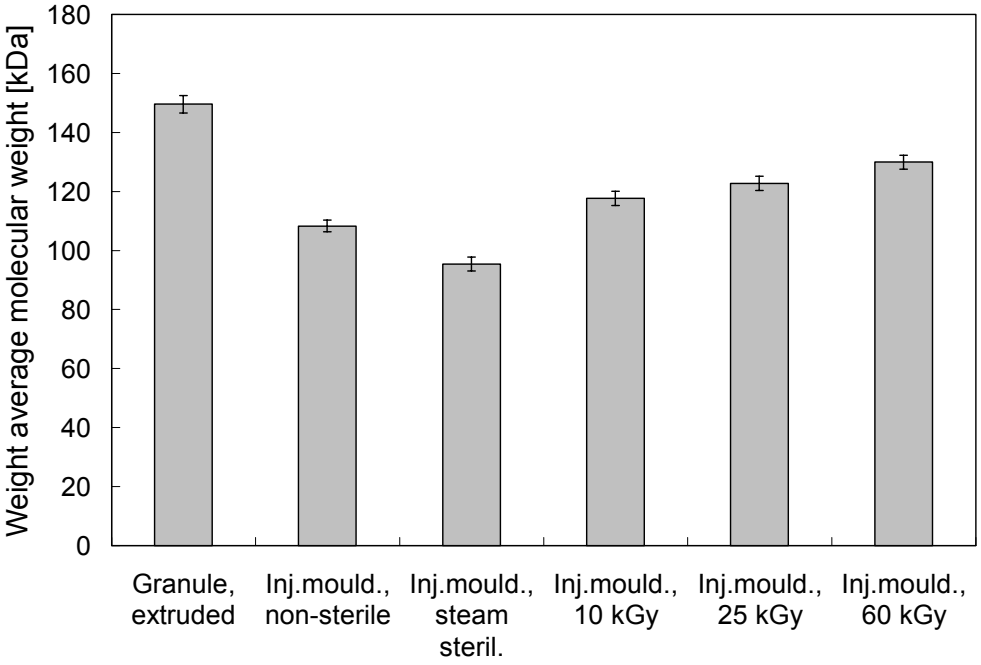

Fig. 67 *Weight average molecular weight number, M_w, of the polyether-urethane after different sterilisation treatment (n=9).*

A plausible reason for the molecular weight increased by the higher γ-dosage was a cross linking between free monomers or polymer chains [185-187]. Similar observations have been made for polyether-urethane [188, 189]; however, the same scientist has found contradicting evidence [190].

The monomers could have been cracked free from the polyether-urethane structure during processing [176, 191, 192] since the molecular weight was changed during production of the implant. Processing degradative behaviour is further discussed in the next chapter.

3 Thermal analysis

The non-sterile and the γ-irradiated samples all had three endothermic peaks. The first one at 70°C, the second at 115°C (Fig. 68) and the last at 175°C.

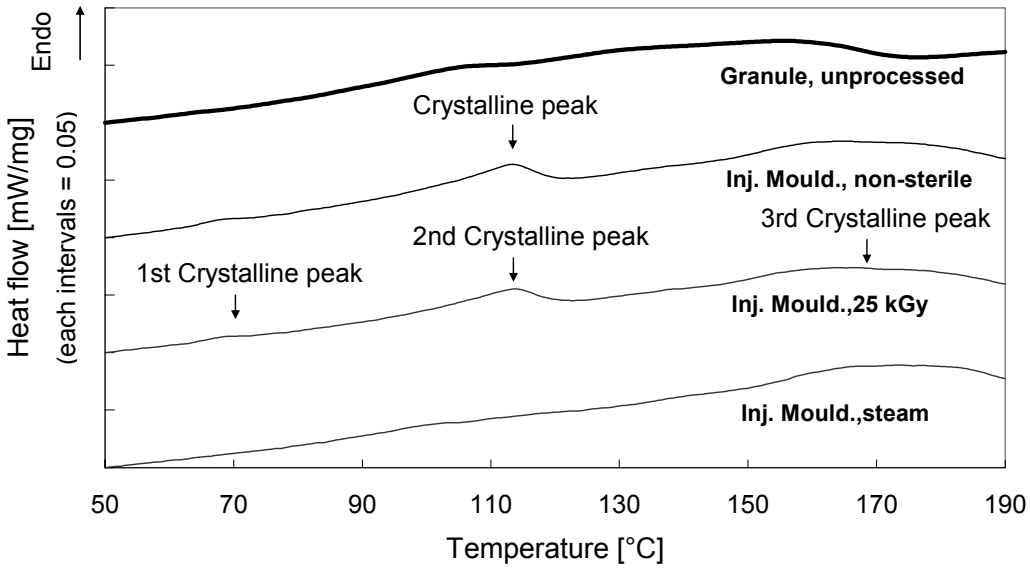

Fig. 68 *DSC curves of the second heat run for different sterilised samples versus untreated.*

The third part was relatively weak, but broad. The first peak (70°C) was melting for the limited short-range order region and the second (115°C) was for the long-range order chains [193]. The last broad peak (175°C) corresponded to the melting of the microcrystal in the hard segment [194-196].

The unprocessed polyether-urethane had only two. The three peaks range in melt enthalpy, ΔH_c, between 0.033-0.08, 0.24-0.72 and 2.59 and 3.61 J/g. The second peak was shifted by increasing radiation doses and found to be at 166°C, for the 60 kGy samples. The different values of the ΔH_c gave the crystallinity (Table 10).

Sample	Crystallinity ± SD
γ-irradiated implant at 10 kGy	2.21 ± 0.021 %
γ-irradiated implant at 25 kGy	1.99 ± 0.223 %
γ-irradiated implant at 60 kGy	1.58 ± 0.296 %
non-sterile implant	1.61 ± 0.378 %
non processed granule	0.28 ± 0.250 %
steam sterilised implant	0.14 ± 0.021 %

Table 10 *Overview of the crystallinity of the GORD implants determined by DSC (n=9).*

The lowest value was found in the steam sterilised implants, where practically no crystalline regions were present. The highest level was obtained for the GORD implant γ-sterilised at 10 kGy, and decreased with higher dosages. This phenomenon can be explained by the increased cross linking observed by the GPC measurement. The cross linking hindered the free motions of the chains, and hence prevented them to organise crystallite regions. The same argument can be used to explain the

increasing crystallinity after injection moulding. Due to shearing and heat, some monomer chains were split and promoted orientation of the molecules [197].
The energy input by steam sterilisation dissolved the crystallite areas and brought the polyether-urethane back to the original amorphous structure.

4 Cell toxicity

The cell toxicity effects of the differently applied sterilisation methods were assessed by tetrazoliumsalz, 4-[3-(4-jodophenyl)-2-(4-nitrophenyl)-2H-5-tertazolio]-1,3-benzen disulfonate, WST-1 assay and vitality colouring. The results can be viewed in Fig. 69 and 70.

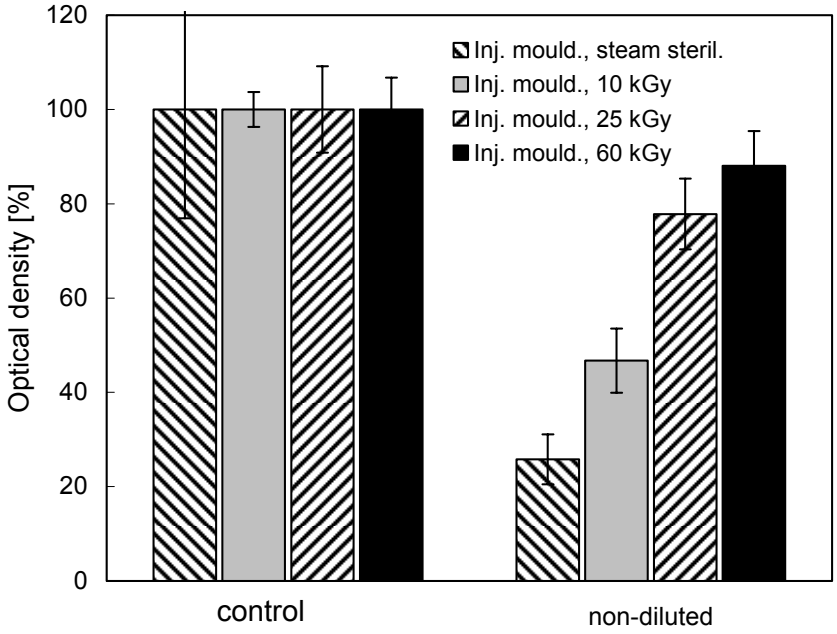

Fig. 69 *WST-1 assays with fibroblastic cells to compare the cytotoxicity of the applied sterilisation methods (n=6).*

Fig. 69 shows an increased optical density (OD) for higher γ-radiation dosage. The OD level for the different dosages were; 10 kGy at 43% ± 8%; 25 kGy at 80% ± 7% and 60 kGy at 90% ± 3%. The worse performing GORD implant was the steam sterilised one (23% ± 4%). These results were also confirmed by vitality colouring, where there was a significant decrease in vital cells for the steam sterilised samples and gradual rise in vital cell numbers for higher γ-radiation dosages Fig. 70. The presences of nuclei of non-vital cells were observed at higher numbers (77). The reason why the samples treated with γ-radiation higher dosage performed better can be attributed to increased molecular weight, where free monomers are bonded back into the polymer structure. The steam sterilisation process accelerated the hydrolysis of the

GORD implant and released toxic degradation products into the eludate medium. The detection and quantification of these hydrolysis products are presented in chapter VII.

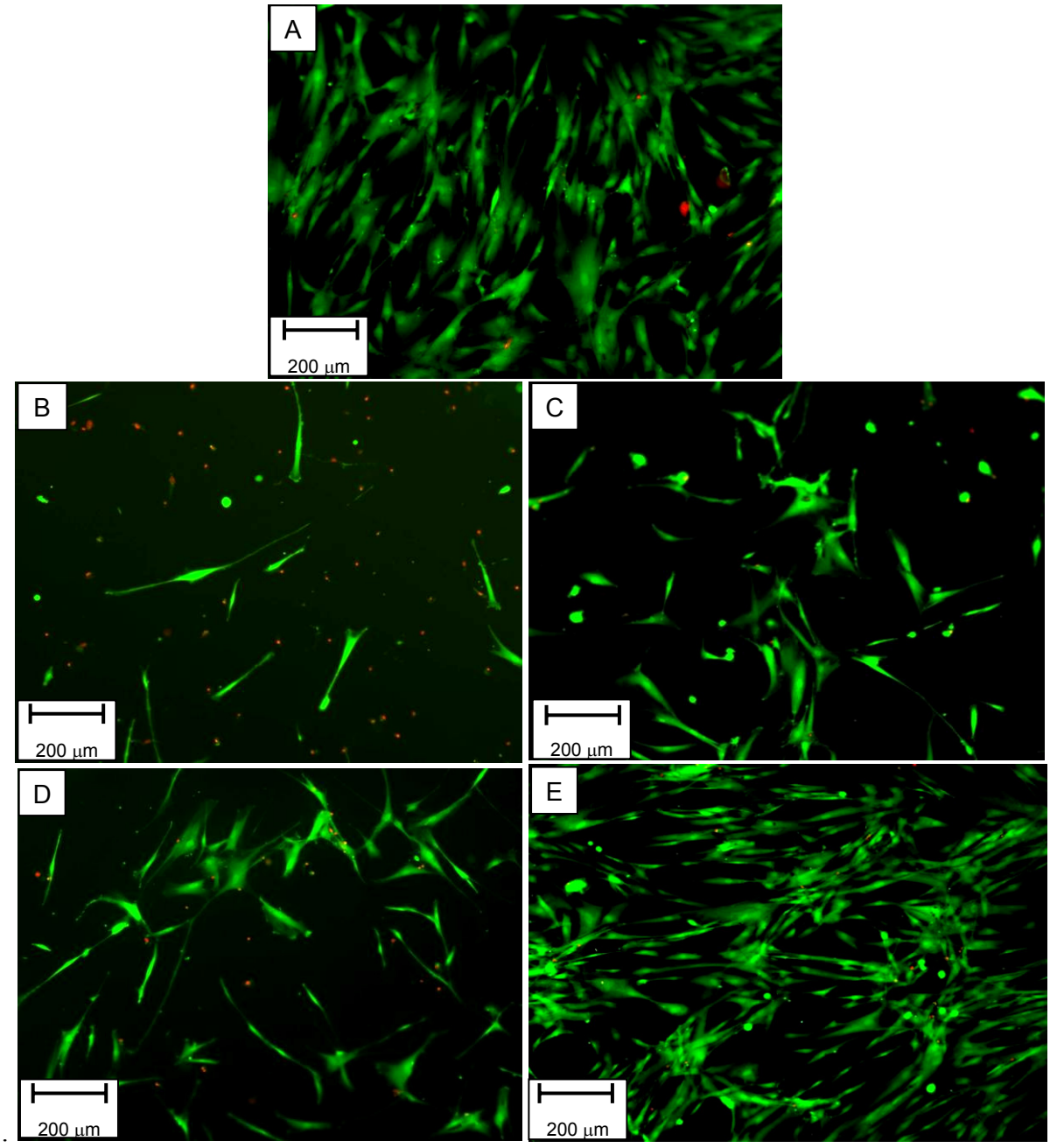

Fig. 70 *Vitality colouring after different sterilisation procedures. The control (A) was pure medium on the seeded fibroblasts. The other images were taken after non-diluted eludate medium was added to the well-plates. The images represent: steam sterilisation (B); γ-radiation with 10 kGy (C); 25 kGy (D); and 60 kGy (E). Green is vital cells and red is nuclei of non-vital cells.*

CHAPTER VII
Results and discussion
Degradation behaviour

1 Degradation due to polymer processing

1.1 Molecular weight

Polyether-urethane is a well-regarded biomaterial due to its mechanical properties, fatigue resistance, blood and tissue compatibility [143]. Nevertheless, problems resulting from degradation *in vivo* have been reported [198]. In chapter V it was shown with biocompatibility tests that the GORD implant processed by hot pressing had a 20% decrease in optical density compared to the one processed by injection moulding. The reason was most likely due to longer processing time (30 min. compared to 60 sec) and release of degradative compounds. The prolonged heat exposure initiated molecular weight loss. Fig. 71 shows that there was a decline in molecular weight distribution for the hot pressed implants, which was 6.5 ± 2.3% lower than in the injection moulded ones. The overall molecular weight loss for the hot pressed samples was 27.2 ± 5.6 and 20.6 ± 4.6% for the injection moulding compared to the M_w value. Similar behaviour was observed in the other molecular weight numbers, M_n, M_z, and M_{z+1}. The graphic presentation (Fig. 71) also shows that the thermal mixing of polyether-urethane and NaCl particles in the extruder had a major impact. The molecular weight M_w was reduced by 25 ± 8.1% in the pure polyether-urethane granules. The molecular weight distribution was not identical to the polydispersity of the polymer and was also changed during processing. The latter effect was most likely due to shear stress of the screw elements. Nevertheless, the remaining issue was to determine the reason why the hot pressed implants performed worse than the injection moulded ones. Since the molecular weight loss during the entire processing was significantly greater than the difference between the two processing methods, it was not clear from the molecular weight changes why the hot pressed samples were less biocompatible.

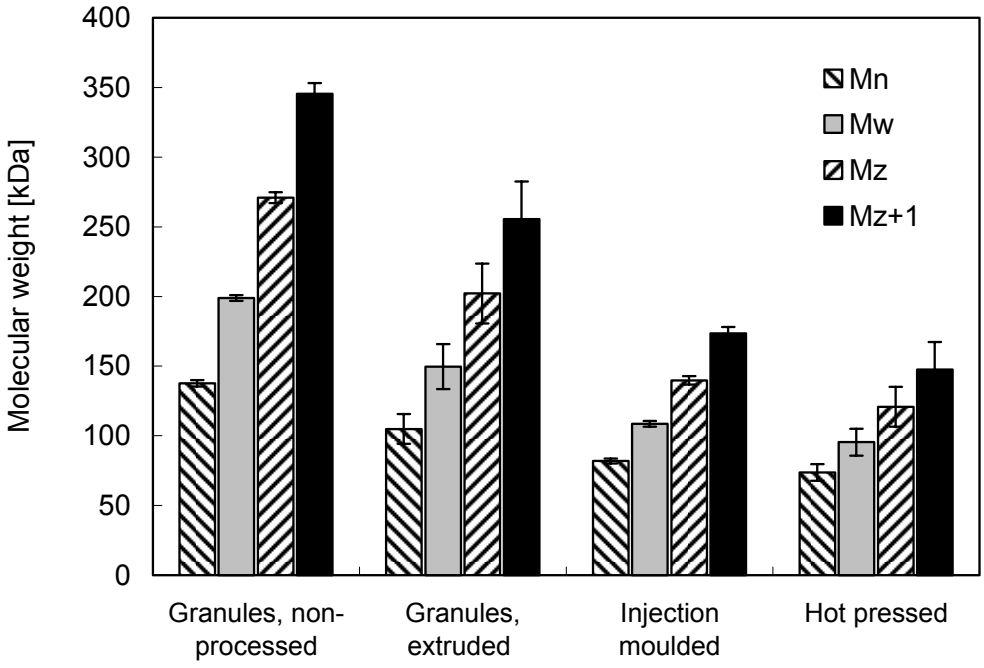

Fig. 71 *Molecular weight distribution of injection moulded and hot pressed implants versus pure polyether-urethane and extruded granules.*

Separation of degradation products by HPLC

An HPLC analysis of the eludate medium revealed that the concentration of break down products and monomers were higher (Fig. 72) when using hot pressing. The peaks at 0.7 and 1.0 minutes had a double detection unit, which meant that the concentration of these compounds were twice as high during hot pressing when compared to injection moulding. The isocyanate monomers reacted in the aqueous environment to a primary amine, i.e. the polyether-urethanes' degradation products resulted in the formation of the amine of the isocyanate (MDA from MDI). MDA is considered to be the most toxic of all degradation products for polyether-urethane [151, 152, 155, 176, 193, 199-201]. A smaller peak at 2.1 minutes was also detected.

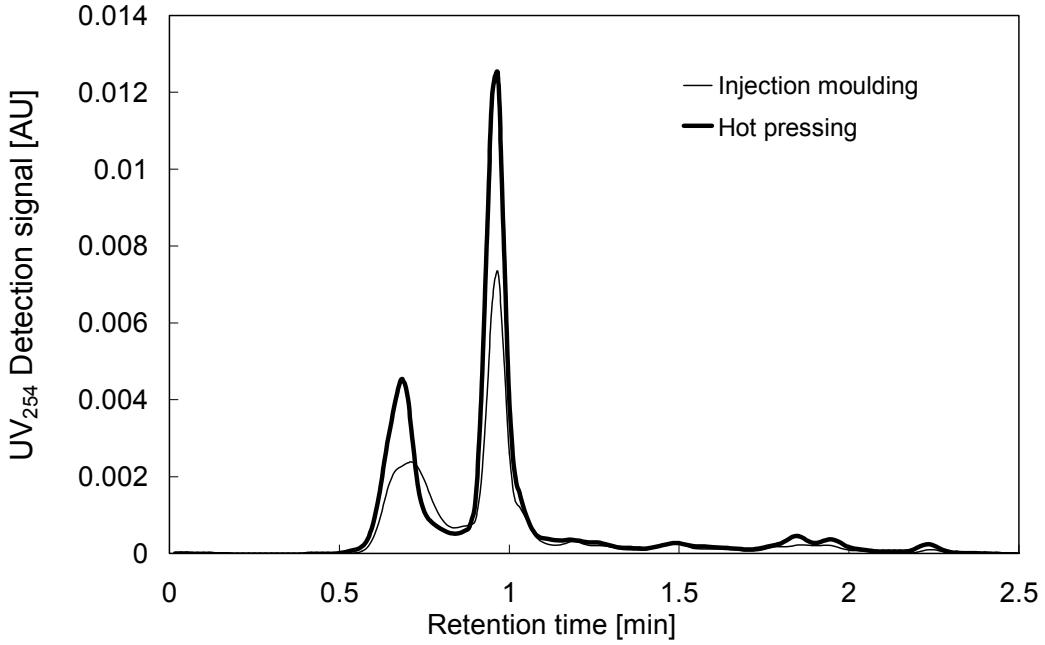

Fig. 72 *An HPLC analysis of the eludate from the injection moulded and hot pressed implant.*

This peak was identified as methyldianaline (MDA) by mass spectroscopy (Fig. 73).

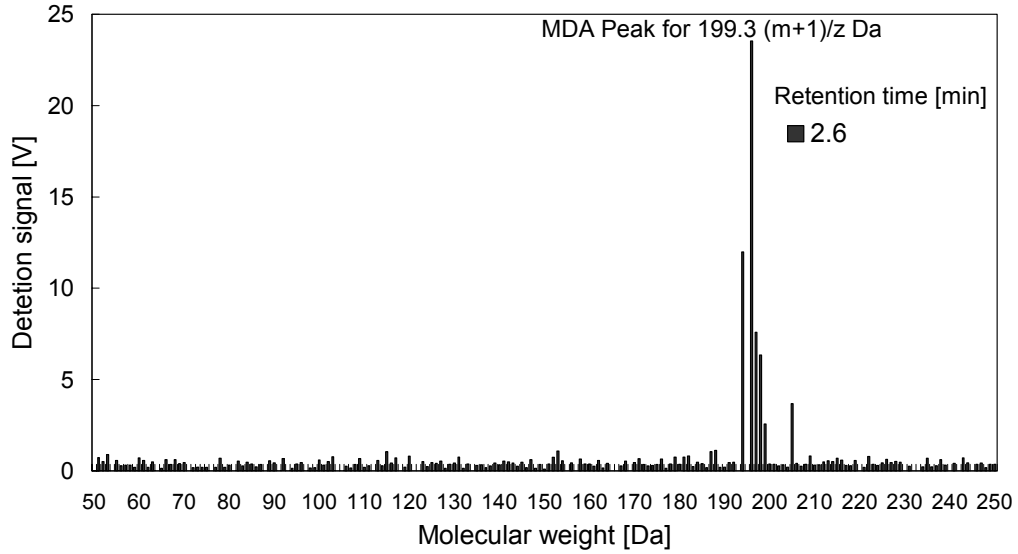

Fig. 73 *Mass spectroscopy scan of the eludate after a retention time for 2.6 minutes. The time delay between the UV and MS detector was measured to be 0.7 minutes.*

MDA has a molecular weight of 198.3 Da. Fig. 73 was recorded 0.7 minutes after a peak was observed by the UV detector. The time delay between the UV and MS detector has been measured to be 0.7 minutes. Therefore, this diagram was the true MS scan of the UV peak at 2.1 min. This diagram proves that the UV peak at 2.1 minutes was, indeed, MDA. Since this signal hit its peak at 199.3 Daltons, the compound detected by the UV detector can only be MDA.

The mean retention time of pure MDA was also found to be at 2.1 ± 0.1 minutes (Fig. 74) using the method described in chapter III (n=50).

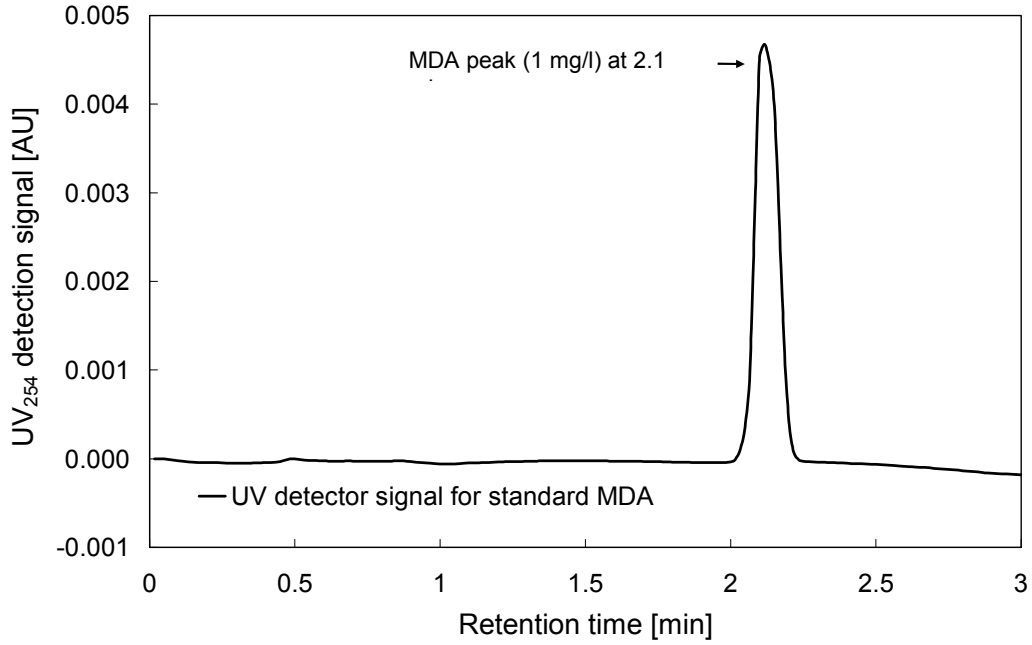

Fig. 74 *UV spectrum for pure MDA. The calibration was done with peak height versus concentration, and determined by linear regression, R^2=0.999.*

The separation method and column used is reliable since the peak is narrow and has low retention time deviation (±0.1) for n=50. The lowest detectable MDA peak, 1.0 x 10^{-4} ppb, was set to be three times the noise of the HPLC system. The fluctuating baseline in the chromatogram (Fig. 77) is due to this noise and drift. MDA calibration curves were generated by recording the UV detector's signal height (Appendix F). For data evaluation, two different calibration curves were calculated on the basis of linear regression. Low MDA amounts (<0.01 ppb) were determined with

a calibration curve ranging from 0-0.01 ppb MDA (n=10, R^2=0.999). However, for higher MDA levels (0.01-100 ppb) a second curve was used (n=50, R^2=0.987). One ng MDA per mL (g) of solvent and HPLC grade water is equivalent to 1 ppb.

The level of MDA form the hot pressed samples were found to be 15 ± 4% higher than their injection moulded counterparts but not in such quantities that it would affect the biocompatibility.

2 Degradation of the polymer due to sterilisation procedure

In the previous chapter the polyether-urethane material was analysed for the effects of sterilisation. It was found that higher γ-sterilisation doses decreased the cell toxicity (Fig. 69 and 70). Steam sterilisation samples had an optical density of 20 %. The question arose whether this was due to MDA formation.

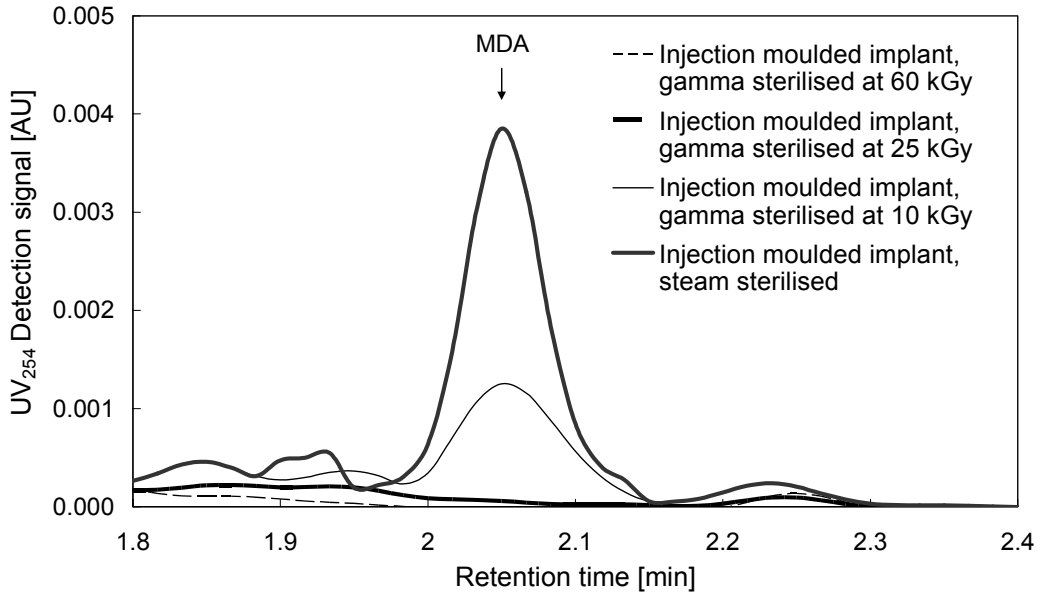

Fig. 75 *UV spectra for the eludate medium used in cell toxicity experiments to test the cell behaviour on the implant sterilised by different methods.*

MDA was indeed found in double quantities for the steam sterilised GORD implant (Fig. 75) (0.7 ± 0.01 ppb) compared to the implant γ-sterilised at 10 kGy (0.3 ± 0.01 ppb). Similar observations were made by Mazzu et al. [156]. The 25 and 60 kGy irradiated implant did not have any peaks for

retention time of 2.1 min. This fact explained the reason for lower optical density levels for the WST-1 assay at higher radiation levels. It is believed that the high energy from the γ-sterilisation binds released MDI, the monomer which causes MDA, back into the polymer chains.

3 Degradation due to enzymatic attack

Enzymatic attack with cholesterol esterase (CE) has been shown to be the most destructive degradation agent [150-152, 200]. Therefore, this enzyme is a crucial component when assessing the biostability of an implant. Enzymatic attack on the polyether-urethane can split the urethane linkage between the isocyanate and the diol [202]. These isocyanate monomers react in the aqueous environment to a MDA [203]. Furthermore, other thermal degradation products such as PhI (phenyl isocyanate) and MIC (methyl isocyanate) can be released [176]. Details regarding different degradation types and reactions are reviewed in Appendix A. In this study, a CE enzymatic attack against thermoplastic polyether-urethane was investigated.

The objective of this study was to monitor the MDA release from the GORD implant during a 28 day period. The toxic level for MDA used was the Lowest Observed Adverse Effect Level LOAEF, which was taken from Reference Exposure Levels, Office of Environmental Health Hazard Assessment, California [204].

3.1 Molecular weight analysis

A molecular weight analysis revealed that the hot pressed GORD implant, which was attacked by enzyme lost 8.5 ± 1.3% of its M_n *and* 13.1 ± 1.9% of its M_w (Fig. 76). The sample, which was attacked at a tenfold enzyme concentration, did not loose more of its molecular weight compared to the other samples. Generally, a 20 % decrease in molecular weight was observed compared to the control.

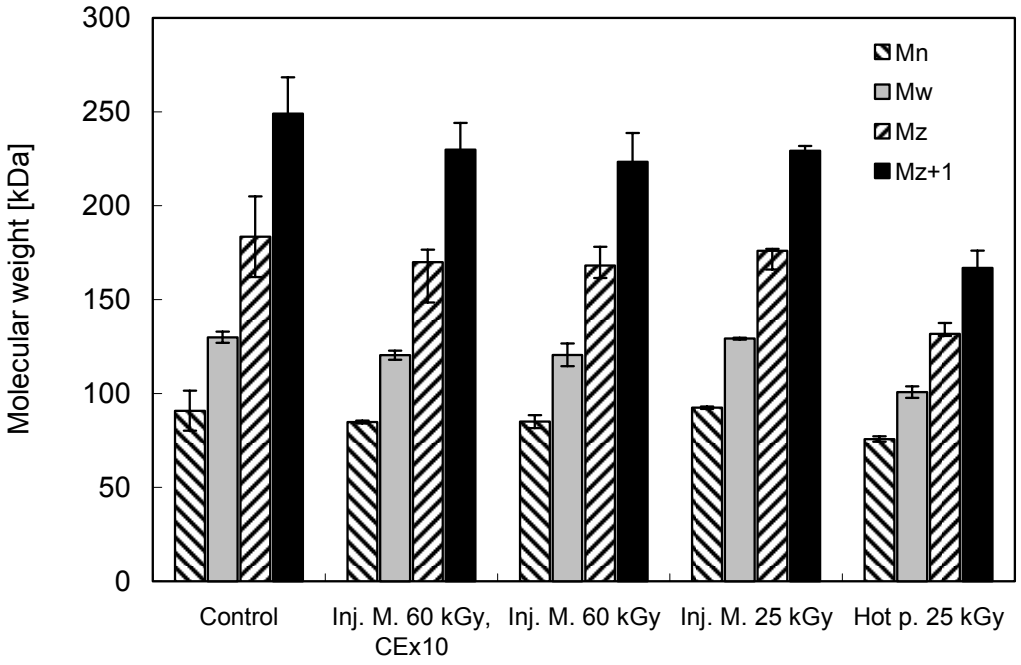

Fig. 76 *Molecular weight distribution of the different samples used in the experiments at the end of the incubation time. The control sample was an injection moulded GORD implant sterilised at 60 kGy. This sample was not attacked by CE enzymes.*

3.2 Separation of MDA by HPLC

The extracts from the incubation media were separated by HPLC in order to isolate individual biodegradation products prior to detection released MDA amounts. Fig. 77 shows selected UV chromatograms for the degradation products of an injection moulded sample and control samples following a 7-day incubation period. The figure shows a distinctive and characterising MDA peak at a retention time of 2.1 minutes. The positive and negative control samples do not display any peaks at the same time. Hence, the control samples do not release MDA into the extract. This ensures the inertness of the specimen holder as well as the embedding medium for MDA detection.

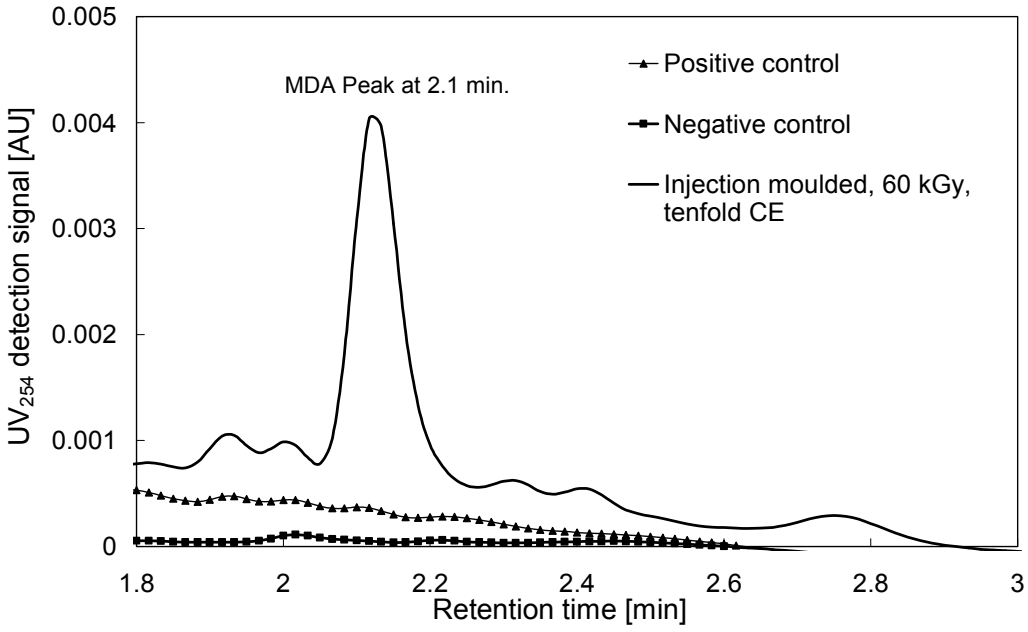

Fig. 77 *MDA detection of injection moulded samples sterilised at 60 kGy with a tenfold CE activity. Measurements were taken on the seventh incubation day.*

The recorded chromatograms for the entire retention time display several peaks, and not only for MDA. Fig. 78 shows a chromatograph with peaks at retention times of 0.75, 1.0 and 1.4 minutes. These peaks were suspected to be other enzyme-catalysed, degradation-related products. Peaks were also generated in the positive and negative control sample. As the positive control has identical peaks, compared to the 25 kGy sterilised injection moulded sample, it is clear that the degradation products come from the testing chamber. The peaks cannot arise from the polyurethane sample as the positive control had none. Hence, the degradation products must arise from the embedding medium, which was the silicone tube, paraffin wax or polystyrene test tube. Interestingly, the negative control neither polyurethane nor enzyme, only silicone tube, paraffin wax and polystyrene test tube) also shows releases of degradation products. However, they are less distinctive. This means that substances are being released from the embedding medium without enzymes. For the peaks at 0.75 and 1.0 minutes, the peak heights are identical to the positive control and implant material. If the polyether-urethane had degradation products for these retention times, one would expect that their peaks would be higher. Since this was not the case, one can conclude that the implants did not have additional degradation products at 0.75 and 1.0

minutes. The peak at 1.4 minutes is even higher for the positive control than the implant material, and additional degradative products from the polyether-urethane are thus not possible.

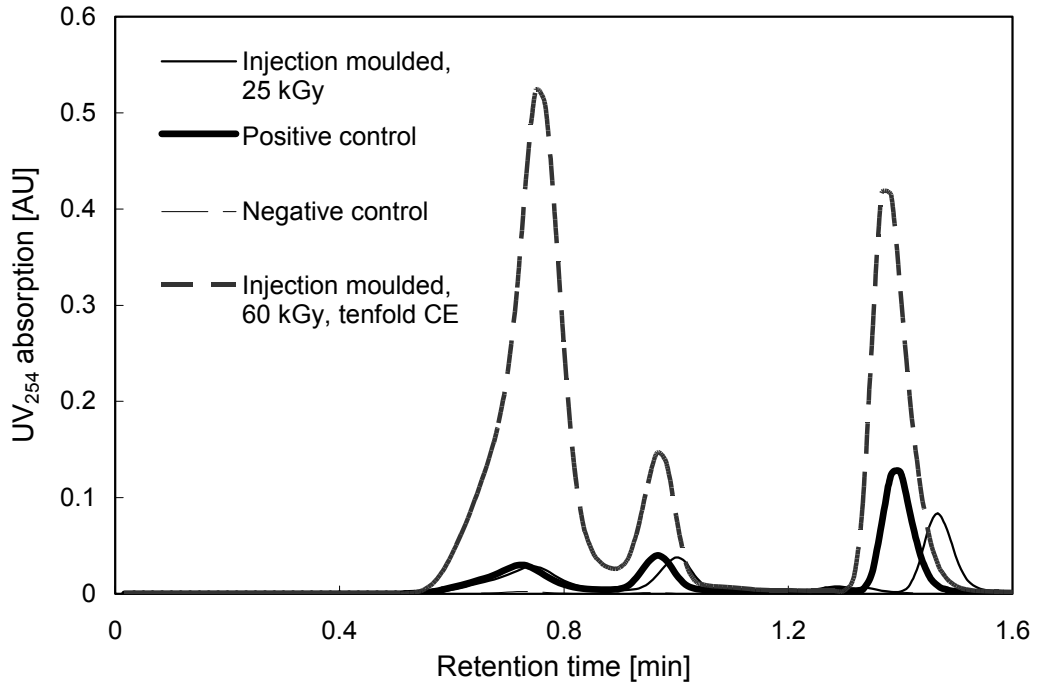

Fig. 78 *Chromatograms of an injection moulded sample, positive and negative control samples. The positive control was an empty testing chamber with a CE solution. The negative control was similar, but was placed in buffer solution without CE.*

Fig. 79 illustrates the progressive MDA release of the polymer samples during cholesterol esterase incubation with a physiologically relevant enzyme activity. All specimens released MDA increasingly over a period of 28 days. No constant level was achieved during this period. This characterising decomposition behaviour was also observed in the injection moulded samples, which were incubated with a 10-fold increased CE activity. There, a mean constant level of $377 \pm 2.2 \cdot 10^{-4}$ ppb MDA (Fig. 80) was obtained after 20 days. The latter accumulated amount of 377 ppb is almost 30,000 to 55,000 times larger when compared to the physiologically incubated implant samples, $0.013 \pm 3.9 \cdot 10^{-4}$ ppb and $0.007 \pm 1.5 \cdot 10^{-4}$ ppb.

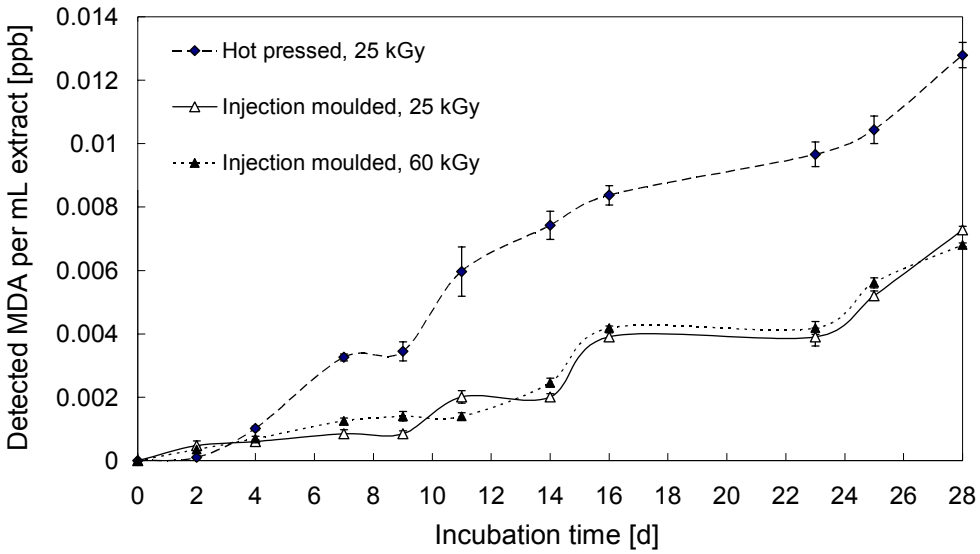

Fig. 79 *MDA release from GORD implant samples exposed to a physiologically normal level of CE. The MDA release is increased overtime, even for the ten incubation days, where the CE concentration was held constant.*

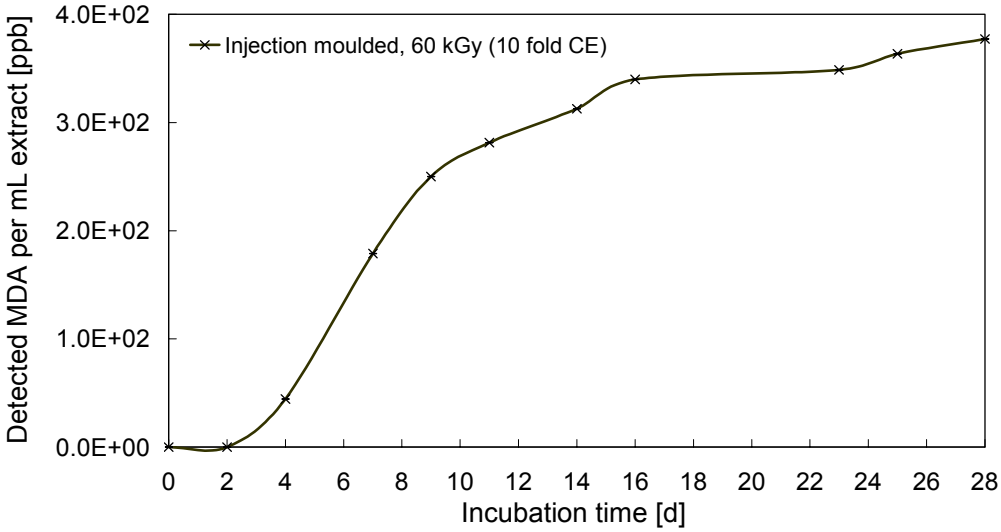

Fig. 80 *MDA release from GORD implant samples exposed to a tenfold of a physiologically normal CE level. The amount of MDA released is 50 000 times higher and reaches a plateau when the CE concentration is kept constant*

Fig. 81 shows the calculated MDA release (n=3) of the entire GORD implant after a 28 day incubation period with cholesterol esterase based on the released MDA amounts per mL extract

(Fig. 79). The numbers on each bar are the mean values with standard deviations. The error bars of the standard deviations are not visible due to the logarithmic scale.

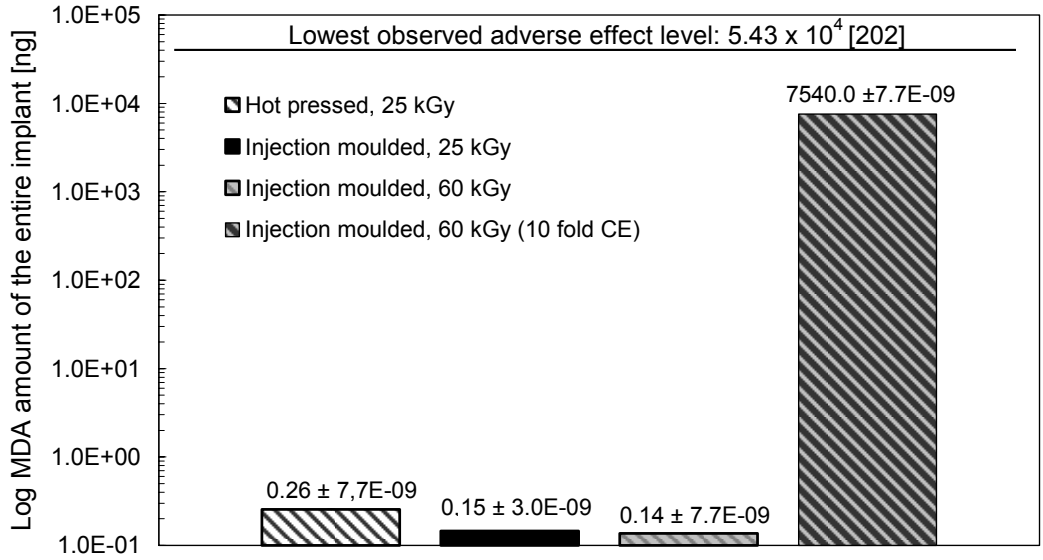

Fig. 81 *Mean MDA release from CE incubated entire GORD implant after 28 days of incubation. The sample that performed best was the injection moulded γ-sterilised at 60 kGy.*

The lowest MDA concentration was released from the GORD implant that was manufactured by injection moulding. The progressive MDA levels and the accumulated value seem to be independent of the γ-irradiation dose (±0.01 ng). Almost double of the MDA amount, 0.26 $\pm 7.76 \cdot 10^{-9}$ ng, was detected in the polymer extracts from the hot pressed samples. The considerably elevated processing time (30 minutes in contrast to a few seconds with injection moulding) can be seen as a potential reason. These MDA amounts are still considerably lower (factor 30,000) in contrast to the sample which was incubated with ten times the increased CE activity. Here a total of $7.5 \pm 7.76 \times 10^{-9}$ µg MDA was released after 28 days. However, all samples were well within the LOAEF [204] toxicity level.

The mean accumulated MDA release (± SD) from the entire implant resulted in a range from 0.136 ± 0.003 ng to 0.256 ± 0.008 ng. From a medical point of view, MDA must be thoroughly monitored due to its carcinogenic potential, which was observed in Weinberger's animal study [205]. The released MDA doses in our study are harmless when comparing the detected amounts with data from literature

[204]. The half-life of MDA-hydrolysed urine is reported to be 70 to 80 hours and 21 days in serum [203, 206]. No data was available for MDA in the gastric region. In the calculation, the half time was not considered and MDA was assumed to constantly accumulate. Hence, the calculated accumulated values represent a worse case scenario.

Incubation with a tenfold increase of CE enzyme activity reveals an elevated mean MDA release of 7540 µg. This enzyme activity was initially defined to simulate an extremely strong inflammation and an abnormal cholesterol esterase attack. However, this value is still more than 8 times lower than LOAFL (54.3 mg) [204]. Table 11 summarises the estimated MDA releases from the entire GORD prosthesis based on our biodegradation test conditions.

Polymer processing method	**Sterilisation γ-dose [kGy]**	**Mean amount of MDA released ±SD [nano g]**	**Incubation enzyme activity**
Hot pressing	25	0.256 ± 0.008	physiological
Injection moulding	25	0.146 ± 0.003	physiological
Injection moulding	60	0.136 ± 0.003	physiological

Table 11 *Accumulated MDA release from the implant based on measured values from samples, which were 1/10 of the entire implant, after a 28 days incubation period.*

The MDA release from the tenfold CE activity compared to the physiological value, shows that the CE enzyme is indeed extremely aggressive towards the polyether-urethane, which has already been described by several scientist [143, 150-152, 160, 200, 207, 208]. Several authors have used techniques such as radiolabelling and MS to detect the small quantities, which is released through a degradation study [151, 152, 209]. This study has shown that the detection of MDA is possible for low quantities (<pg) by means of modern columns and HPLC chromatographic techniques.

CHAPTER VIII
Conclusions and outlook

1 Conclusions

1.1 Processing

It has been proven that moisture (H_2O), which is always removed from granules prior to polymer processing, can be used to form a porous structure with a defined pore size diameter. A new processing method for a porous polymer has been established. This method has been utilized to produce an implant to treat oesophageal reflux disease. The method utilizes thermal mixing of NaCl particles of 200-500 μm and polyether-urethane (Fig. 82). The polymer/NaCl granules were exposed to a humid atmosphere, where the granules absorbed water. After that, the polymer/NaCl granules containing H_2O were plasticized by hot pressing or injection moulding. Due to the applied heat, the water evaporated but could not leave the polymer due to the low diffusion rate and was, therefore, evenly distributed in the melted polymer. By applying a sudden pressure drop, a thermodynamically unstable state was generated. This forced the moisture to form nucleation sites. In these sites, pores were produced. After the polymer had vitrified, the produced samples were placed in water. The previously added NaCl particles were leached out and left behind interconnective pores.

The method was tested on two different processing machines (hot pressing and injection moulding) successfully. The GORD implant, defined in Chapter I, was obtained with the required porous structure for both processing methods.

This study showed that the main important parameters that influenced the pore building were filling volume, NaCl-concentration, temperature, time and water-uptake rate. Decreasing filling volume and increasing NaCl-concentration, temperature, time and water-uptake rate increased the pore size and the porosity of the porous structure. Hence the pore structure was adjustable. The leaching process period was shorten by using an ultra sonic bath and was speeded up at about three

times, compared to conventional methods. Seven days was needed for complete dissolution of the NaCl particles.

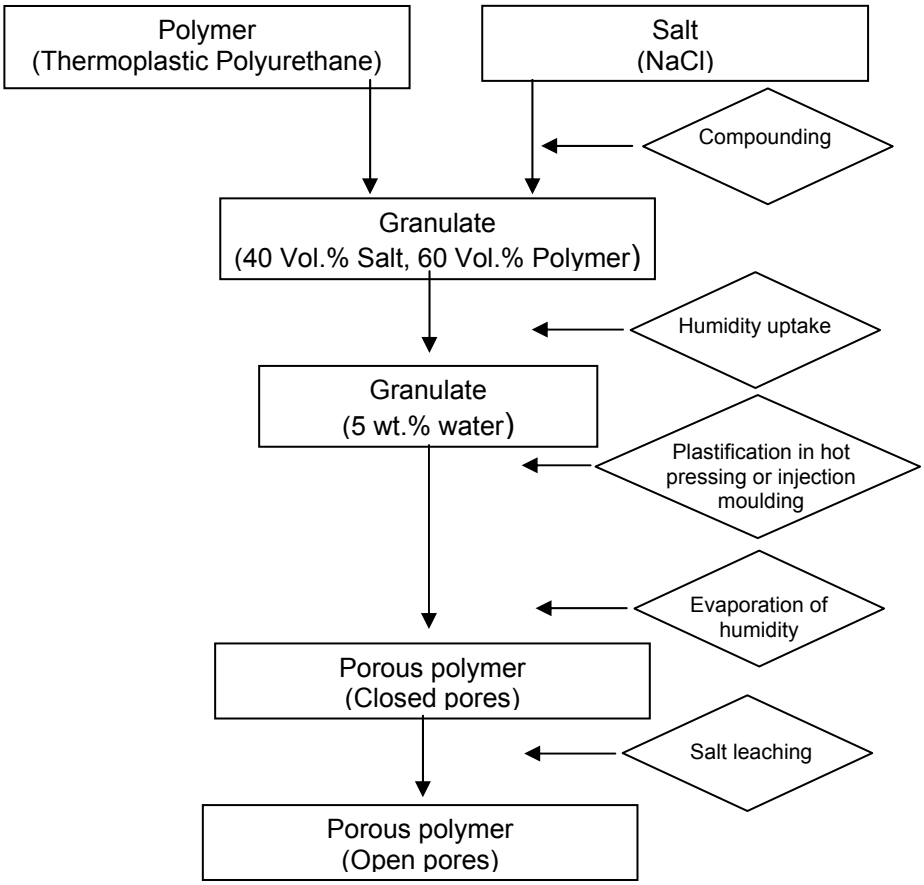

Fig. 82 *Flow chart of the new production method developed in this study to produce biocompatible porous structures*

The GORD implant processed in this study with a NaCl-concentration of 46 vol.% and a water-uptake rate of 5 wt.% led to a porosity of about 64% and a pore size ranging from 50 µm to 500 µm when applied to the heated press (Fig. 83). No significant chemical changes of the polyether-urethane were found with an ATR FT-IR analysis, where pure unprocessed granules were used as control.

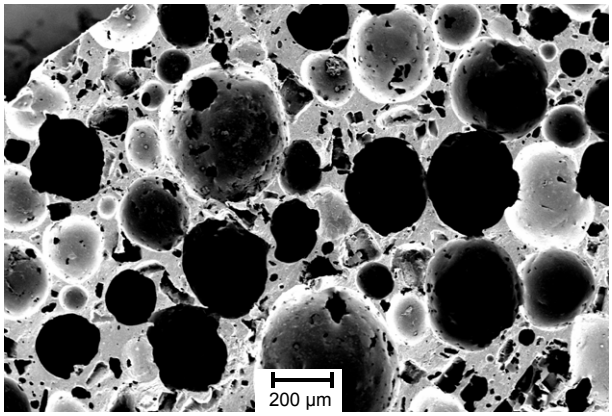

Fig. 83 *Cross section of the GORD implant produced by hot pressing*

It has been demonstrated for the injection moulding that the pore structure (pore size, porosity and interconnectivity) depended on several adjustable processing parameters. The porosity and pore size were adjustable by the NaCl-amount and water-uptake rate. In addition to NaCl-concentration of 40% and a water-uptake rate of 5%., pore size and porosity was adjustable by the plasticize – rotation, -speed and –pressure, by tool- and cylinder temperature. A rotation of 20 rpm, a speed of 5 mm/s and a pressure of 10 bar were adjusted for the plasticize unit. The mould temperature was kept at 70°C and the cylinder temperature at 220°C. The most important parameters were the injection pressure and the injection temperature. A short overview of the parameters above discussed is presented in Table 12.

Investigated parameter	**Effect on pore size diameter**	**Effect on porosity**
plasticizing speed	increased	unchanged
plasticizing rotation	decreased	unchanged
plasticizing pressure	increased	unchanged
mould temperature	increased	increased
cylinder temperature	increased	increased
NaCl concentration	slight increased	slight increased

Table 12 *Overview of the effect on pore structure important injection moulding parameters (Effects as the parameters are increased).*

The most favourable processing parameters for generate the required pore structure for the GORD implant on the injection moulding machine were found through a parameter study (Table 13).

Ideal parameters	Value
Plasticizing rotation	20 rpm
Plasticizing speed	3 mm/s
Plasticizing pressure	10 bar
Mould temperature	70°C
Cylinder temperature	220°C
Injection pressure	800 bar
Injection speed	38 mm/s
NaCl content	50 vol.%
Moisture	5 wt.%

Table 13 *The most favourable processing parameters for the GORD implant on the injection moulding machine.*

When applying these parameters to the injection moulding machine, it was possible to produce implants with a porosity of 64%, a pore size distribution from 30 – 450µm, and a mean pore diameter of 270µm. The interconnective pores were found to lie between 5 and 58 µm. The added NaCl particles, which generate these interconnections, were crushed by the injection moulding's screw to 1/10 of their original size. A SEM micrograph of the structure inside the GORD implant is presented in Fig. 84.

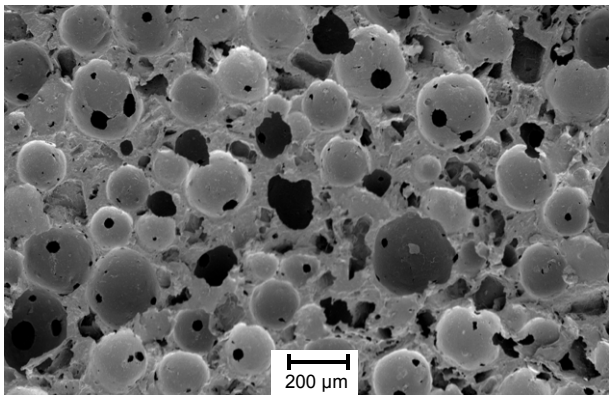

Fig. 84 *Cross section of the GORD implant produced by injection moulding with the optimal processing parameters.*

Moulds for hot pressing and injection moulding were successfully constructed to produce the GORD implant. The constructed moulds produced the GORD implants very well. The one for the injection moulding was capable of producing six implants within 1 minute, whereas the heated press needed 30 minutes for one. The implants had a solid outer layer after processing, which was

mechanically removed to expose the porous core. This core had a uniform porous structure. The standard deviation of pore structure within one ring was 2 % (n=7). The deviation on the six implants, which were simultaneously injection moulded, was found to be 5% (n=36).

Analysis of the implants after processing revealed that only minor alteration to their chemical structures had occurred. Mechanical analysis showed doubled tensile strength and elongation of break for injection moulded implants versus the hot pressed.

1.2 Biocompatibility testing

Biocompatibility tested proved that only a slight decrease in cell cytotoxicity was present from the injection moulded GORD implant (Mean optical density = 80%). The sample for the hot pressed had mean value optical density of about 20% lower than the injection moulded one. The best overall performing processing method was, therefore, injection moulding. Cell seeding studies also showed that fibroblasts adhered to the surface and proliferated. The spread of the adhered fibroblasts was uniform on the surface. This cell layer thickened with increased incubation time.

Initial 3D seeding failed, as the GORD implant at this stage did not have enough interconnective pores. These seeding tests were not repeated after modifying the injection moulding parameter to increase the number and pore size of the interconnective pores.

It has been proven that it was possible to produce biocompatible porous structures on an industrial polymer production machine with the novel technique of using water as a foaming agent.

1.3 Fitting foaming theory to experimental data

The pore development of the moisture content in the polyether-urethane may be described by the nucleation theory [108]. Chapter III dealt with the modelling of the pore growth and porosity using water as a foaming agent in polyether-urethane. The nucleation theory revealed that several parameters govern pore growth. Pressure drop seemed to be the main driving force for pore growth, whereas the porosity was dependent on the amount of gas dissolved in the polymer and gas diffusion rate. These parameters were again dependent variables on temperature, pressure and

its rate of change. It was shown that the Gibbs free energy, which was the pressure barrier initiate nucleation, was heavily dependent on pressure. The same results were found in the experiments. However, the theory predicted a plateau at 1000 bar for the Gibbs free energy. At higher pressure, the Gibbs free energy would be constant, which meant that at higher injection pressure pore growth could not be altered. This situation was not observed. A 10% alteration for injection pressure (from 1000 to 1100 bar) resulted in a doubling of the pore size diameter. This observation would also be applied to lower pressure changes. The model also described that the pore building would depend on diffusion (Peclet number) and solubility, where an increase in temperature would produce larger pores. This fact was supported by the experiments. One can conclude that the effect of the processing parameters followed the Shafi model, but the calculated numbers did not correspond with the experiments.

1.4 Sterilisation method

This study has shown, in contrast to Zhang [210], that it was possible to detect differences by thermal analysis in polyether-urethane sterilised by γ-radiation and steam sterilisation. The crystallinity of the material decreased with higher γ-radiation doses. The reason was that the energy input by the irradiative waves cross linked monomers and molecular chains within the polyether-urethane. GPC analysis supported this theory where an increase in molecular weight and polydispersity were observed by increasing irradiative strength.

Steam sterilisation showed no crystalline regions and had the lowest molecular weight of all samples test. This sterilisation method also generated MDA, the most toxic degradative compound for polyether-urethane, in such amounts that it had a large impact on the biocompatibility. The OD decreased by only 20% during the steam sterilisation of the GORD implants. The γ-irradiative samples showed a different behaviour, where the 60 kGy dosed samples had an OD of 90% ± 3%, and decreased evenly with lower radiation doses. MDA was not found in samples sterilised at 25 kGy and 60 kGy. This was due to the high irradiation energy, which bounded the MDA back into the polymer structure. It is, therefore, recommended that the GORD implant should be γ-radiated at 25 kGy or higher.

1.5 Degradation studies

The goal of this section was to compare two different processing methods for the GORD implant, as well as the effect of high γ-sterilisation dosage as it relates to resistance against degradation. Degradation may release compounds at toxic levels. Biodegradation tests were conducted with four different polyether-urethane samples, following incubation with an inflammation enzyme. Cholesterol esterase (CE) attack over 28 days caused methylene dianiline (MDA) release from all test specimens. Very low amounts of MDA were released and their concentrations were well within safe toxic levels (<50 000), according to LOAFEL [204]. The mean accumulated MDA released from the entire implant (injection moulded, γ-sterilised with 60 kGy) was found to be 0.136 ng. The mean released MDA amounts were constant for lower γ-sterilised doses, but double for these implants processed with the heat press 0.256 ± 0.008 ng (n=3). Incubation with a tenfold increased CE enzyme activity revealed a considerable elevated MDA release 7540 ± 0.004 µg (n=3). This enzyme activity was initially employed to simulate an extremely strong inflammation and an abnormal cholesterol esterase attack. However, this value is still more than 8 times lower than the lowest observed adverse effect level (54.3 mg) [204]. The amount of MDA released at normal physiologically enzyme levels did not reach a plateau during the test period, which was the case with CE concentrations ten times higher.

1.6 Summary

The main goal of the project has been reached. It has been shown that a biocompatible porous structure could be industrially produced with injection moulding and hot pressing through the newly developed processing method. The desired porous structure may be obtained by either hot pressing or injection moulding. The pore size and porosity was adjustable by altering the processing parameters. It has also been demonstrated that a GORD implant, with a porous inner surface and solid outer coating, can be processed applying this water foaming method on these machines. Biocompatibility tests and enzymatic degradation studies have proven that the injection moulded GORD samples performed better. Enzyme degradation products were found to lie within safe toxic levels when using either machine. The injection moulding machine was also capable of producing far more implants per unit time compared to hot pressing. Material analysis and cell toxicity tests revealed that the most desirable sterilisation method was γ-sterilisation, with a minimum dose of 25 kGy.

2 Outlook

Since the injection moulding machine performed better in all test and was capable of producing more implants per unit time compared to hot pressing, it was useless to continue producing the GORD implant with the latter method. Even tough the goals of the project having been met, some modifications on the machine are still necessary.

The shear rate of the plastification screw crushed the NaCl particles (200 – 500 µm) to a size of approximately 10 µm. Some particles were seen in SEM images to be even smaller. Hence, NaCl particles mixed with the polyether-urethane must have a size from 500 to 800 µm to ensure even more interconnections. After injection moulding, the implants had a smooth surface. A cylindrical metal punch was used to expose the open porous structure of the inner-side of the implant. This method is time consuming and should be automated. A water-jet cutting tool would provide a finer cut and reduce labour time. A rotating placer has to be developed for this procedure to ensure that the interface between the solid and porous surface is kept smooth. Sharp edges are not desirable for an implant as excessive connective tissue formation could be induced.

The porous structure was found to be sensitive to injection pressure. Means must be found to keep this parameter stable for longer production cycles. It is also recommended that a production testing protocol should be established to ensure good quality.
In this study water was used as a blowing agent. A new technology called MuCell®, where CO_2 is used as a blowing agent, was recently installed on the injection moulding machine. The potential advantages of this method compared to the one used in this study would be worth to be examined.

The testing chamber for the enzymatic degradation study, including paraffin wax and silicone, is not recommended for further studies. These components released degradation products, which interfered with the detection of the all degradation products from the GORD implant. It is advisable to prolong the incubation time and to analyse the polyether-urethane behaviour further.

The cell studies showed that the optical density biocompatibility of the implant increased by increasing γ-sterilisation dosage. The reason was assumed to be the cross linkage of free monomers. A study on the

surface modification through the radiation was not conducted, but is worth looking into. A device with a plug connector has been designed to function as a closing mechanism (Fig. 85). The plug can be pulled to different positions in order to fit any oesophagus' diameter. Adequate application instrument for the implantation is under development in a collaborative research group.

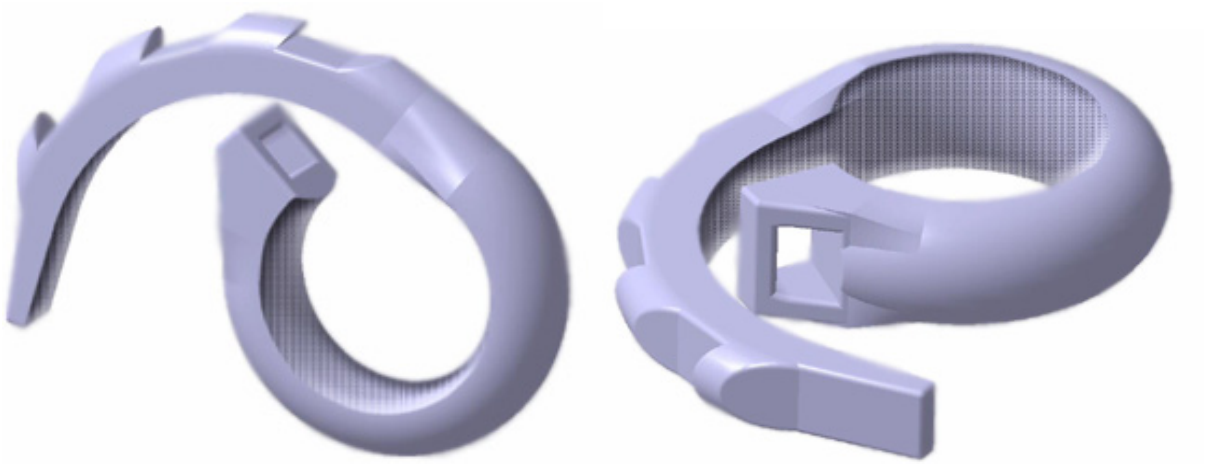

Fig. 85 *Model of the closing mechanism on the GORD implant, where the plug connector is inserted into a socket. The implant can be adjusted to the desired size by pushing the plug through the socket (Scale 1:1).*

FEM analysis with the standard setup in the CAD-software CATIA V.5 has been performed to analyse the mechanical stability when different levels and types of stresses are applied to the implant. A simulation of the behaviour of the socket when the plug was pulled through is displayed below. Fig. 86 A displays the implant without any stresses and Fig. 86 B shows the stress distribution when the socket is stretched to its maximum (100% elongation). The latter diagram shows a maximum stress peak of 2.6 MPa and a minimum of 2.3 MPa.

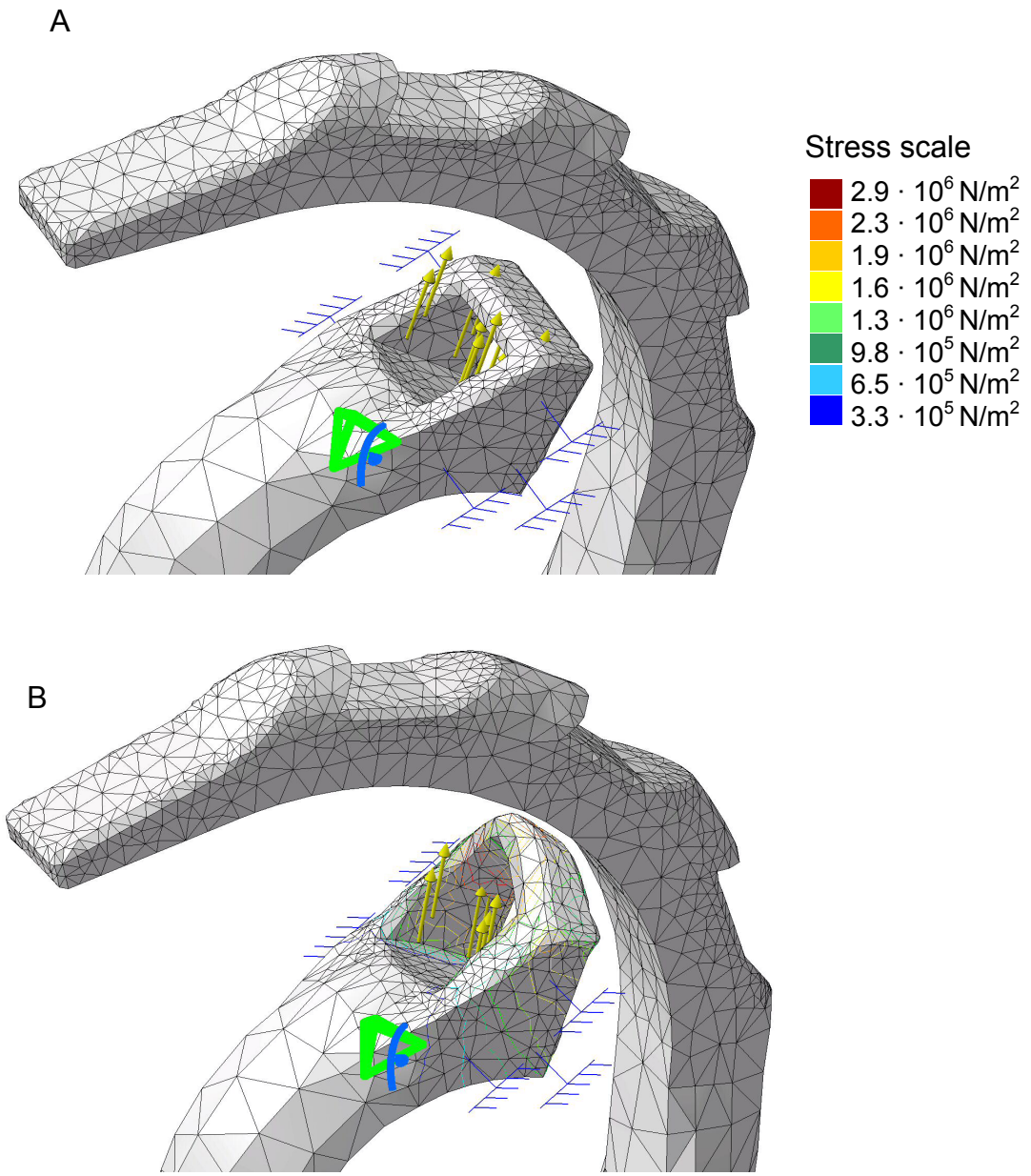

Fig. 86 *FEM analysis of the closing mechanism on the GORD implant. This model simulates the stress on the bracket as the connector is pushed through by 100% elongation.*

Furthermore, test on the stress distribution on the sockets as the connector has been pushed through the bracket, was performed (Fig. 87). The maximum stress was 0.22 MPa for the sockets and was situated at the top of the socket (Fig. 87 A). The peak stress for the bracket was 0.24 MPa (Fig. 87 B). All these values are within the safety factor of four. The initial test showed satisfactory results but should be refined in Marc Patran.

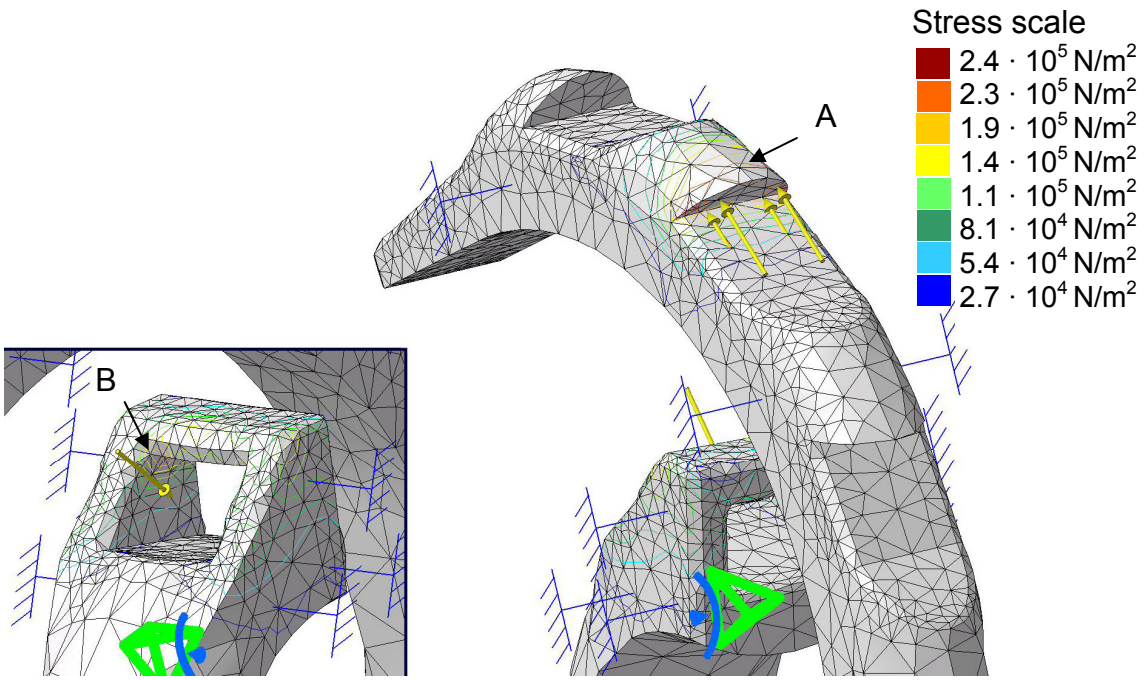

Fig. 87 *FEM analysis of the closing mechanism on the GORD implant. This model simulates the stress on the socket as the connector has been pushed through the bracket.*

Following design a mould for producing this model should also a surgery instrument be made in order to test it functionality and reliability. Valuable input from surgeons could then be acquired to ensure for the best possible implant results. Animal testing should be used to confirm the long term biocompatibility and anti-refluxing functionality of the implant.

Nomenclature

A	Surface area of the riser strips
AAP	Angelchik antireflux prosthesis
ATR FT-IR	Annotated total reflexion Fourier transform infrared
AU	Absorption units
b	Thickness
CE	Cholesterol Esterase
c_S	Nucleation threshold
C_0	Concentration
c	Dissolved gas concentration
c_p	Specific heat capacity
D	Gas diffusivity in polymer melt
DIN	Deutsches Institut für Normung
DSC	Differential scanning calorimetry
DMSO	Dimethylsulfoxid
E	E-Modulus
EDX	Energy dispersive X-ray analysis
ESC	Environmental stress cracking
ESI	Electronspray Ionisation
EthD	Ethidiumhomodimer
f_0	Frequency factor
F	Maximum clamping pressure
FBGC	Foreign body giant cells
F_K	Flexural stress on riser strips
$F_{K,}$	Flexural stress
FV	Filling volume
ΔG_n	Free energy of formation of pore of size n
GORD	Gastro-Oesophageal Reflux Disease
Gy	Gray [1 J/kg]
HPLC	High Performance Liquid Chromatography
h	Height
I	Moment of inertia of area
J_S	Steady state nucleation rate
k	Boltzmann constant
K	Henry's law constant
LC	Liquid chromatography
L_K	Free flexural length
LOS	Lower oesophageal sphincter
M	Highest order of polynomials
M_b	Bending moment
MDA	Methylene dianiline, diamino-diphenylmethane
MDI	Methylene-diphenyl-diisocyanate
MDMs	Monocyte-derived macrophages
MIC	Methyl isocyanate
MS	Mass spectrometry
MTT	3-(4,5-dimethylthiazolyl-2)-2,5-diphenyltetrazolium bromide

N	Density of dissolved gas
n	Number of measured values
N_B	Number of pores per cm^3
N_G	Free energy number
N_{homo}	Number of nuclei formed per second
N_{Pl}	Dimensionless ambient pressure
N_{Pe}	Péclet number
N_{Sl}	Solubility number
OD	Optical density
P	Pressure
PBS	Phosphate Buffered Saline
PhI	Phenyl isocyanate
PMT	Photomultiplier
$PMNs$	Polymorphonuclear leukocytes
PPI	Proton pump inhibitor
R^2	Stability index from regression analysis
r	Radial coordinate
Re	Reynolds number
R	Pore radius
$\dot{R}$	Pore growth rate
$\mathfrak{R}$	Gas constant
S	Radial position where the dissolved gas concentration is equal to the nucleation threshold
s	Wall thickness of sprue
SEM	Scanning electron microscopy
SIM	Single ion monitoring
SIR	Single ion recording
S_K	Safety factor
STA	Simultaneous temperature analysis
SD	Standard deviation
t	Time
t	Depth of riser strips
T	Temperature
t'	Time when pore nucleated
TPU	Thermoplastic polyether-urethanes
U	Unit
V	Volume
$UV\text{-}Vis$	UV-Visible Spectrometry
W_b	Stress resistance
$WST\text{-}1$	4-[3-(4-jodophenyl)-2-(4-nitrophenyl)-2H-5-tertazolio]-1,3-benzene disulfonate
Z	Zeldovich factor

Greek letters:

ρ	Density
ν	Kinematic viscosity
η	Melt kinematic viscosity
χ	Mole fraction
σ	Stress
σ	Surface tension
β	Surface area of critical nuclei
λ	Thermal conductivity
τ	Time elapsed since pore was nucleated

Superscript

*	Dimensionless quantities
0	Base case values listed in Table 2

Subscript

0	Quantities before the onset of nucleation
all	Allowed
b	Bending
c	Cooling
crit	Critical
d	Compressive
F,bend	Safety factor, bending stresses
F,S c	Safety factor, compressive stress
G	Inside pore
i	Impinge
L	Ambient
p	Polymer
sb	Static bending stress factor

List of figures

List of tables

References

[1] Lagergren, J., et al., Symptomatic gastroesophageal reflux as a risk factor for esophageal adenocarcinoma. The New England Journal of Medicine, 340, 11 (1999), 825-831.

[2] Powell, J. and McConkey, C.C., The rising trend in oesophageal adenocarcinoma and gastric cardia. European Journal of Cancer Prevention, 1, 3 (1992), 265-269.

[3] Blot, W.J., et al., Rising incidence of adenocarcinoma of the esophagus and gastric cardia. Journal of the American Medical Association : JAMA, 265, 10 (1991), 1287-1289.

[4] Hansson, L.E., Sparen, P., and Nyren, O., Increasing incidence of both major histological types of esophageal carcinomas among men in Sweden. International Journal of Cancer, 54, 4 (1993), 402-407.

[5] Pera, M., et al., Increasing incidence of adenocarcinoma of the esophagus and esophagogastric junction. Gastroenterology, 104, (1993), 510-513.

[6] Landis, S.H., et al., Cancer statistics, 1999. Cancer Journal for Clinicians, 49, (1999), 8-31.

[7] Bytzer, P., et al., Adenocarcinoma of the esophagus and Barrett's esophagus: a population-based study. The American Journal of Gastroenterology, 94, 1 (1999), 86-91.

[8] Devesa, S.S., Blot, W.J., and Fraumeni, J.F., Jr., Changing patterns in the incidence of esophageal and gastric carcinoma in the United States. Cancer, 83, 10 (1998), 2049-2053.

[9] Petersen, H., The prevalance of gastro-oesophageal reflux disease. Scandinavian journal of gastroenterology, 30, (Suppl. 211) (1995), 5-6.

[10] Bashford, J.N.R., Norwood, J., and Chapman, S.R., Why are patients prescribed proton pump inhibitors? Retrospective analysis of link between morbidity and prescribing in the General Practice Research Database. British Medical Journal, 317, 7156 (1998), 452-456.

[11] Royal College of General Practitioners, Morbidity statistics from general practice 1981–1982; third national study, Her Majesty's Stationary Office, London, 1986.

[12] O'Connor, J.B., Provenzale, D., and Brazer, S., Economic considerations in the treatment of gastroesophageal reflux disease: a review. The American Journal of Gastroenterology, 95, 12 (2000), 3356-3364.

[13] Johnston, B.T., The significance of heartburn. The Quarterly Journal of Medicine, 93, 6 (2000), 321-322.

[14] Allgöwer, M., et al., eds. Chirurgische Gastroenterologie. Refluxkrankheit, ed. Siewert, J.R. and Blum, A.L. Springer Verlag, Berlin 1981, pp. 291-305.

[15] Yamada, T., Reflux oesophagitis, In: Textbook of Gastroenterology, Orlando, R.C., Editor. JB Lippincott Co, Philadelphia, Pa. 1991, pp. 1123-1147.

[16] Beckmann, I.A., Speiseröhrenkrebs - ein Ratgeber für Betroffene, Angehörige und Interessierte. Deutsche Krebshilfe und Deutsche Krebsgesellschaft 2002.

[17] Lindsetmo, R.-O. and Paulssen, E.J., Endoskopisk cardiaplastikken ny behandlingsmetode ved gastroösofageal reflukssykdom. Tidsskrift for den Norske Laegeforening, 13, 122 (2002), 1282-1284.

[18] Edwards, D.A., The antireflux mechanism. Journal of Clinical Gastroenterology, 3, 2 (1981), 109-113.

[19] Miller, G. and Savary, M., Lóesophage Manuel et atlas d'endoscopie, Gassamann Sleure Suisse, Basel, Switzerland, 1977.

[20] Lundell, L.R., et al., Endoscopic assessment of oesophagitis: clinical and functional correlates and further validation of the Los Angeles classification. Gut, 45, 2 (1999), 172-180.

[21] Tauber, S., Gross, M., and Issing, W.J., Association of laryngopharyngeal symptoms with gastroesophageal reflux disease. Laryngoscope, 112, 5 (2002), 879-886.

[22] Rothstein, R.I. and Filipi, C.J., Endoscopic therapy for gastroesophageal reflux disease. Gastrointestinal Endoscopy Clinical North America, 13, 1 (2003), 7-14.
[23] Hogan, W.J., Endoscopic therapy for gastroesophageal reflux disease. Current Gastroenterology Reports, 5, 3 (2003), 206-212.
[24] Stein, H.J., Ambulante 24-h--Manometrie der tubulären Speiseröhre, In: Gastric Cancer, Siewert, J.R., Kelsen, D., and Maruyama, K., Editors. Springer-Verlag, Heidelberg, Germany 2001, pp. 47-60.
[25] Dent, J., et al., Mechanisms of lower oesophageal sphincter incompetence in patients with symptomatic gastrooesophageal reflx. Gut, 29, (1988), 1020-1028.
[26] Fennerty, M.B., et al., Gastroesophageal Reflux Disease. Hospital Medicine, 29, 4 (1988), 28-40.
[27] Prasad, M., Rentz, A.M., and Revicki, D.A., The impact of treatment for gastro-oesophageal reflux disease on health-related quality of life: a literature review. Pharmacoeconomics, 21, 11 (2003), 769-790.
[28] Hochberger, J., et al., Endoscopic antireflux treatment: fact, fiction or future? Drugs Today (Barc), 39 Suppl A, (2003), 21-28.
[29] Martini, G.A., Wienbeck, M., Does alcohol favour the development of Barret's syndrome (endobrachy-oesophagus)? Deutsche medizinische Wochenschrift, 99, 10 (1974), 434-439.
[30] Henderson, R.D. and Marryatt, G., Total fundoplication gastroplasty. Long-term follow-up in 500 patients. The Journal of Thoracic and Cardiovascular Surgery, 85, 1 (1983), 81-87.
[31] Isolauri, J., et al., Natural course of gastroesophageal reflux disease: 17-22 year follow-up of 60 patients. American Journal of Gastroenterology, 92, 1 (1997), 37-41.
[32] Cohen, S. and Parkman, H., Heartburn -- A Serious Symptom. The New England Journal of Medicine, 340, 11 (1999), 878-879.
[33] Haering, R. and Zilch, H., Chirurgie. 4th ed, de Gruyter, Berlin, 1997.
[34] Makkar, R.P. and Sachdev, G.K., Gastric asthma: a clinical update for the general practitioner. Medscape General Medicine, 5, 3 (2003), 4.
[35] Katunaric, M., et al., Some periodontological parameters in patients with oesophagogastric passage insufficiency. Collegium Antropologicum, 22 Suppl, (1998), 199-203.
[36] Spechler, S.J., Epidemiology and natural histroy of the gastro-oesophageal reflux disease. Digestion, 51, (suppl. 1) (1992), 24-29.
[37] Rosaida, M.S. and Goh, K.L., Gastro-oesophageal reflux disease, reflux oesophagitis and non-erosive reflux disease in a multiracial Asian population: a prospective, endoscopy based study. European Journal of Gastroenterology & Hepatology, 16, 5 (2004), 495-501.
[38] Fraser-Moodie, C.A., et al., Weight loss has an independent beneficial effect on symptoms of gastro-oesophageal reflux in patients who are overweight. Scandinavian Journal of Gastroenterology, 34, 4 (1999), 337-340.
[39] Richter, J.E. and Castell, D.O., Gastroesophageal reflux. Pathogenesis, diagnosis, and therapy. Annals of Internal Medicine, 97, 1 (1982), 93-103.
[40] Classen, M., Diehl, V., and Kochsiek, K., Innere Medizin. 3. neubearbeitete Auflage ed. Vol. 526, Urban&Schwarzenberg, München, Wien, Baltimore, Köln, Würzburg, 1994, pp. 540.
[41] Vigneri, S., et al., A Comparison of Five Maintenance Therapies for Reflux Esophagitis. The New England Journal of Medicine, 333, 17 (1995), 1106-1110.
[42] Katz, P.O., Gastroesophageal reflux disease. Reviews in Gastroenterological Disorders 3, 2 (2003), 118-120.
[43] Dekel, R., Morse, C., and Fass, R., The role of proton pump inhibitors in gastro-oesophageal reflux disease. Drugs, 64, 3 (2004), 277-295.
[44] Feussner, H., Treatment of gastroesophageal reflux disease: an european view. Digestive Endoscopy, 12, 2 (2000), 107-113.

[45] Fernando, H.C., et al., Quality of life after antireflux surgery compared with nonoperative management for severe gastroesophageal reflux disease. Journal of the American College of Surgeons, 194, 1 (2002), 23-27.
[46] Savarino, V. and Dulbecco, P., Optimizing symptom relief and preventing complications in adults with gastro-oesophageal reflux disease. Digestion, 69 Suppl 1, (2004), 9-16.
[47] Kawaura, Y., et al., Immunohistochemical study of p53, c-erbB-2, and PCNA in barrett's esophagus with dysplasia and adenocarcinoma arising from experimental acid or alkaline reflux model. Journal of Gastroenterology, 36, 9 (2001), 595-600.
[48] Benz, L.J., et al., A comparison of clinical measurements of gastroesophageal reflux. Gastroenterology, 62, 1 (1972), 1-74.
[49] Van Den Boom, G., et al., Cost effectiveness of medical versus surgical treatment in patients with severe or refractory gastroesophageal reflux disease in the Netherlands. Scandinavian Journal of Gastroenterology, 31, 1 (1996), 1-9.
[50] Anvari, M., Allen, C., and Borm, A., Laparoscopic Nissen fundoplication is a satisfactory alternative to long-term omeprazole therapy. British Journal of Surgery, 82, 7 (1995), 938-942.
[51] Fuchs, K.H., et al., Current status and trends in laparoscopic antireflux surgery: results of a consensus meeting. The European Study Group for Antireflux Surgery (ESGARS). Endoscopy, 29, 4 (1997), 298-308.
[52] Katada, N., et al., Laparoscopic Nissen fundoplication. Gastroenterologist, 3, 2 (1995), 95-104.
[53] Nissen, R. and Rossetti, M., Modern operations for hiatal hernia and reflux esophagitis: gastropexy and fundoplication. Archivio di Chirurgia del Torace, 13, (1959), 375-387.
[54] Lortat Jacob, J.L., Pathology and surgery of esophageal reflux. Medical Chirurgic Digest, 10, 3 (1981), 193-195.
[55] Stewart, GD, et al., Comparison of three different procedures for antireflux surgery. British Journal of Surgery ;91,6, (2004), 724-9.
[56] Hinder, R.A., et al., Laparoscopic Nissen fundoplication is an effective treatment for gastroesophageal reflux disease. Annals of Surgery, 220, 4 (1994), 472-481; discussion 481-473.
[57] Trondsen, E., et al., Day-case laparoscopic fundoplication for gastro-oesophageal reflux disease. British Journal of Surgery, 87, 12 (2000), 1708-1711.
[58] Klingler, P.J., et al., Laparoscopic antireflux surgery for the treatment of esophageal strictures refractory to medical therapy. American Journal of Gastroenterology, 94, 3 (1999), 632-636.
[59] Cohn, J.C., Klingler, P.J., and Hinder, R.A., Laparoscopic Nissen fundoplication as an ambulatory surgery center procedure. Today's Surgical Nurse, 19, 4 (1997), 27-30.
[60] Cadiere, G.B., et al., Laparoscopic Nissen fundoplication: technique and preliminary results. British Journal of Plastic Surgery, 81, 3 (1994), 400-403.
[61] Perdikis, G., et al., Laparoscopic Nissen fundoplication: where do we stand? Surgical Laparoscopy & Endoscopy, 7, 1 (1997), 17-21.
[62] Siewert, J.R., Histologic tumor type is an independant prognostic parameter in esophageal cancer: lessons from more than 1000 consecutive resections at a single center in the Western World: Siewert JR, Stein HJ, Feith M, Bruecher B, Fink U. Ann Surg 2001 ; 234 : 360-9. Annales de Chirurgie, 127, 2 (2002), 157-158.
[63] Jennings, R.W., et al., A novel endoscopic transgastric fundoplication procedure for gastroesophageal reflux: an initial animal evaluation. Journal of Laparoendoscopic Surgery, 2, 5 (1992), 207-213.
[64] Roy-Shapira, A., et al., Endoluminal methods of treating gastroesophageal reflux disease. Diseases of the Esophagus 15, 2 (2002), 132-136.
[65] Mason, R.J., et al., Endoscopic augmentation of the cardia with a biocompatible injectable polymer (Enteryx) in a porcine model. Surgical Endoscopy 16, 3 (2002), 386-391.

[66] Dua, K.S., et al., Self-expanding metal esophageal stent with anti-reflux mechanism. Gastrointestinal Endoscopy, 53, 6 (2001), 603-613.
[67] Hill, L.D. and Kozarek, R.A., The gastroesophageal flap valve. Journal of Clinical Gastroenterology, 28, 3 (1999), 194-197.
[68] Angelchik, J.P. and Cohen, R., A new surgical procedure for the treatment of gastroesophageal reflux and hiatal hernia. Surgical Gynecoligical Obstetic, 148, 2 (1979), 246-248.
[69] Swain, C.P. and Mills, T.N., An endoscopic sewing machine. Gastrointestinal Endoscopy, 32, 1 (1986), 36-38.
[70] Bonavina, L., et al., Surgical treatment of reflux stricture of the oesophagus. British Journal of Surgery, 80, 3 (1993), 317-320.
[71] Martinez-Serna, T., et al., Endoscopic valvuloplasty for gastroesophageal reflux disease. Gastrointestinal Endoscopy, 52, 5 (2000), 15A.
[72] Triadafilopoulos, G., et al., Radiofrequency energy delivery to the gastroesophageal junction for the treatment of GERD. Gastrointestinal Endoscopy, 53, 4 (2001), 407-415.
[73] Triadafilopoulos, G., et al., The Stretta procedure for the treatment of GERD: 6 and 12 month follow-up of the U.S. open label trial. Gastrointestinal Endoscopy, 55, 2 (2002), 149-156.
[74] Davies, R.P., Kew, J., and Byrne, P.D., Treatment of post-stent gastroesophageal reflux by anti-reflux Z-stent. Cardiovascular and Interventional Radiology, 23, 6 (2000), 487-489.
[75] Do, Y.S., et al., Malignant esophagogastric junction obstruction: palliative treatment with an antireflux valve stent. Journal of Vascular and Interventional Radiology, 12, 5 (2001), 647-651.
[76] Bowles, B.J., et al., Fifteen years' experience with an antirefluxing biliary drainage valve. Journal of Pediatric Surgery, 34, 11 (1999), 1711-1714.
[77] Young, M.A., et al., The Angelchik anti-reflux prosthesis (AARP) for gastroesophageal reflux disease (GERD): A 10 to 23 years follow up. American Journal of Gastreosurgery, 95, 9 (2000), 2442-2443.
[78] Maxwell-Armstrong, C.A., et al., Long-term results of the Angelchik prosthesis for gastro-oesophageal reflux. British Journal of Surgery, 84, 6 (1997), 862-864.
[79] Varshney, S., et al., Angelchik prosthesis revisited. World Journal of Surgery, 26, 1 (2002), 129-133.
[80] Willmen, H.R., Simplified laparoscopic surgery in reflux disease by a modified polyglactin scarf. Langenbecks Archiv fur Chirurgie. Supplement. Kongressband. Deutsche Gesellschaft fur Chirurgie, 113, (1996), 614-616.
[81] Horvath Ors, P., et al., Can gastroesophageal reflux be prevented by inducing a scar tissue ring around the cardia? Orv Hetil, 133, 28 (1992), 1751-1754.
[82] Feussner, H., Horvath, O.P., and Siewert, J.R., Vicryl-scarf-induced scarring around esophagogastric junction as treatment of esophageal reflux disease. An experimental study in the dog. Digestive Diseases and Sciences, 37, 6 (1992), 875-881.
[83] Feussner, H., et al., Experimental evaluation of the safety and biocompatibility of a new antireflux prosthesis. Diseases of the Esophagus 13, 3 (2000), 234-239.
[84] O'Connor, K.W. and Lehman, G.A., Endoscopic placement of collagen at the lower esophageal sphincter to inhibit gastroesophageal reflux: a pilot study of 10 medically intractable patients. Gastrointestinal Endoscopy, 34, 2 (1988), 106-112.
[85] Feretis, C., et al., Plexiglas (polymethylmethacrylate) implantation: technique, pre-clinical and clinical experience. Gastrointest Endosc Clin N Am, 13, 1 (2003), 167-178, xi.
[86] Feretis, C., et al., Endoscopic implantation of Plexiglas (PMMA) microspheres for the treatment of GERD. Gastrointestinal Endoscopy, 53, 4 (2001), 423-426.
[87] Louis, H. and Deviere, J., Endoscopic implantation of enteryx for the treatment of gastroesophageal reflux disease: technique, pre-clinical and clinical experience. Gastrointestinal Endoscopy Clinical North America, 13, 1 (2003), 191-200.

[88] FDA, GERD implant approved. FDA Consum, 37, 4 (2003), 7.
[89] Johnson, D.A., et al., Endoscopic implantation of enteryx for treatment of GERD: 12-month results of a prospective, multicenter trial. American Journal of Gastroenterology, 98, 9 (2003), 1921-1930.
[90] Hogan, W.J. and Shaker, R., A critical review of endoscopic therapy for gastroesophageal reflux disease. The American Journal of Medicine, 115 Suppl 3A, (2003), 201S-210S.
[91] van Tienen, T.G., et al., Tissue ingrowth and degradation of two biodegradable porous polymers with different porosities and pore sizes. Biomaterials, 23, 8 (2002), 1731-1738.
[92] Wake, M.C., Patrick, C.W., Jr., and Mikos, A.G., Pore morphology effects on the fibrovascular tissue growth in porous polymer substrates. Cell Transplantation, 3, 4 (1994), 339-343.
[93] Zeltinger, J., et al., Effect of pore size and void fraction on cellular adhesion, proliferation, and matrix deposition. Tissue Engineering, 7, 5 (2001), 557-572.
[94] Jemal, A., et al., Cancer Statistics, 2003. CA: Cancer Journal for Clinicians, 53, 1 (2003), 5-26.
[95] Thomson, R.C., et al., Hydroxyapatite fiber reinforced poly([alpha]-hydroxy ester) foams for bone regeneration. Biomaterials, 19, 21 (1998), 1935-1943.
[96] Mikos, A.G., et al., Preparation and characterization of poly(L-lactic acid) foams. Polymer, 35, (1994), 1068-1077.
[97] Thomson, R.C., et al., Polymer Scaffold Processing, In: The principles of tissue engineering, Lanza, R.P., Langer, R., and Vacanti, J., Editors. Academic Press, San Diego, USA 2000, pp. 251-261.
[98] Mooney, D.J., et al., Novel approach to fabricate porous sponges of poly(D,L-lactic-co-glycolic acid) without the use of organic solvents. Biomaterials, 17, 14 (1996), 1417-1422.
[99] McClurg, R.B., Nucleation rate and primary particle size distribution. Journal of Chemical Physics, 117, 11 (2002), 5328-5336.
[100] Rodeheaver, B.A. and Colton, J.S., Open-celled microcellular thermoplastic foam. Polymer Engineering and Science, 41, 3 (2001), 380-400.
[101] Goel, S.K. and Beckman, E.J., Nucleation and growth in microcellar materials: supercritical CO2 as foaming agent. International Journal of Multiphase Flow, 22, Supplement 1 (1996), 93.
[102] Delale, C.F., Hruby, J., and Marsik, F., Homogeneous bubble nucleation in liquids: The classical theory revisited. Journal of Chemical Physics, 118, 2 (2003), 792-806.
[103] Frenkel, J., Kinetic Theory of Liquids, Oxford University Press, Oxford, 1941.
[104] Abraham, F.F., Homogeneous Nucleation, Academic Press, New York/London, 1974.
[105] Skripov, V.P., Metastable Liquids, Wiley, New York/London, 1974.
[106] Reiss, H., The kinetics of phase transition in binary systems. The Journal of Chemical Physics, 18, (1950), 840-848.
[107] Kagan, Y., The kinetics of boiling of a pure liquid. The Russian Journal of Physical Chemistry, 34, (1960), 42-46.
[108] Lothe, J. and Pound, G.M., Reconsiderations of Nucleation Theory. The Journal of Chemical Physics, 36, (1962), 2080-2085.
[109] Feder, J., et al., Homogeneous nucleation and growth of droplets in vapors. Advances in Physics 15, (1966), 111-178.
[110] Katz, J.L. and Blander, M., Condensation and boiling: Corrections to homogeneous nucleation theory for nonideal gases. Journal of Colloid and Interface Science, 42, (1973), 496-502.
[111] Blander, M. and Katz, J.L., Bubble nucleation in liquids. American Institute of Chemical Engineerings Journal, 21, (1975), 830-848.
[112] Wilt, P.M., Nucleation rates and bubble stability in water-carbon dioxide solutions. Journal of Colloid and Interface Science, 112, (1986), 530-538.

[113] Colton, J.S. and Suh, N.P., The nucleation of microcellular thermoplastic foam;process model and experimental data. Advanced Manufacturing Processes, 1, 3/4 (1986), 341-364.
[114] Narsimhan, G. and Ruckenstein, E., A new approach for the prediction of the rate of nucleation in liquids. Journal of Colloid and Interface Science, 128, (1989), 549-565.
[115] Ruckenstein, E. and Nowakowski, B., A kinetic theory of nucleation in liquids. Journal of Colloid and Interface Science, 137, (1990), 583-592.
[116] Zurek, W.H. and Schiever, W.C., Molecular dynamics study of clustering. The Journal of Chemical Physics, 68, (1978), 840-846.
[117] Barlow, E.J. and Langlois, W.E., Diffusion of gas from a liquid into an expanding bubble. IBM Journal of Research and Develeopment, 6, (1962), 329-337.
[118] Street, J.R., Arthur, L.F., and Reiss, L.P., Dynamics of phase growth in viscous, non-Newtonian liquids. Industrial and Engineering Chemistry Fundamentals, 10, (1971), 54-64.
[119] Patel, R.D., Bubble growth in viscous Newtonian liquid. Chemical Engineering Science, 35, (1980), 2352-2356.
[120] Arefmanesh, A. and Advani, S.G. Modelling of bubble growth in viscoelastic foams. in The Winter Annual Meeting of the ASME. 1990.
[121] Amon, M. and Denson, C.D., A study of the dynamics of foam growth: analysis of the growth of closely spaced spherical bubbles. Journal of Polymer Science, 24, (1984), 1026-1034.
[122] Arefmanesh, A., Advani, S.G., and Michaelides, E.E., A numerical study of bubble growth during low pressure structural foam molding process. Journal of Polymer Science, 30, (1990), 1330-1337.
[123] Shafi, M.A., Joshi, K., and Flumerfelt, R.W., Bubble size distributions in freely expanded polymer foams. Chemical Engineering Science, 52, 4 (1997), 635-644.
[124] Zeldovich, J.B., On the theory of new phase formation; cavitation. Acta Physicochem, 18, (1943), 1-22.
[125] Reid, R.C., Parusnitz, J.M., and Poling, B.E., The properties of Gases and Liquids. 4th Edition ed, McGraw Hill Books Company, New York, 1986, pp. 644.
[126] Beckman, E.J. and Goel, S.K., Generation of Microcellular Polymeric Foams Using Supercritical Carbon Dioxide - 2: Effect of Pressure and Temperature on Cell Growth. Journal of Polymer Science, 14, (1994), 1148.
[127] Colton, J.S. and Suh, N.P., The nucleation of microcellular thermoplastic foam with additives. Part 1: Theoretical considerations. Polymer engineering & science, 27, 7 (1987), 485-492.
[128] Russell, K.C., Nucleation in solids: The induction and steady state effects. Advances in Colloid and Interface Science, 13, 3-4 (1980), 205-318.
[129] Goel, S.K. and Beckmann, E.J., Plasticization of poly(methylmethacrylate) (PMMA) networks by supercritical carbon dioxide. Polymer, 34, 7 (1993), 1410-1417.
[130] Goel, S.K. and Beckmann, E.J., Generation of Microcellular Polymers using Supercritical CO2. Cellular Polymers 2nd International Conference held at Heriot-Watt University, Edinburgh, UK, (1993).
[131] Beckman, E.J. and Goel, S.K., Generation of Microcellular Polymeric Foams Using Supercritical Carbon Dioxide - 1: Effect of Pressure and Temperature on Cell Density. Journal of Polymer Science, 14, (1994), 1137.
[132] Shen, V.K. and Debenedetti, G., A kinetic theory of homogeneous bubble nucleation. Journal of Chemical Physics, 118, 2 (2003), 768-783.
[133] DeWitt, D.P. and Incropera, F.P., Fundamentals of heat and mass transfer. 4th ed, John Wiley & Sons, New York, 1996.
[134] Shafi, M.A. and Flumerfelt, R.W., Initial bubble growth in polymer foam processes. Chemical Engineering Science, 52, 4 (1997), 627-633.

[135] Fujimoto, K., et al., Porous polyurethane tubes as vascular graft. Journal of Applied Biomaterials, 4, 4 (1993), 347-354.
[136] Matsuda, T. and Nakayama, Y., Surface microarchitectural design in biomedical applications: in vitro transmural endothelialization on microporous segmented polyurethane films fabricated using an excimer laser. Journal of Biomedical Materials Research, 31, 2 (1996), 235-242.
[137] Spaans, C.J., et al., Solvent-free fabrication of micro-porous polyurethane amide and polyurethane-urea scaffolds for repair and replacement of the knee- joint meniscus. Biomaterials, 21, 23 (2000), 2453-2460.
[138] Spector, M., et al., Porous polysulfone coatings for fixation of femoral stems by bony ingrowth. 176 (1983), 34-41.
[139] Whang, K., et al., Engineering bone regeneration with bioabsorbable scaffolds with novel microarchitecture. Tissue Engineering, 5, 1 (1999), 35-51.
[140] Thomson, R.C., Yaszemski, M.J., and Powers, J.M., Fabrication of biodegradable polymer scaffolds to engineer trabecular bone. Journal of Biomaterials Science - Polymer Edition, 7, 1 (1995), 23-38.
[141] Hutmacher, D.W., Scaffold design and fabrication technologies for engineering tissues- state of the art and future perspectives. Journal of Biomaterial Science Polymer Edition, 12, 1 (2001), 107-124.
[142] Lu, L. and Mikos, A.G., The importance of new processing techniques in tissue engineering. MRS Bulletin / Materials Research Society, 21, 11 (1996), 28-32.
[143] Lamba, N., Woodhouse, K., and Cooper, S., Polyurethanes in biomedical applications. CRC Press, Boca Raton, USA 1998, pp. 181-205.
[144] Beyersdorf, J., Polyurethan-Präpolymere zur Immobilisierung von lebenden Zellen und Enzymen - Entwicklung von Immobilisierungsverfahren und Charakterisierung der Biokatalysatoren, in Naturwissenschaftliche Fakultät. Technischen Universität Carolo-Wilhelmina: Braunschweig 1992.
[145] Lelah M. D., C.S.L., Polyurethanes in Medicine, CRC Press, Boca Raton, USA, 1986.
[146] Kiremitci, M., et al., Structural and cellular characterization of solvent-casted polyurethane membranes. Clinical Materials, 6, 3 (1990), 227-237.
[147] Saechtling, H., Kunststoff Taschenbuch. 28 ed, Carl Hanser, Munich, Germany, 2000, pp. 599.
[148] Menges, G., Michaeli, W., and Mohren, P., Anleitung zum Bau von Spritzgießwerkzeugen. 5 ed, Carl Hanser Verlag, München, 1999, pp. 513-518.
[149] Wintermantel, E. and Ha, S.-W., Medizintechnik mit biokompatiblen Werkstoffen und Verfahren., Springer-Verlag Berlin, 2002, 3rd ed., pp. 89.
[150] Labow, R., Duguay DG, and JP, S., The enzymatic hydrolysis of a synthetic biomembrane: a new substrate for cholesterol and carboxyl esterases. Journal of Biomaterial Science Polymer Edition, 6, 2 (1994), 169-179.
[151] Santerre, J.P., et al., Biodegradation evaluation of polyether and polyester-urethanes with oxidative and hydrolytic enzymes. Journal of Biomedical Materials Research, 28, 10 (1994), 1187-1199.
[152] Santerre, J.P., Labow, R.S., and Adams, G.A., Enzyme-biomaterial interactions: effect of biosystems on degradation of polyurethanes. Journal of Biomedical Materials Research, 27, 1 (1993), 97-109.
[153] Gerhardt, L.-C., Review regarding in-vitro test procedures to detect biodegradation products of thermoplastic polyurethanes. HIWI-Arbeit (ZIMT, H. Haugen), (2003), 1-12.
[154] Bayer AG, Desmopan, the link between rubber and engineering thermoplastics: Leverkusen 1998.
[155] Mathur, A.B., et al., In vivo biocompatibility and biostability of modified polyurethanes. Journal of Biomedical Materials Research, 36, 2 (1997), 246-257.

[156] Mazzu, A.L. and Smith, C.P., Determination of extractable methylene dianiline in thermoplastic polyurethanes by HPLC. J Biomed Mater Res, 18, 8 (1984), 961-968.
[157] Wen, T.-C., Du, Y.-L., and Digar, M., Compositional effect on the morphology and ionic conductivity of thermoplastic polyurethane based electrolytes. European Polymer Journal, 38, 5 (2002), 1039-1048.
[158] Harris, L.D., Kim, B.S., and Mooney, D.J., Open pore biodegradable matrices formed with gas foaming. Journal of Biomedical Material Research, 42, 3 (1998), 396-402.
[159] Tang, Y.W., Labow, R.S., and Santerre, J.P., Isolation of methylene dianiline and aqueous-soluble biodegradation products from polycarbonate-polyurethanes. Biomaterials, 24, 17 (2003), 2805-2819.
[160] Labow, R.S., Meek, E., and Santerre, J.P., Hydrolytic degradation of poly(carbonate)-urethanes by monocyte-derived macrophages. Biomaterials, 22, 22 (2001), 3025-3033.
[161] Tang, Y.W., Labow, R.S., and Santerre, J.P., Enzyme induced biodegradation of polycarbonate-polyurethanes: dose dependence effect of cholesterol esterase. Biomaterials, 24, 12 (2003), 2003-2011.
[162] Labow, R.S., Meek, E., and Santerre, J.P., Model systems to assess the destructive potential of human neutrophils and monocyte-derived macrophages during the acute and chronic phases of inflammation. Journal of Biomedical Materials Research, 54, 2 (2001), 189-197.
[163] Wintermantel, E., Medizintechnik mit biokompatiblen Werkstoffen und Verfahren.. Springer Verlag, Berlin 2002, 3rd ed., pp. 219-222.
[164] Schmitz-Moormann, P., et al., Verdauungsapparat. 1 ed. Grundlagen der klinischen Medizin, ed. 2, Schattauer Verlagsgesellschaft mbH, Stuttgart, New York, 1989, pp. 187.
[165] Kühnel, W., Taschenatlas der Zytologie, Histologie und mikroskopischen Anatomie, Georg Thieme Verlag, Stuttgart, New York, 1999, pp. 96.
[166] Lindl, T., Zell- und Gewebekultur. 4 ed, Spektrum - Akademischer Verlag, München, 2000, pp. 110.
[167] Sugarman, B.J., et al., Recombinant human tumor necrosis factor-alpha: effects on proliferation of normal and transformed cells in vitro. Science, 230, 4728 (1985), 943-945.
[168] Freshney, R.I., Culture of animal cells -a manual of basic techniques. 4th ed, John Wiley and Sons, New York, 2000, pp. 185-187.
[169] Belinsky, S.A., et al., Trypan blue uptake as a new method to investigate hepatotoxicity in periportal and pericentral regions of the liver lobule: studies with allyl alcohol in the perfused liver. The Journal of Pharmacology and experimental Therapeutics, 230, 3 (1984), 755-760.
[170] Medzihradsky, F. and Marks, M.J., Measures of viability in isolated cells. Biochem Med, 13, 2 (1975), 164-177.
[171] Schärfe-System, ed. Gebrauchsanleitung Casy 1 Model TT. ed. Schärfe System GmbH, Reutlingen 2000, pp. 4.
[172] Biologische Beurteilung von Medizinprodukten, in ISO 10993-5 1999.
[173] Girotto, D., et al., Tissue-specific gene expression in chondrocytes grown on three-dimensional hyaluronic acid scaffolds. Science direct, 24, 19 (2003), 3265-3275.
[174] Aigner, J., et al., Distribution and viability of cultured human chondrocytes in a three-dimensional matrix as assessed by confocal laser scan microscopy. In vitro Cellular & Developmental biology - Animal, 33, 6 (1997), 407-409.
[175] Hirata, N., et al., Gamma-ray irradiation, autoclave and ethylene oxide sterilization to thermosetting polyurethane: sterilization to polyurethane. Radiation Physics and Chemistry, 46, 3 (1995), 377-381.
[176] Lastbom, L., et al., Effects of thermal degradation products from polyurethane foams based on toluene diisocyanate and diphenylmethane diisocyanate on isolated, perfused lung of guinea pig. Scandinavian Journal of Work and Environmental Health, 29, 2 (2003), 152-158.

[177] Labow, R.S., Meek, E., and Santerre, J.P., Differential synthesis of cholesterol esterase by monocyte-derived macrophages cultured on poly(ether or ester)-based poly(urethane)s. Journal of Biomedical Materials Research, 39, 3 (1998), 469-477.
[178] Henson, P., Mechanisms of exocytosis in phagocytic inflammatory cells. American Journal of Pathology, 101, 3 (1980), 494-511.
[179] Inaba, T., et al., Macrophage colony-stimulating factor regulates both activities of neutral and acidic cholesteryl ester hydrolases in human monocyte-derived macrophages. The Journal of Clinical Investigation, 92, 2 (1993), 750-757.
[180] Lo, H., Ponticiello, M.S., and Leong, K.W., Fabrication of controlled release biodegradable foams by phase separation. Tissue Engineering, 1 (1995), 15-28.
[181] Balkovsky, E., Fouxon, A., and Lebedev, V., Turbulence of polymer solutions. Phyical Review, Series E, 64, 5 Pt 2 (2001), 056301.
[182] Szycher, M., Szycher's handbook of polyurethanes. CRC Press, New York 1999, pp. 22-21.
[183] Cheremisinoff, N.P., Encyclopedia of fluid mechanics, Gulf Publishing Co., Houston, Tex., 1986, pp. 10 bd.
[184] Granville, P.S., The frictional resistance and velocity similarity laws of drag-reducing dilute polymer solutions. Report / Naval Ship Research and Development Center 2502, Washington, D.C. ,, 1967, pp. vi, 34 s.
[185] Ravat, B., et al., Electron irradiation of polyurethane using UV spectroscopy, GPC and swelling analyses. Radiation Physics and Chemistry, 63, 1 (2002), 93-99.
[186] Lee, H.J. and Matsuda, T., Surface photograft polymerization on segmented polyurethane using the iniferter technique. Journal of Biomedical Materials Research, 47, 4 (1999), 564-567.
[187] Gheysari, D. and Behjat, A., Radiation crosslinking of LDPE and HDPE with 5 and 10 MeV electron beams. European Polymer Journal, 37, 10 (2001), 2011-2016.
[188] Bruck, S.D. and Mueller, E.P., Radiation sterilization of polymeric implant materials. Journal of Biomedical Materials Research, 22, A2 Suppl (1988), 133-144.
[189] Zahraoui, C. and Sharrock, P., Influence of sterilization on injectable bone biomaterials. Bone, 25, 1 (1999), 63S-65S.
[190] Shintani, H., The relative safety of gamma-ray, autoclave, and ethylene oxide gas sterilization of thermosetting polyurethane. Bio-medical instrumentation, 29, 6 (1995), 513-519.
[191] Sendijarevic, V., et al., Hydrolytic stability of toluene diisocyanate and polymeric methylenediphenyl diisocyanate based polyureas under environmental conditions. Environ Sci Technol, 38, 4 (2004), 1066-1072.
[192] Herrera, M., Matuschek, G., and Kettrup, A., Thermal degradation of thermoplastic polyurethane elastomers (TPU) based on MDI. Polymer Degradation and Stability, 78, 2 (2002), 323-331.
[193] Shintani, H., Formation and elution of toxic compounds from sterilized medical products: methylenedianiline formation in polyurethane. Journal of Biomaterials Applications, 10, 1 (1995), 23-58.
[194] Turi, E., Thermal Characterization of Polymeric Materials. 2.edition ed, Academic press, Oxford, 1997.
[195] Rudnik, E., Resiak, I., and Wojciechowski, C., Thermoanalytical investigations of polyurethanes for medical purposes. Thermochimica Acta, 320, 1-2 (1998), 285-289.
[196] Teo, L.-S., Kuo, J.-F., and Chen, C.-Y., Study on the morphology and permeation property of amine group-contained polyurethanes. Polymer, 39, 15 (1998), 3355-3364.
[197] Dickie, B.D., Investigation of an engineering thermoplastic polyurethane by MDSC. Thermochimica Acta, 304-305, (1997), 347-352.
[198] Glasmacher-Seiler, B., Zur Kalzifizierung von Polyurethan-Biowerkstoffen im kardiovaskulären System, in Helmholtz Institut. RWTH Aachen: Aachen 1991.

[199] Lamba, N., Woodhouse, K., and Cooper, S., Polyurethanes in biomedical applications, Boca Raton, USA, 1998, pp. 5.
[200] Santerre, J.P. and RS., L., The effect of hard segment size on the hydrolytic stability of polyether-urea-urethanes when exposed to cholesterol esterase. Journal of Biomedical Materials Research, 36, 2 (1997), 223-232.
[201] Shintani, H. and Nakamura, A., Formation of 4,4'-methylenedianiline in polyurethane potting materials by either g-ray or autoclave sterilization. Journal Biomedical Material Research, 25, (1991), 1275.
[202] Lamba, N., Woodhouse, K., and Cooper, S., Polyurethanes in Biomedical Applications. 1 ed, CRC Press, Boca Raton, Bosteon, London, New York, Washington, D. C., 1998, pp. 277.
[203] Skarping, G. and Dalene, M., Determination of 4,4'-methylenediphenyldianiline (MDA) and identification of isomers in technical-grade MDA in hydrolysed plasma and urine from workers exposed to methylene diphenyldiisocyanate by gas chromatography-mass spectrometry. Journal of Chromatography B: Biomedical Sciences and Applications, 663, 2 (1995), 209-216.
[204] CalEPA, California Environmental Protection Agency, Office of Environmental Health Hazard Assessment, Support Document for the Determination of Noncancer Chronic Reference Exposure Levels, Berkeley, CA
[205] Weisburger, E.K., et al., Neoplastic response of F344 rats and B6C3F1 mice to the polymer and dyestuff intermediates 4,4'-methylenebis(N,N-dimethyl)-benzenamine, 4,4'-oxydianiline, and 4,4'-methylenedianiline. Journal of the National Cancer Institute, 72, 6 (1984), 1457-1463.
[206] Littorin, M., et al., Acute respiratory disorder, rhinoconjunctivitis and fever associated with the pyrolysis of polyurethane derived from diphenylmethane diisocyanate. Scandinavian Journal of Work and Environmental Health, 20, 3 (1994), 216-222.
[207] Labow, R., Meek E, and JP, S., Synthesis of cholesterol esterase by monocyte-derived macrophages: a potential role in the biodegradation of poly(urethane)s. Journal of Biomaterials Applications, 13, 3 (1999), 187-205.
[208] Labow, R.S., Adams, K.A.H., and Lynn, K.R., Porcine cholesterol esterase, a multiform enzyme. Biochimica et Biophysica Acta (BBA) - Protein Structure and Molecular Enzymology, 749, 1 SU - (1983), 32-41.
[209] Wang, G.B., Labow RS, and JP., S., Biodegradation of a poly(ester)urea-urethane by cholesterol esterase: isolation and identification of principal biodegradation products. Journal of Biomedical Materials Research, 36, 3 (1997), 407-417.
[210] Zhang, Y.-Z., et al., Tissue response to commercial silicone and polyurethane elastomers after different sterilization procedures. Biomaterials, 17, 23 (1996), 2265-2272.
[211] Pulat, M. and Senvar, C., Structural and surface properties of polyurethane membranes of different porosities. Polymer Testing, 14, 2 (1995), 115-120.
[212] Lamba, N., Woodhouse, K., and Cooper, S., Polyurethanes in biomedical applications, Boca Raton, USA 1998, pp. 5.
[213] Anderson, J.M., Inflammatory response to implants. Transactions, 34, (1988), 101-107.
[214] Zhao, Q., et al., Foreign-body giant cells and polyurethane biostability:In vivo correlation of cell adhesion and surface cracking. Journal Biomedical Material Research, 25, (1991), 177.
[215] Stokes, K., Coury, A., and Urbanski, P., Autooxidative degradation of implanted polyether polyurethane devices. Journal of Biomaterials Applications, 1, (1987), 411.
[216] Pinchuk, L., A review of the biostability and carcinogenicity of polyurethanes in medicine and the new generation of biostable polyurethanes. Journal of Biomaterials Science, Polymer Edition, 6, 3 (1994), 225-267.
[217] Stokes, K., McVenes, R., and Anderson, J.M., Polyurethane elastomer biostability. Journal of Biomaterial Applications, 9, 4 (1995), 321-354.

[218] Joshi, R., et al., Phosphonated polyurethanes that resist calcification. Journal of Applied Biomaterials, 5, (1994), 65.
[219] Pierce, W.S., et al., Calcification inside artifical hearts: Inhibition by warfarin-sodium. Science, 9, (1980), 601.
[220] Dostal, M., et al., Mineralization of polyurethane membranes in the total artifical heart (TAH): a retrospective study from long-term animal experiments. International Journal of Artificial Organs, 13, (1990), 498.
[221] Zitats, N.P., Miller, K.M., and Anderson, J.M., In vitro and in vivo interactions of cells with biomaterials. Biomaterials, 9, 5 (1988).
[222] Bakker, D., et al., Tissue/biomaterial interface characteristics of four elastomers. a transmission electron microscopical study. Journal of Biomedical Materials Research, 24, 277 (1990).
[223] Mohanty, M., et al., Evaluation of soft tissue response to a poly(ether urethane ureas). Biomaterials, 13, (1992), 651.
[224] Wilkins, E.S., Tissue reaction to intraperitoneally implanted catheter materials. Journal of Biomedical Engineering, 13, (1991), 173.
[225] Fischer, U., et al., Tabellenbuch Metall. 42. ed, Verlag Europa-Lehrmittel, Haan-Gruiten, 2002, pp. 40-47.
[226] Niemann, G. and Hirt, M., Maschinenelemente. 2. ed, Springer-Verlag, Berlin, 1981, pp. 44-83.

Appendix A, TPU as biomaterial

1 Use of polyether-urethanes

Due to their physiological compatibility, relatively good blood tolerability, excellent stability over long implant periods and excellent physical and mechanical properties [146, 211], polyether-urethanes are widely used in blood-contacting applications, such as catheters, heart assist pumps and chambers for artificial hearts, *Table A.1* shows biomedical applications of polyether-urethane. In general, thermoplastic polyether-urethanes, which comprise the most important group of implantable materials, have very high tensile strength, toughness, abrasion resistance, and resistance to degradation, in addition to biocompatibility, which has sustained their use as biomaterials [182, 212]. Polyether-urethane is regarded as an excellent biomaterial [144-146]

Purpose	**Examples**
Implants	Artificial heart, cardiac pacemaker leads, vascular tube prosthesis, breast implants, membrane for the reconstruction of the meniscus, materials to fix bones, implants for the reconstruction of facial bones
Materials with membrane properties	Adhesive materials, materials for drug-delivery-systems, inclusion membrane for the fixation of inner organs, dialyses-membrane, filtration of oxygen-adsorption-module, artificial skin
Auxiliary material	Catheter, cannula, blood sack, wound dressing

Table A.1 *Biomedical applications of polyether-urethane [144].*

2 Advantages/Disadvantages of polyether-urethane

Polyether-urethane is a well-regarded biomaterial, due to its mechanical properties, particularly good tensile strength, fatigue resistance, and blood and tissue compatibility [143]. Nevertheless, problems occur due to degradation and calcification [198].

2.1 Mechanisms of decomposition

The degradation of polyether-urethane is still an unsolved problem, as it often leads to significant changes in the polymers mechanical properties, surface chemistry and structure [143]. The most important degradation mechanisms are described below.

Hydrolysis

Hydrolysis is one of the dominant mechanism that leads to the degradation of polyether-urethane in an aqueous environment [143]. Polyester-based polyurethane is known not to be resistant against to hydrolysis. The ester-group starts to degrade after the implantation and this leads to strong inflammatory reactions. This problem was solved with the invention of a hydrolysis stable polyether-urethane [163], which is based on polyether. Hence, presently polyester-based polyether-urethanes are no longer used to produce implants [155].

Generally, the hydrolytic degradation of polyether-urethanes in pure water is minimal. But the aqueous environment of the body, i.e. cations and anions, has a strong catalytic effect and in terms of the hydrolysis. Polyether-based polyether-urethanes are generally less susceptible to hydrolysis compared to those that are polyester-based. However, at high temperatures in the presence of water they also degrade hydrolytically. These conditions often exist in polymer processing methods like injection moulding and extrusion [199].

Oxidation

As already mentioned, polyether-based polyether-urethanes are relatively resistant to hydrolysis. However, degradation of this polymer occurs more often through oxidative routes. Oxidation mechanisms include oxidation by hydrogen peroxide or free radicals as well as auto-oxidation. Accordingly, auto-oxidation is considered to be thermal degradation. Thermal degradation results from overheating the polyether-urethane during processing. Elevated temperatures, approximately 150°C can split the urethane link between the isocyanate and the diol [202]. Subsequently, the isocyanate monomers react to the aqueous environment, or in the presence of water, to produce carbon dioxide and a primary amine, that is, the polyether-urethanes' degradation products result in the formation of the amine of the isocyanate (MDA from MDI). These compounds are toxic [205]. The detailed thermal degradation reactions are shown in Fig. *A.1*. Furthermore, other thermal degradation products such as PhI (phenyl isocyanate) and MIC (methyl isocyanate) can be released when polyether-urethanes are heated [176].

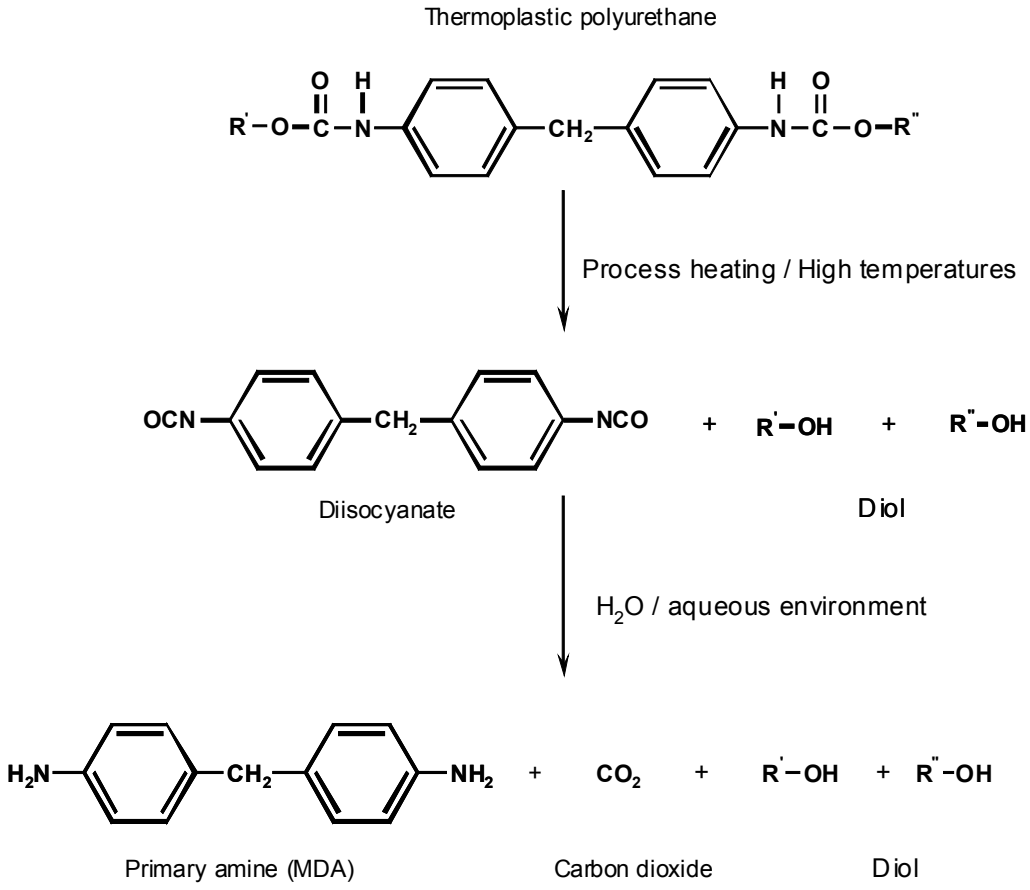

Fig. *A*.1 *Thermal degradation scheme of polyether-urethanes*

Chemical degradation

The exposure of aromatic polyether-urethanes to sunlight changes the mechanical properties (embrittlement and loss of tensile strength) and the polyether-urethanes' colour. Methylene diisocyanate-based (MDI) polyether-urethanes like Texin change their colour from a light yellow to amber, or a dark brown as a result of exposure to sunlight.

Various chemicals can induce degradation during the processing stages. However, during processing the polyether-urethane is only briefly exposed to chemicals compared to the implantation duration for medical applications. Thus, chemical degradation during processing of polyether-urethane is irrelevant. The aggressive biological environment has a much greater influence on degradation because it interacts with the polymer over a very long period of time [143].

Enzymatic degradation

Enzymes are biological catalysts, i.e. they are modified proteins that serve a specific purpose in the human organism, such as digestion or metabolism. They support coordination of the cellular activity and regulate several intracellular processes. Furthermore, they activate and deactivate several proteins and produce oxidative or hydrolytic components. Therefore, enzymes are responsible for initiating biodegradation. Other malfunction phenomena have also been found in association with cells and enzymes, e.g. calcification and environmental stress cracking [143, 198].

Surface cracking

The term auto-oxidation is also used to describe the cause of cracking, which occurs in a very shallow zone (< 10µm) at the surface of the material. It occurs in the absence of stress, and this differentiates it from environmental stress cracking. Explanted polyether-urethanes frequently show shallow random cracks that do not appear to be multiplied. Auto-oxidation, and the resultant surface cracking appear to result from the foreign body response associated with biomaterials *in vivo* [213]. Zaho et al. [214] found that macrophages adhered to the surface of the polyether-urethane, formed foreign body giant cells (FBGCs), and subsequently areas of surface cracking were found in association with the FBGC. Those conducting the experiments found no cracking in the absence of adherent cells. Since surface cracking does not result in significant changes in the polymer's mechanical properties it should not have an impact on the structural integrity of the GORD implant.

Environmental stress cracking

Environmental stress cracking (ESC) is a problem associated with polymers across their spectrum of applications. ESC of a material occurs under conditions that provide an active chemical agent and tensile stress [215]. Stress may be inherent due to the phase-separated nature of polyether-urethanes. It may also be applied to a device during manufacturing, implantation, or through intracorporeal movement. The failure of a pacemaker's leads was believed to have been caused by environmental stress cracking, and led to many studies of the ESC of implanted medical devices. It was suspected that the manufacturing method employed to produce lead insulation was the cause of stress in the sheaths, which in turn contributed to lead failure. Environmental stress cracking is characterized by deep, ragged fractures within the polyether-urethane, often occurring perpendicular to the direction of

stress [216, 217]. Tissue surrounding an implant which has environmental stress cracking is often well integrated into the material due to in growth into the cracks. As a phenomenon, it has been difficult to show ESC *in vitro*, and it appears to require tissue contact [216]. Further studies of environmental stress cracking of polyether-urethanes in the biological environment have reported that cracks appear within six months of implantation, yet they do not propagate more than 20 – 30 μm within three years [216]. Cracking may also lead to a reduction in the tensile strength of the polyether-urethane.

Two different theories have been proposed to explain environmental stress cracking. The first was proposed by Sutherland [215]. It involves HOCl and NO_3 release from PMNs. The other was proposed by Stokes [217].

2.2 Calcification

The use of polyether-urethanes as a biomaterial is often limited by calcification. [218] Both *in vitro* and *in vivo* calcification of polyether-urethanes have been reported and they are associated with stiffening, failure in flexure and perforations. [143, 219, 220] Most of the effects of calcification on polyether-urethanes have been investigated in relation to cardiovascular devices [143, 218] and have not been tested on soft tissue.

Soft tissue interactions with polyether-urethanes

The first event in soft tissue interactions with polyether-urethane is the adsorption of water and protein onto the surface followed by an acute inflammatory response characterised by the presence of polymorphonuclear leukocytes. The consequence of the adsorbed protein layer on the biomaterial is that cells never actually come into contact with the material itself. Subsequent to protein adsorption, an acute response, is followed by chronic inflammation, which includes a wound healing mechanism and a foreign body reactions that involves both macrophages and fibroblasts. Polyether-urethanes, like many other biomaterials, elicit a foreign body response, which are determined by the presence of multinucleated giant cells found in contact with their surfaces. Additionally, researches have found that polyether-urethanes, like many other materials, become encapsulated in a fibrous capsule [143, 221, 222].

Surface chemistry, the relative hydrophobicity and hydrophilicity of polyether-urethanes has been found to influence the proteins adsorbed by the surface. Ultimately, this influences the subsequent

cell migration and implant's function. Mohanty [223] and others [224] have found a relationship between pore size and the infiltration of macrophages into a polymer implant. The researches found that a pore size of 5 - 10 μm inhibits cellular infiltration of the material, while larger pore sizes (200 - 300 μm) encourage cell infiltration [143]. Mohnty's work also indicates that a porous implant delays the incidence of capsule formation and contracture for about 10 years.

Toxicity and carcinogenicity

All the components of polyether-urethane, the soft segment, hard segment and chain extenders could potentially be toxic by themselves or as part of degradation products. As of yet, there have been no published reports of cancer linked to polyether-urethane implants or to the degradation of polyether-urethanes [143].

Appendix B, Injection moulding mould

1 Strength calculations for the aluminium alloy mould

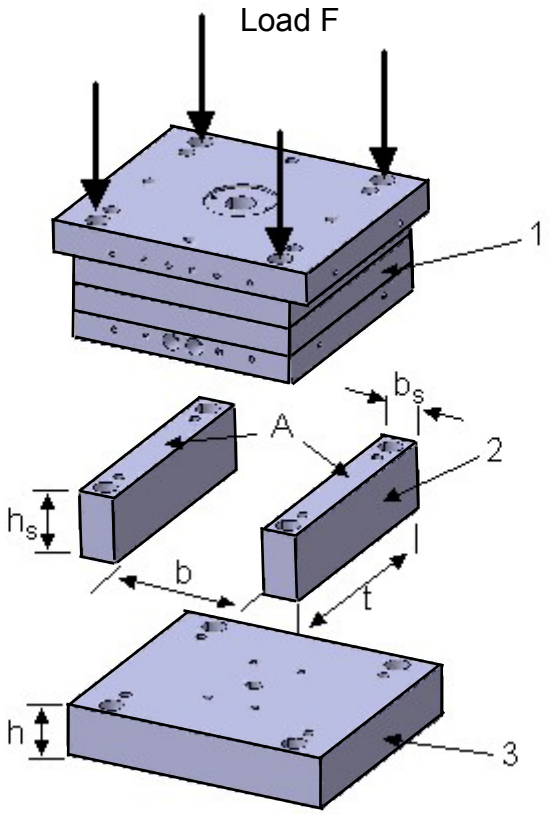

Fig. B.1 Nomenclature for strength calculations

It has been proven that the aluminium alloy mould does not have a plastic behaviour although it has a low density compared to steel.

To prove that the constructed mould can withstand the load, the maximum load, M_L, is compared to the maximum strength, M_s, of the mould. If the M_L is greater than M_s a plastically deformation of the mould takes place ($M_L / M_s > 1$).

The maximum compressive stress upon the mould is equal to the maximum clamping force of the injection moulding machine. This pressure is evenly distributed throughout the mould. The strength

is greatest on the smallest part, e.g. the riser strips (Part No. 2 in Fig. B.1). Verification that plastical deformation of the riser strips due to compression [225] is calculated by Eq. B.1:

Base values used for the calculations:

F	= 1250 kN	maximum clamping pressure
A	= 23832 mm²	surface area of the riser strips
$\sigma_{d,all}$	= 410 N/mm²	allowable compressive stress
σ_S	= 410 N/mm²	yield strength of aluminium alloy

$$\sigma_d = \frac{F}{A} = \frac{1250\,kN}{2*(46\,mm*296\,mm - 2*((15\,mm)^2\pi + (6{,}75\,mm)^2\pi)} = 52.5\frac{N}{mm^2} \qquad \text{Eq.B.1}$$

$$\sigma_{d,alll} = \sigma_S = 410\frac{N}{mm^2} \qquad \text{Eq.B.2}$$

$$S_{F,S.c.} = \frac{\sigma_{d,zul}}{\sigma_d} = 7.8 \qquad \text{Eq.B.3}$$

Solution:

σ_d	= 52.5 N/mm	compressive stress
$S_{F,S\,c.}$	= 7.8	Safety factor against plastical deformation

Since the safety factor is 7.8, a plastical deformation is not possible under the experimental boundary conditions.

Another mechanical failure of the mould that might occur is bending. The calculation for bending stress is found by using the bending momentum and resistance of the clamping plate (Part No. 3 in Fig. B.1).

Base values used for the calculation in Eq. B.4:

M_b	= 31875000 Nmm	bending stress momentum
W_b	= 148104 mm³	bending stress resistance
F	= 1250 kN	maximum clamping pressure

b	= 204 mm	distance between the riser strips
h	= 66 mm	thickness of clamping plate
σ_S	= 410 N/mm²	yield strength of aluminium alloy

The safety factor, $S_{F,\ Bending}$, on bending deformation of the clamping plates (Part No. 3 in Fig. B.1) is expressed [225, 226] through:

$$\sigma_b = \frac{M_b}{W_b} = \frac{Fb}{8} * \frac{6}{b^2 h} = \frac{1250\,kN * 204\,mm}{8} * \frac{6}{(204\,mm)^2 * 66\,mm} = 69{,}6\,\frac{N}{mm^2} \qquad \text{Eq.B.4}$$

$$\sigma_{b,all} = \sigma_S * v_{sb} = 410\,\frac{N}{mm^2} * \left(1 + 0{,}37 * \left(\frac{300}{410}\right)^{0{,}25}\right) = 550\,\frac{N}{mm^2} \qquad \text{Eq.B.5}$$

$$S_{F,Bending} = \frac{\sigma_{b,zul}}{\sigma_b} = 7.9 \qquad \text{Eq.B.6}$$

Solution:

σ_b	= 69.6 N/mm²	bending stress
v_{sb}	= 1.34	static bending stress factor
$\sigma_{b,all}$	= 550 N/mm²	allowable bending stress
$S_{F,bending}$	= 7.9	safety factor for bending stresses

Again, the safety factor is well within the allowable mechanical limits.

Thirdly, to be sure that the riser strips do not flex axially, the critical flexural stress was calculated using Eq. B.7.

Base values used for the calculation:

E	= 72000 N/mm²	E-Modulus of aluminium alloy
b_S	= 46 mm	thickness of riser strips
t	= 296 mm	depth of riser strips
h_S	= 86 mm	height of riser strips
S_K	= 6	safety factor
F	= 1250 kN	maximum clamping pressure

Calculation of the flexural strength of the riser strips based on Euler [226]:

$$F_K = \frac{\pi^2 E * I}{L_K^2} = \frac{\pi^2 E b_S t^3}{\left(\frac{1}{2} h_s\right)^2 * 12} = \frac{\pi^2 * 72000 \frac{N}{mm^2} * 46mm * (296mm)^3}{\left(\frac{1}{2} * 86mm\right)^2 * 12} = 3.82 * 10^{10} N \qquad \text{Eq.B.7}$$

$$F_{K,crit} = \frac{2 * F_K}{S_K} = \frac{2 * 3.82 * 10^{10} N}{6} = 1.27 * 10^{10} N \quad >> \quad F = 1.25 * 10^6 N \qquad \text{Eq.B.8}$$

Solution:

I	= 9.94*10^6 mm^4	moment of inertia of area
L_K	= 43 mm	free flexural length
F_K	= 3.82*10^{10} N	flexural stress on riser strips
$F_{K,crit}$	= 1.27*10^{10} N	critical flexural stress

The maximum clamping pressure of the injection moulding machine is less than the critical flexural stress. It has, therefore, been proven that the aluminium alloy mould cannot be flexed axially during the processing of the implant.

Based on the calculations above (Eqs.B.3, B.4 and B.8), deformation of the mould, neither by clamping, bending nor flexing, can occur when being used in the injection moulding machine.

Appendix C, Polymer processing

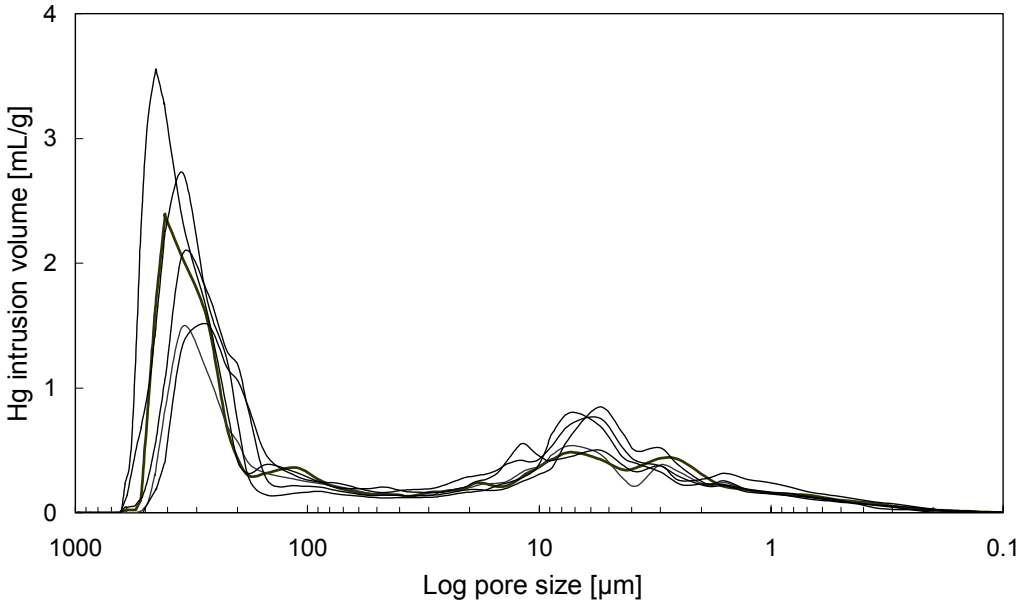

Fig. C.1 *Pore size distribution within the porous kernel of the GORD implant depended in one mould cycle*

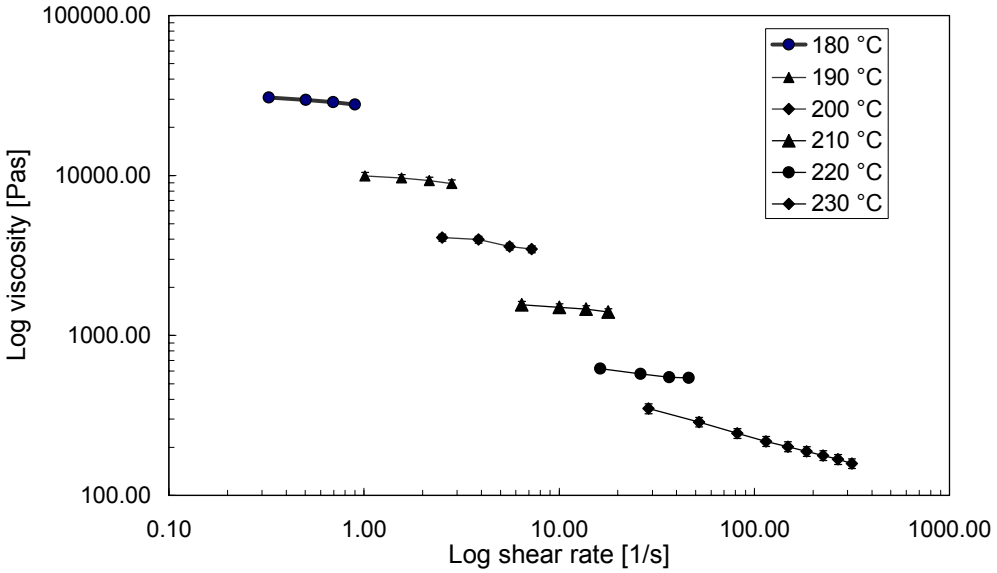

Fig. C.2 *Viscosity of TPU with NaCl particles against shear rate at different temperatures*

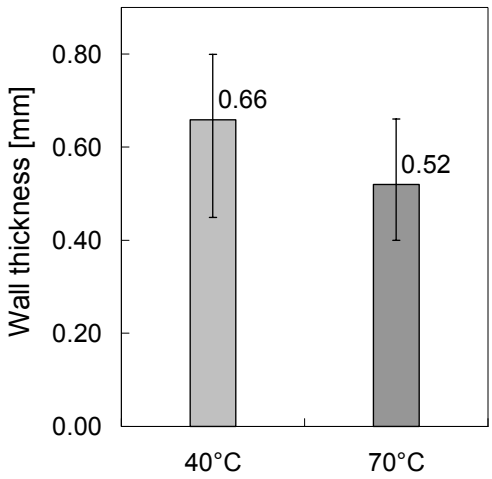

Fig. C.3 *Wall thickness of the solid outer layer of the GORD implant at different mould temperatures*

Appendix D, Culture medium additives

D.1 Medium for cultivation of Detroit 551 fibroblasts

Minimum essential medium (Eagle) 1x	Biochrom AG, Cat.no. FG0325
+ 0.1 mM Non-essential amino acids	Biochrom AG,, Cat.no. K0293
+ 1.0 mM Sodium Pyruvat (100mM)	Biochrom AG, Cat.no. L0473
+ 10% Fetale bovine serum (heat inactivated)	Biochrom AG, Cat.no. S0115
+ 1% Penicillin/Streptavidin (10000U/10000ug/ml)	Biochrom AG, Cat.no. A2213
+ 1% Partricin (Fungicide, 50ug/ml)	Biochrom AG, Cat.no. A2812

D.2 Trypsination

Trypsin/EDTA-Solution (0.05%/0.02%)	Biochrom AG,Cat.no. L2143
Cryo tubes	Nalge Nunc International, Brand Products, 343958

D.3 Culture dishes

Well-Plates (6, 12, 24, 48, 96)	TPP, Trasadingen, Schweiz
Cell culture dishes (T25, T75)	TPP, Trasadingen, Schweiz
Centrifuge tubes (15 ml, 50 ml)	TPP, Trasadingen, Schweiz